

Portland State University

PDXScholar

Dissertations and Theses

Dissertations and Theses

Summer 6-10-2016

Biomimetic Tools in Oxidative Metabolism: Characterization of Reactive Metabolites from Antithyroid Drugs

Kudzanai Chipiso

Portland State University

Follow this and additional works at: https://pdxscholar.library.pdx.edu/open_access_etds

 Part of the [Chemistry Commons](#)

Let us know how access to this document benefits you.

Recommended Citation

Chipiso, Kudzanai, "Biomimetic Tools in Oxidative Metabolism: Characterization of Reactive Metabolites from Antithyroid Drugs" (2016). *Dissertations and Theses*. Paper 3083.

<https://doi.org/10.15760/etd.3078>

This Dissertation is brought to you for free and open access. It has been accepted for inclusion in Dissertations and Theses by an authorized administrator of PDXScholar. Please contact us if we can make this document more accessible: pdxscholar@pdx.edu.

Biomimetic Tools in Oxidative Metabolism: Characterization
of Reactive Metabolites from Antithyroid Drugs

by

Kudzanai Chipiso

A dissertation submitted in partial fulfillment of the
requirements for the degree of

Doctor of Philosophy
in
Chemistry

Dissertation Committee:
Reuben H. Simoyi, Chair
Bradley Buckley
Dean Atkinson
Robert Strongin
Shankar Rananavare

Portland State University
2016

ABSTRACT

Toxicities of sulfur-based drugs have been attributed to formation of highly reactive sulfur oxo-acids and depletion of glutathione by the formation of reactive metabolites. Metabolic activation of these sulfur centers to conceivably toxic reactive metabolites (RMs) that can covalently modify proteins is considered the initial step in drug-induced toxicity. Despite considerable effort and research, detection and characterization of these RMs during drug development and therapy remains a challenge. Methimazole (MMI) and 6-propyl-2-thiouracil (PTU) are two commonly used antithyroid, sulfur-based drugs. Though effective, these drugs are associated with idiosyncratic toxicity. PTU has acquired a black box warning and physicians are calling for its withdrawal. RMs resulting from bioactivation of these drugs have been implicated in the aforementioned adverse reactions. Unfortunately, isolating and detecting RMs using traditional analytical techniques has not been successful due to their high reactivity and short life span, typically less than a minute.

Current approaches in drug metabolism studies use microsomal incubations to generate RMs, which are then trapped using nucleophiles. Antithyroid drugs, however, are known to deactivate enzymes involved in their oxidation. Moreover, due to the complex nature of biological matrices and low abundance of possible toxic conjugates, this technique results in poor selectivity and sensitivity. This study developed and optimized an analytical method based on coupling electrochemical redox reactions and mass spectrometry to generate, detect and identify RMs from antithyroid drugs. The metabolites were also compared to those that were generated using chemical oxidants and

biological microsomes. Mimicry of enzymatic oxidation of the antithyroid drugs was carried out by electrochemically oxidizing them using a coulometric cell coupled on-line to electrospray ionization mass spectrometry (EC/ESI-MS). Oxidation of MMI and subsequent trapping with nucleophile resulted in formation of adducts with N-acetylcysteine, revealing reactive metabolites. The most-postulated metabolite, sulfenic acid, had never been isolated or detected until now, using electrochemistry on-line with electrospray ionization. The results showed that bioactivation of MMI proceeds predominantly through the S-oxide and not through formation of thiyl radicals. These same trapping experiments were also conducted with PTU, but no conjugates were detected. The lack of conjugates from PTU does not preclude formation of RMs, but asserts radical pathway might be dominant in EC oxidation. A double mixing stopped flow was used to investigate the kinetics and mechanism of reaction of the MMI and the biologically relevant hypochlorous acid (HOCl), a product of oxidation of chloride (Cl⁻) ions by myeloperoxidase. The products from the chemical oxidations were compared to the electrochemically generated metabolites, some differences were apparent. Human liver microsomes (HLM) were also used, to investigate oxidation of PTU. Oxidation of PTU, resulted in the supposedly toxic S-oxide, but this has never been isolated, save for speculation. A comparison of metabolites that were found with HLM to those generated electrochemically showed some degree of similarity. These results show that *in vitro* techniques such as chemical oxidations and electrochemistry coupled to mass spectrometry can be used to mimic oxidative metabolism and subsequent high throughput screening of reactive metabolites.

DEDICATION

*This dissertation is dedicated to my late father, Stephen Chipiso.
Who had confidence in me.*

ACKNOWLEDGEMENTS

I would like to acknowledge my advisor Prof R.H. Simoyi for his support, guidance and encouragement during my studies at Portland State University. His unwavering support in both my academic and social life made this thesis a reality.

I would also want to thank the members of my dissertation committee: Drs. Bradley Buckley, Dean Atkinson, Shankar Rananavare and Robert Strongin for their contributions towards completion of my degree requirements. I am also grateful to the faculty, staff and members of PSU Chemistry Department for their support, including uninterrupted financial support during my studies.

I would also want to thank past and current members of the Simoyi research group; Dr Mashood Morakinyo, Dr Wilbes Mbiya, Dr Risikat Ajibola, Dr Morgen Mhike, Matt Eskew, Isabelle Logan , Vusimuzi Sibanda and the undergraduates I have worked with, Sylvie Tran, Thai Tran, Trang Duc, Anh Nguyen for their advice and invaluable support.

I greatly appreciate the love and support of my wife Tsitsi for being there for me, in every way and her words of encouragement. I am indebted to my mom, who despite being single parent, after the death of my father was able to see me through my undergraduate studies, paying every cent for my college education. My profound gratitude goes to my siblings for their support and encouragement throughout the years. Finally I give glory to the God that I believe in for giving me faith to trust in him.

TABLE OF CONTENTS

ABSTRACT	i
DEDICATION	iii
ACKNOWLEDGEMENTS	iv
LIST OF TABLES	ix
LIST OF FIGURES	x
LIST OF SCHEMES	xiii
LIST OF ABBREVIATIONS	xiv
CHAPTER ONE: INTRODUCTION AND RATIONALE	1
1.1: Methods for characterization of reactive metabolites.....	4
1.2: Electrochemistry/liquid chromatography/mass spectrometry (EC/LC/MS) in drug metabolism.....	5
1.3: Bioactivation of sulfur based drugs	6
1.4: Mechanism of action of antithyroid drugs	8
1.5: Significance of this research	8
CHAPTER TWO: INSTRUMENTATION, MATERIALS AND METHODS	9
2.1 INSTRUMENTATION	9
2.1.1 Electrochemical apparatus	9

2.1.2 LTQ-Orbitrap Electrospray-Ionization Mass Spectrometry (ESI-MS)	11
2.1.3 Coupling electrochemical apparatus to LTQ Orbitrap MS	13
2.1.4 Nuclear Magnetic Resonance (NMR) Spectroscopy	15
2.1.5 Conventional UV/Vis Spectrophotometry	15
2.1.6 Stopped Flow Spectrometry	16
2.2 MATERIALS AND METHODS	18
2.2.1 Chemicals	18
2.2.2 On-line EC/ESI-MS electrochemical oxidation of analytes	18
2.2.3 Experimental procedure for trapping experiment	19
2.2.4 Purification and Standardization of Chlorite	19
2.2.5 Reaction dynamics	20
2.2.6 Microsomal enzymatic oxidation	21
2.2.7 LC-MS analysis	22
2.2.8 Structural elucidation, mass accuracy and theoretical m/z calculations	23
2.3 OPTIMIZATION OF PARAMETERS	27
2.3.1 Optimization of electrochemical methods	27
2.3.2 Sample preparation and delivery	28
2.3.3 Results and discussion from optimization	29
CHAPTER THREE: ELECTROCHEMICAL OXIDATION OF METHIMAZOLE	
.....	34
3.1 INTRODUCTION	34

3.2 RESULTS AND DISCUSSION	36
3.2.1 Electrochemical oxidation in basic media	36
3.2.2 Electrochemical oxidation in acidic media	40
3.2.3 Choice of supporting electrolyte and effect of pH.....	42
3.2.4 Assessment of stability and reactivity of metabolites	43
3.2.5 Experimental results derived from nucleophilic trapping	42
3.2.6 NMR experiments	48
3.2.7 Mechanism	49
3.2.8 Proposed mechanism for electrochemical oxidation of MMI.....	52
3.2.9 Comparison with biological oxidations	55
3.4 CONCLUSION.....	56

CHAPTER FOUR: KINETICS AND MECHANISM OF OXIDATION OF METHIMAZOLE BY CHLORITE IN SLIGHTLY ACIDIC MEDIA57

4.1 INTRODUCTION.....	57
4.2 RESULTS AND DISCUSSION	58
4.2.1 Stoichiometry of reaction.....	59
4.3 Reaction Kinetics.....	64
4.3.1 Chlorine dioxide and MMI reaction kinetics	69
4.3.2 Chlorite-MMI reactions at λ_{max} 260 nm.....	73
4.4 Mechanisms	77
4.4 1Oxychlorine chemistry.....	79

4.4.2 Effect of Chloride	80
4.4.3 Effect of acid.....	81
4.4.4 Reaction of chlorine dioxide and MMI.....	83
4.4.5 Oligooscillations	84
4.5 Overall reaction scheme.	85
4.6 CONCLUSION.	88
CHAPTER FIVE: ELECTROCHEMICAL AND ENZYMARTIC OXIDATION OF 6-PROPYL-2-THIOURACIL	89
5.1 INTRODUCTION.....	89
5.2 RESULTS AND DISCUSSION	91
5.2.1 Electrochemical oxidation of PTU in basic media	91
5.2.2 Effect of oxidation potential	96
5.3 IN VITRO ENZYMATIC OXIDATIONS	98
5.3.1 Oxidation Mechanism.....	102
5.3.2 Comparison of electrochemical oxidation with biological oxidations	106
5.4 CONCLUSION	107
REFERENCE LIST.....	108

LIST OF TABLES

Table 4.1:	Chlorite –Chlorine- MMI reactions	87
-------------------	---	----

LIST OF FIGURES

Figure 1.1:	Hypothesis in etiology of drug induced liver injury.....	3
Figure 2.1:	Basic Potentiostat circuit and a three-electrode cell.....	9
Figure 2.2:	Schematic diagram of LTQ- orbitrap mass spectrometry	11
Figure 2.3:	Schematic representation of electrospray ionization source	12
Figure 2.4:	Schematic of EC/ESI –MS system.	13
Figure 2.5:	Sample Handling Unit (SHU) flow circuit diagram for SF-61DX-2 Double-Mixing Hi-Tech Stopped Flow Spectrometer	16
Figure 2.6:	Qual Browser™ simulation for elemental composition, showing 10 possible molecular combinations of m/z 129 at low accuracy of +/- 100 ppm.....	24
Figure 2.7:	Qual Browser™ simulation for elemental composition, showing 10 possible molecular combination of m/z 129 at low accuracy of +/- 4 ppm	25
Figure 2.8:	ESI(+) mass spectrum showing simulation of the proposed elemental composition	26
Figure 2.9:	ESI (+) mass spectrum of APAP and GSH mixture, after APAP oxidation at 650mv vs Pd/H ₂	30
Figure 2.10:	Cyclic voltammetry: catalytic oxidation of GSH to GSSG and subsequent reduction of NAPQI to APAP	31
Figure 3.1:	On-line ESI(-)mass spectrum analysis of MMI oxidized in ammonium buffer	36
Figure 3.2:	Putative metabolites from oxidation of MMI.....	37
Figure 3.3:	On-line ESI (+) mass spectrum showing the oxides of MMI in basic medium.....	38
Figure 3.4:	Off-line ESI (-) mass spectrum of MMI oxidized in basic medium	39
Figure 3.5:	Off-line ESI (+) mass spectrum of MMI oxidation products neutral medium	40
Figure 3.6:	On-line ESI(+) mass spectrum of oxidized MMI in acidic medium.....	41
Figure 3.7:	On-line ESI (+) mass spectrum MMI-n-acetyl cysteine conjugate in basic medium.....	44

Figure 3.8	List of structure of metabolites that are known and those that were observed during oxidation of methimazole	46
Figure 3.9:	NMR spectrum of oxidized MMI products.....	48
Figure 3.10:	ESI (+) mass spectrum of oxidation of MMI with bromine, 1:1 mixture ratio.....	51
Figure 4.1:	Spectral scans showing intrinsic absorption of the reactants	58
Figure 4.2:	Iodometric titration to determine stoichiometry.....	60
Figure 4.3:	On-line ESI (+) mass spectrum for oxidation of MMI by chlorite	62
Figure 4.4:	On-line ESI (-) mass spectrum of oxidation of MMI by chlorite.....	63
Figure 4.5:	Multiple scans of MMI oxidation by chlorite in aqueous acidic medium at 60 seconds intervals	65
Figure 4.6:	Variation of [MMI] ₀ and its oxidation by chlorite	66
Figure 4.7:	Effect of [ClO ₂] ₀ variation on the reaction with MMI.	67
Figure 4.8:	Effect of [H ⁺] ₀ variation on the reaction with MMI with ClO ₂ ⁻	68
Figure 4.9.	Variation of [ClO ₂] ₀ and its effect on rate of reaction.	70
Figure 4.10:	Variation of [MMI] ₀ and their effect on rate of reaction with ClO ₂	72
Figure 4.11:	Effect of [MMI] ₀ variation on its oxidation by chlorite at λ _{max} 260 nm ..	74
Figure 4.12:	Effect of varying chlorite on oxidation of MMI at λ _{max} 260 nm	75
Figure 4.13:	Effect of acid variation on oxidation of MMI.	76
Figure 4.14:	Effect of chloride ions on the oxidation of MMI	80
Figure 5.1:	Tautomeric forms of PTU	89
Figure 5.2:	On-line ESI (-) mass spectrum of PTU at 0 mV in basic medium.....	91
Figure 5.3:	On-line ESI (-) mass spectrum generated with the cell potential at 400 mV	93
Figure 5.4:	On-line ESI (-) mass spectrum of oxidized PTU at 800 mV.....	97
Figure 5.5:	LC-MS chromatograms from metabolites generated by incubation with human liver microsomes (HLM)	99

Figure 5.6:	ESI (+) mass spectrum, showing PTU-S-oxide as the product of oxidation from microsomal incubation.	101
Figure 5.7	ESI (+) mass spectrum showing sulfinic acid and sulfonic acid as products of oxidation of PTU.....	104
Figure 5.8:	Putative zwitterion structures	105

LIST OF SCHEMES

Scheme 2.1 : Reaction scheme for the oxidation of APAP in the presence of GSH	32
Scheme 3.1 : Reaction scheme for the oxidation of MMI and subsequent formation of sulfenic acid.....	54
Scheme 3.2 : Summary of fate of sulfenic acid.....	55
Scheme 4.1 : Proposed MMI-Chlorite adduct formation	74
Scheme 4.2 : The keto and enol forms of MMI	77
Scheme 4.3 : The initial oxidation scheme of MMI to form the sulfenic and S-oxide.....	77
Scheme 5.1 : Proposed oxidation scheme for PTU and its dimerization	94
Scheme 5.2 : Proposed mechanism for FMO oxidation of PTU in microsomes	102

LIST OF ABBREVIATIONS

Abbreviation	Meaning
ADRs	Adverse drug reactions
APAP	Acetaminophen
CYP450	Cytochrome P450
EC/MS	Electrochemistry-Mass Spectrometry
ESI (-)	Electrospray negative mode
ESI (+)	Electrospray positive mode
ESI-MS	Electrospray ionization mass spectrometer
FMO	Flavin monooxygenase
GSH	Glutathione
GSSG	Glutathione dimer
HLM	Human liver microsomes
HPLC	High pressure liquid chromatography
IADRs	Idiosyncratic Adverse Drug reactions
IDRs	Idiosyncratic drug reactions
LC/MS/	Liquid chromatography mass spectrometry
LTQ	Linear Trap Quadrupole
MMI	Methimazole
NAC	N-acetyl-l-cysteine
NADP+	Nicotine Adenine Dinucleotide Phosphate
NADPH	Nicotine Adenine Dinucleotide Phosphate reduced
NAPQI	N-acetyl-para-benzoquinimine
NMR	Nuclear Magnetic Resonance
PTU	6-Propyl-2-thiouracil
RLM	Rat liver microsomes
RM _s	Reactive metabolites
RSO ₂ H	Generic sulfinic acid

RSO₃H

Generic sulfonic acid

RSOH

Generic sulfenic acid

FTMS

Fourier Transformation Mass Spectrometer

ITMS

Ion Trap Mass Spectrometer

UV/Vis

Ultra Violet/ Visible

CHAPTER ONE

INTRODUCTION AND RATIONALE

Drugs undergo different phase I biotransformations such as oxidations, reductions, hydrolysis, hydration and condensation followed by phase II conjugation reactions such as glucuronidation which results in detoxification.^{1,2} Oxidative reactions catalyzed by cytochrome CYP450 enzymes forms the bulk of these biotransformations.³ The enzymatic biotransformation of drugs and xenobiotics usually results in detoxification and subsequent elimination of the drug metabolites from the body.⁴ However, in some cases, the drugs are bioactivated to toxic reactive metabolites.⁵ Reactive metabolites have been found to play a major role in drug-induced toxicity, leading to adverse drug reactions.⁶ These transient metabolites are electrophilic in nature and have the capacity to bind covalently and irreversibly to cellular macromolecules resulting in formation of haptens.⁷ These can then induce drug adverse events such as direct target damage e.g., liver injury or immune mediated toxicity.⁸

ADRs rank between 4th and 6th leading cause of death and results in withdrawal of drugs from the market.⁹⁻¹¹ These adverse drug reactions can be classified as either idiosyncratic (unpredictable) or intrinsic; which are non-idiosyncratic (predictable), as in the case of liver injury due to acetaminophen overdose as they are dose dependent.^{12,13} Utrecht defined idiosyncratic toxicities as adverse drug reactions that do not occur in most patients and do not involve the known pharmacological effects of a drug.¹⁴ Several drugs have been withdrawn from market or from use after reports of hepatotoxicity were noted.¹⁵⁻¹⁸ Some of them have been in use for years e.g., the anti-diabetic troglitazone,¹⁹

talcapone, trovafloxacin²⁰ and the anti-inflammatory drug (NSAID) sudoxicam²¹. The common feature with all these drugs was their bioactivation to reactive metabolites during metabolism.

Although there has been extensive research in the field of chemical toxicology; reliably predicting the occurrence of idiosyncratic adverse drug reactions (IADRs) still remains elusive²². Three main hypotheses have been suggested to explain how reactive metabolites might induce immune-mediated idiosyncratic reactions. These are the hapten hypothesis, the danger hypothesis, and the pharmacological interaction (PI), as shown in Figure 1.1, below. The PI's hypothesis suggests that drugs which lack hapten characteristics actually bind covalently and irreversibly to cell receptors resulting in an immune response.^{23,24}

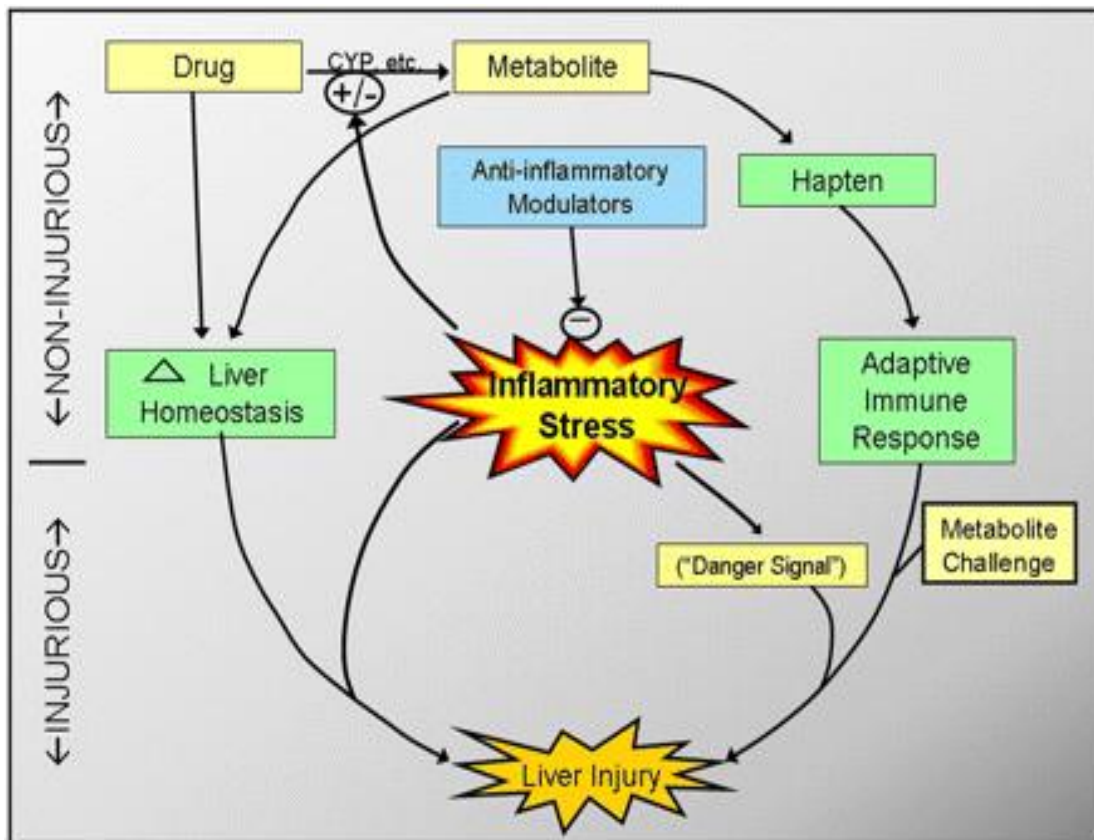


Figure 1.1 Hypothesis in etiology of drug induced liver injury. Adapted from Deng et al *Pharmacol Rev* 61:262–282, 2009²⁵

The current understanding of IADRs indicates that there are several molecular/cellular mechanisms that are not mutually exclusive and can arise from either direct or off-target effects either from the parent drug or its metabolites^{14,25} as shown in figure 1.1. Although the relationship between idiosyncratic adverse reactions and reactive metabolites is not well established, evidence in figure 1.1 and other sources show that drugs and their reactive metabolites are involved at the onset of idiosyncratic toxicities.²⁶⁻

²⁹ In general, the formation of reactive metabolites in drug metabolism is considered unsafe.³⁰ Therefore it is important to understand mechanisms by which bioactivation occurs for the purpose of screening and structural characterization of metabolites in order to mitigate the risk associated with these reactive metabolites during drug design and even during therapy. This will go a long way in reducing attrition rates in drug development.

1.1 Methods for characterization of reactive metabolites

Toxicity of drug candidates contributes about 21% towards failure of lead drug candidates during development.^{31,32} As mentioned above, the major culprits are the unexpected and sometimes reactive metabolites. Different methods have been employed in screening and characterization of reactive metabolites. Techniques using mass spectrometry have become the workhorse in drug development and discovery.³³ Current methods to detect and identify reactive metabolites are based on indirect measurements by mass spectrometry.³⁴ The reactive metabolites from bioactivation of drugs are electrophilic and sometimes radical in nature.⁷ These metabolites are short-lived, with half-lives of usually less than 1 minute, and are not normally detectable in plasma or urine,³⁵ but they can be detected as phase II conjugates.³⁶ Most reactive metabolites can be captured by trapping them with nucleophiles such as N-acetyl cysteine, methoxylamine and GSH to form stable adducts in microsomal incubations.³⁷ The trapped conjugates are usually analyzed using a combination of liquid chromatography and tandem mass spectrometry (LC/MS/MS). Other techniques such as infrared spectroscopy (IR) and NMR may also be used for full structural elucidation. A slightly similar method of trapping and identifying the conjugates uses radiolabeled compounds such as [³⁵S]

cysteine, [¹⁴C] sodium cyanide and [³⁵S] glutathione.³⁸ However, this is a low throughput technique and is also expensive, which makes it unsuitable during lead optimization.³⁹ Measurement of covalent binding to liver microsomal proteins in presence and absence of NADPH is another method that is used to screen for metabolites.⁴⁰

1.2 Electrochemistry/liquid chromatography/mass spectrometry (EC/LC/MS) in drug metabolism

The conventional method of studying oxidative drug metabolism during preclinical experiments is through animal models (*in vivo*) or perfused organs *in vitro*.⁴¹ However, the use of animals in experiments involving scientific research and biological testing has raised concerns over the years among animal advocates.⁴² In view of this as well as the large number of drug candidates emerging and those existing, there has been a renewed interest in the development of complementary tools for mimicry of oxidative metabolism. Although it remains a challenge to extrapolate data generated from such systems to actual *in vivo* systems, these biomimetic tools offer some advantages that are not inherent in the conventional methods.

Electrochemistry coupled on-line to liquid chromatograph/mass spectrometer (EC/LC/MS) has the potential to mimic redox metabolism. Research has shown that electrochemistry can be coupled to mass spectrometer in order to detect products of oxidation.⁴³⁻⁴⁸ The EC/LC/MS method offers the advantage of generating and isolating reactive metabolites in the absence of physiological endogenous material, where usually

the endogenous matrix components will immediately bind to the reactive metabolites resulting in evasion of detection.⁴⁹⁻⁵¹ Jurva and co-workers reported that reactions such as N-Dealkylation, S-Oxidation, P-Oxidation, alcohol oxidation and dehydrogenation that proceed via a mechanism initiated by single electron transfer or hydrogen abstraction are amenable to electrochemical oxidation.⁵² Therefore EC/LC/MS can be used to mimic biotransformation, synonymous to CYP450's. Different experimental setups can be used; a column may be used between the cell and the mass spectrometer, for purification if needed. However, this may slow the time taken by metabolites to be detected from mass spectrometer.

1.3 Bioactivation of Sulfur based drugs

Microsomes contain both flavin-containing monooxygenases (FMO) as well as CYP450's. CYP450's are usually involved in bioactivation of drugs, through oxidative metabolism⁵³. They both use molecular oxygen and NADPH for the oxidation of substrates (S).



The bulky of oxidation process is simply insertion of oxygen on to the substrate. Our research in the past has focused on investigating the mechanism of S-oxidation of organosulfur compounds.^{54,55} Extensive studies from our laboratory have shown that nearly every organosulfur compound presents a unique reactivity and no generic oxidation pathway can be easily derived. The sulfur atom has been implicated as a site of

bioactivation, resulting in formation of reactive and potentially toxic metabolites from bioactivation of sulfur containing drugs.⁵⁶ Many of the adverse reactions produced by penicillamine and other compounds with an active sulfhydryl group form a distinctive pattern when viewed as a class. Alterations in taste perception, mucocutaneous lesions, proteinuria due to immune-complex membranous glomerulopathy, and pemphigus are adverse reactions that have been encountered with all of these compounds. Classic examples include the thiol, captopril, a still-used antihypertensive drug which comes with a black box warning and is associated with hepatotoxicity.⁵⁷⁻⁵⁹ It can only be used in low doses and after careful selection of patients to avoid idiosyncratic drug reactions and thus cannot be used for patients with severe hypertension.⁵⁸ Troglitazone, a thiazolidinedione, developed for diabetes mellitus type 2, had to be withdrawn from market because it caused severe liver injury. Thiazoles such as Sudoxicam were withdrawn in Phase III trials when it was already apparent that the drug was rife with IDR's; while a closely-related drug, Meloxicam, has not been associated with any IDR's. This study investigates the bioactivation of two sulfur based drugs, methimazole and 6-propyl-2-thiouracil. These two drugs are used as antithyroid drugs. Bioactivation of thionamides to reactive intermediates have been implicated in adverse drug reactions. Thionamides drugs are associated with idiosyncratic toxicity, characterized by skin reactions, leucopenia, agranulocytosis, aplastic anemia, hepatitis and cholestasis.⁶⁰

1.4 Mechanism of action of antithyroid drugs

Peroxidases oxidize iodides in the presence of H_2O_2 to form I^+ ions, which in the presence of this enzyme, binds to thyroglobulin.⁶¹ 6-propyl-2-thiouracil (PTU) and methimazole (MMI) block the thyroid hormone synthesis by inhibiting the thyroid peroxidase (TPO) or diverting oxidized iodides away from thyroglobulin.

1.5 Significance of this research

This research has the potential of being informative on the design of *in vitro* experiments, and to refine as well as reduce *in vivo* animal trials. This is crucial in early drug development and can be used to weed out unsuitable candidates for further development, thus reducing late stage compound failures. This technique can be adopted by the pharmaceutical industry as an alternative or complementary technique to existing screening methods. Successful isolation and synthesis of additional/novel reactive metabolites can enhance further studies in bioassays and toxicological studies. This will also add value in understanding the generation of reactive metabolites, for example, the long speculated sulfenic acid responsible for hepatotoxicity in oxidation of methimazole was first reported as part of this work.⁶² Further development of this method can lead to automation and thus reduce the time required for analysis. Apart from metabolism, this technique has potential to be used as an analytical tool for detection and determination of other compounds or drug concentrations; e.g., in plasma samples, as electrochemistry is a sensitive technique that can be used at very low concentrations.

CHAPTER TWO

INSTRUMENTATION, MATERIALS AND METHODS

2.1 INSTRUMENTATION

2.1.1 Electrochemical apparatus

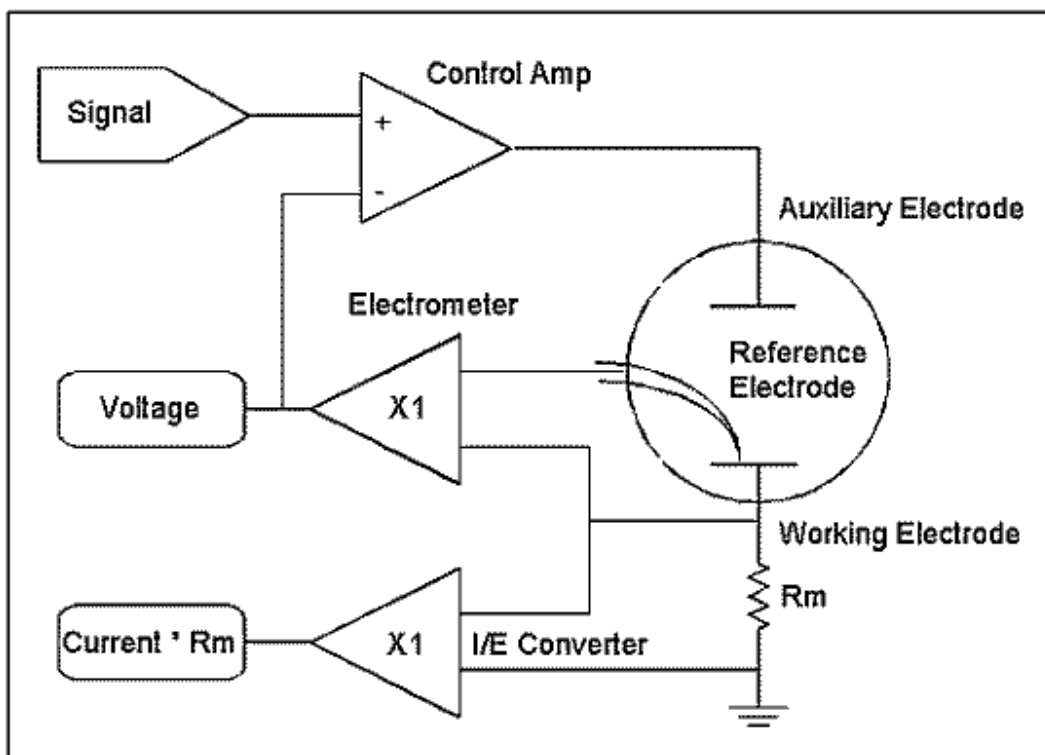


Figure 2.1 Basic potentiostat circuit and a three-electrode cell, [Courtesy of Gamry Instruments® application notes]

Figure 2.1, above shows a basic three electrode cell (sensor) that utilizes a potentiostat hardware, which is used to control the electrode cells for running electroanalytical experiments. The electrode cell is composed of a working electrode

(WE), whose function is to serve as a platform on which the electrochemical reaction takes place. The second electrode is the reference electrode (RE), its function is to measure any potential quantity present in WE electrode.⁶³ A third electrode, the counter electrode (CE) completes the circuit. Its sole purpose is to conduct current into or out of the cell. This current has to exactly balance the current generated at the working electrode. Cyclic voltammetry was used in the initial phase of these experiments, to optimize the technique of coupling electrochemistry to mass spectrometry. Where the oxidation potential of an electroactive compound in a given medium was not known, preliminary studies were conducted using cyclic voltammetry which gave an insight on the required optimum potentials. Despite the difference between cyclic voltammetry and the technique that was mostly used here, the electrochemical apparatus have similar design and same principle of operation as the cell shown above, except that the analyte flows through the working electrode, *vide infra*. The ESA Coulochem III[®] Multi-Electrode Detector used here is equipped with the DC Potentiostat Board as well as Pulse/Scan Potentiostat Board. The analogue signals were controlled by electronic circuits, in the logic module.⁶⁴

2.1.2 LTQ-orbitrap Electropray-Ionization Mass Spectrometry (ESI-MS)

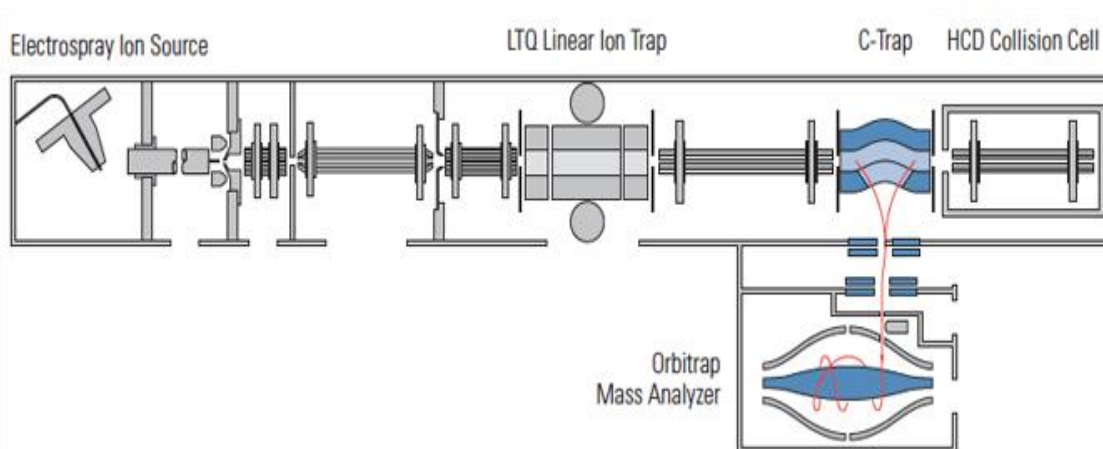


Figure 2.2. Schematic diagram of LTQ- Orbitrap Mass Spectrometry [Courtesy of Thermofisher Scientific Application Notes]

Mass spectra of the electrochemical oxidation metabolites were acquired on a high-resolution ($m/\Delta m = 30\,000$) Thermo Scientific LTQ-Orbitrap Discovery mass spectrometer (San Jose, CA) equipped with an electrospray ionization source. Figure 2.2 shows a schematic diagram of an LTQ-orbitrap mass spectrometer. It is a hybrid instrument that combines the linear trap and orbitrap thus making it more robust in detection, identification, and characterization of samples, including biological complexes.^{65,66} It has high mass accuracy, high resolving power, high sensitivity and MSⁿ capability, although tandem mass spectrometry was not utilized in these experiments.⁶⁷ The instrument above uses electrospray ionization for its ion source. See figure 2.3 below.

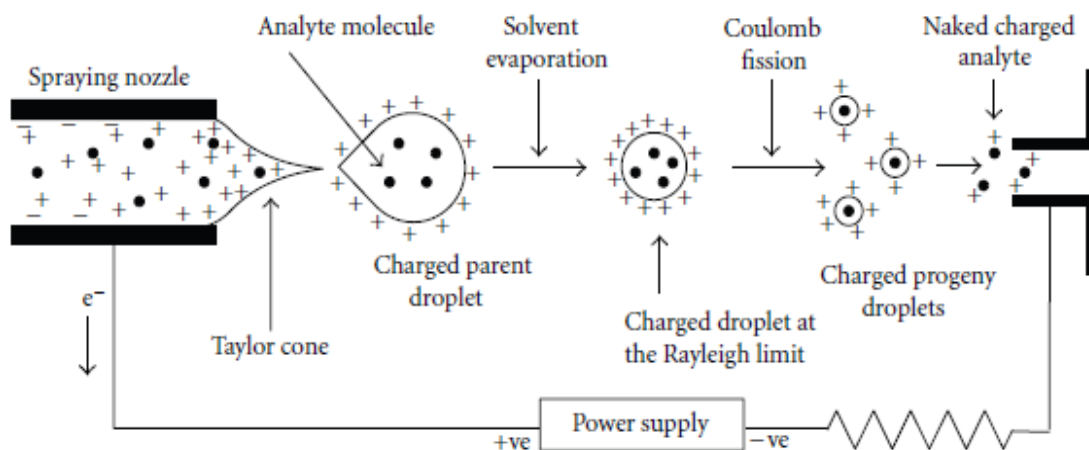


Figure 2.3: Schematic representation of electro spray ionization source⁶⁸

Electrospray ionization (ESI) is a soft ionization technique used for production of gas phase ions, without fragmentation of the molecule being observed. Figure 2.3 shows an ESI process, the transfer of ionic species from solution into the gas phase by ESI involves three steps: (a) dispersal of a fine spray of charge droplets, (b) solvent evaporation and (c) ion ejection from the highly charged droplets.⁶⁸ The charged droplets generated at the exit of the electro spray tip pass down a pressure and potential gradient toward the linear trap analyzer, then into the C-trap where the ions are cooled and slowed down, then into another analyzer, the orbitrap, and finally to the detector.⁶⁹ The mass spectrum is a graphical display of the relative abundance of ion signals against the m/z ratios. It is a common practice that the highest signal is taken as 100% abundance and all the other signals are expressed as a percentage of this peak. Details of full operation of each component of the mass spectrometer are described elsewhere in literature.⁷⁰

2.1.3 Coupling electrochemical apparatus to LTQ Orbitrap MS

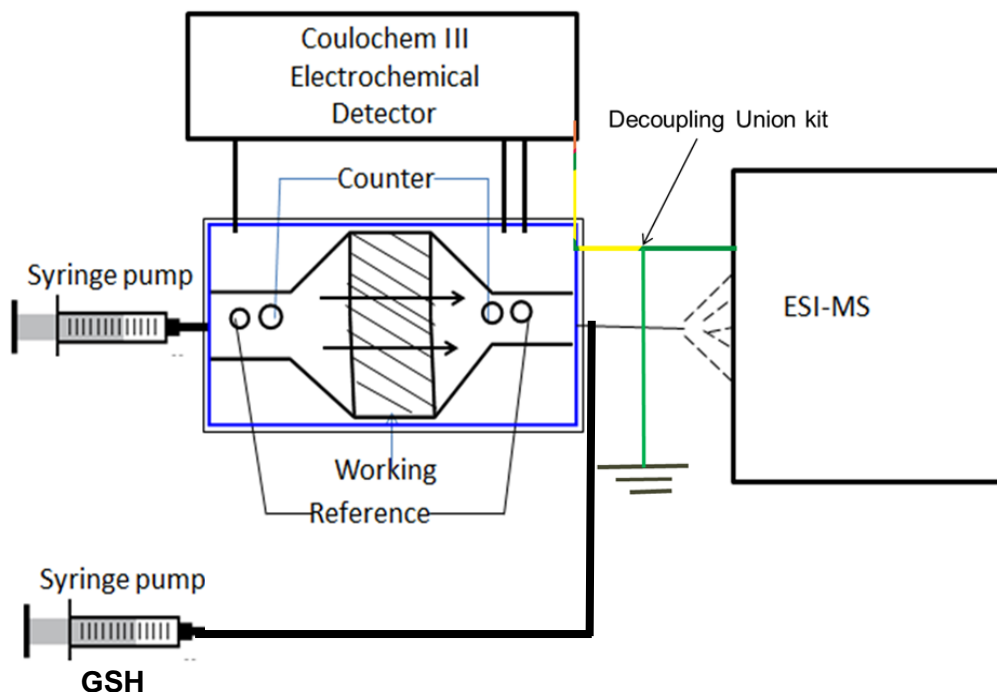


Figure 2.4. Schematic of EC/ESI-MS system. Coulochem III Electrochemical Detector® controls potential of the flow through cell.

A schematic representation of EC-MS coupling is shown in Figure 2.4. ESA Coulometric cells 5150 and 5021A or 5130 and 5021A were interfaced to an LTQ Orbitrap mass spectrometer. The potential to the cells was controlled using a potentiostat in the form of an ESA Colouchem III detector. This unit has a front panel with key controls to input and change different parameters such as potential and current output. The cells described above are equipped with a flow through graphite working electrode, solid-state palladium (Pd/H₂) reference electrode and a palladium counter electrode.⁶⁴

Solutions of analytes and electrolytes were infused into the flow through cells using a syringe pump at different flow rates, depending on the requirements of the experiment. In trapping experiments, the effluent from the cell was directed into a T-junction where it would be mixed with a trapping solution also pumped from another syringe pump into the mass spectrometer.

Coupling electrochemistry techniques to a mass spectrometer is not trivial and is not common. Several practical aspects have not yet been fully explored. Optimum coupling conditions are required for EC/MS technique. Electrospray Ionization Mass Spectrometry is associated with high voltage at the ionization source, for example the spray voltage used during positive mode experiments was +4.5 kV. This can result in backward electric currents flowing through the electrolyte into the cell and detector. The magnitude of this current can be large and dangerous resulting in electric shock to the operator as well as damage to the cells and detector. In order to avoid this, a ground point was introduced between the mass spectrometer and the electrochemical equipment. On-line experiments coupling the cell to mass spectrometer were performed with a decoupling union kit that was used to ground and decouple the high voltage from the ESI- MS as shown in Figure 2.4. Optimum performance of the above setup was realized with ESI source parameters set as follows: spray voltage, 2.5 kV in negative mode and 4.5 kV in positive mode; spray current, 1.96 (μ A); sheath gas flow rate, 20 L/min; auxiliary gas flow rate, 0.01 L/min; capillary voltage, -16 V; capillary temperature, 300 ($^{\circ}$ C); and tube lens, -115 V. Detection was carried out in both the negative and positive ionization mode (-ESI) for 4 min. The detection parameters were set up as follows:

Analyzer: FTMS, positive and negative polarity; mass range, normal; resolution, 30 000; scan type, centroid.

2.1.4 Nuclear Magnetic Resonance (NMR) Spectroscopy

Nuclear magnetic resonance spectrometry (NMR) spectroscopy was also used in structural characterization and verification of products and intermediates. However, it was of little use in EC-MS experiments. Stability of reactive intermediates is dictated by local environment. After lyophilizing and purifying the products for NMR analysis, there were changes in environment and morphology, hence intermediates were not observed in NMR spectra. By their nature the intermediates are short lived and isolating them is not trivial. Hence we tried to do a real time analysis. NMR results obtained showed mostly substrate, even after oxidation, it is as expected since the S-OH bond is unstable. NMR experiments described above were conducted using a Bruker AMX-400 MHz Nuclear Magnetic Resonance (NMR) spectrometer. The atomic nucleus is a spinning charged particle, and it generates a magnetic field.

2.1.5 Conventional UV/Vis Spectrophotometry

Kinetics and reaction dynamics were carried out using spectrophotometric techniques. Slow reactions that occurred in more than sixty seconds were measured using a Perkin Elmer Lambda 25 UV/Vis spectrophotometer system within the range 200 to 800 nm. For these instruments, holographic grating was used as the monochromator and

two radiation sources, a deuterium lamp (UV) and a halogen lamp (visible range) were used in sequence as the polychromator light sources. The Perkin Elmer spectrophotometer was interfaced to a desktop computer and uses the UV WinLab Software for data collection and analyses. Path length of the cuvette was 1 cm. Constant temperature was maintained by use of a circulating water bath attached to the cell holders.

2.1.6 Stopped Flow Spectrometry

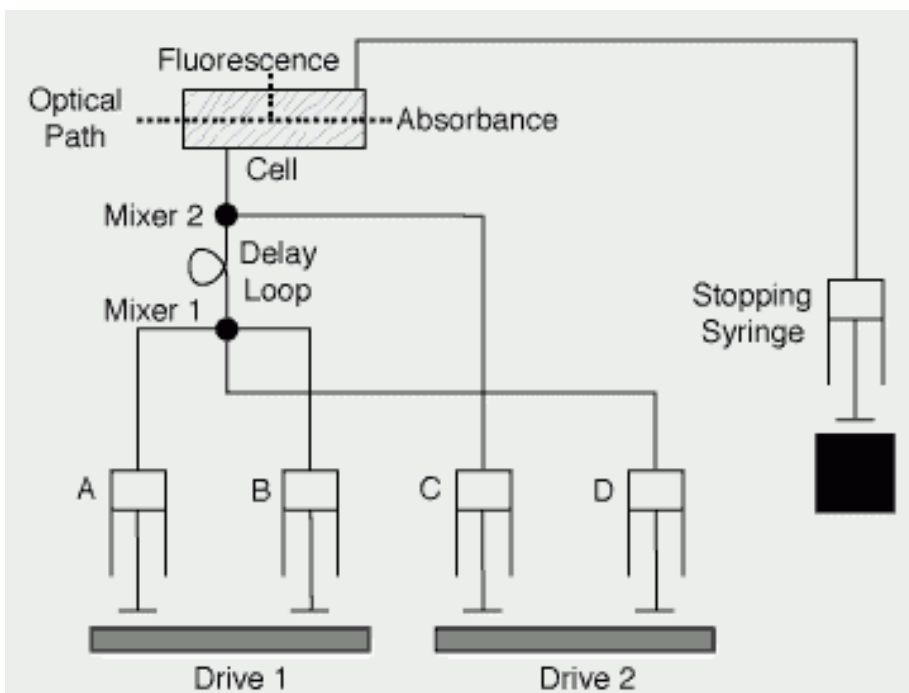


Figure 2.5. Sample Handling Unit (SHU) flow circuit diagram for SF-61DX2 Hi Tech Kinet Asyst Stopped flow Spectrometer. [Courtesy of Hi- Tech Scientific Operators Manual]

Rapid reactions with time scales of less than 10 seconds were measured using the stopped-flow technique, which can follow reactions with time scales as short as 1 millisecond. The Hi-Tech Scientific SF61 – DX2 Double mixing stopped-flow spectrophotometer was used for the acquisition of absorbance data, it allows for changes in optical properties as a result of reactions to be monitored using UV/VIS. A stable Xenon Arc lamp was used as the light source. The instrument was interfaced to a desktop computer via a 413 kHz 16 bit A/D converter to enable the conversion of analog data to digital form. Small volumes of solutions are driven from high performance syringes through a high efficiency mixer(s). The sample handling unit (Figure 2.5) facilitates both the single mixing of two reagents, using only one of the drives, and double mixing of three reactants by a push-push mode of operation. However, experiments were conducted in single mixing mode. Double mixing mode enables transient species formed by mixing reactants in A and B to be subsequently mixed with a third reactant, C, after a delay period. Reactant reservoir D is reserved for the buffer and this will push the premixed solutions A and B (from mixer 1) to a second mixer (mixer 2) where it reacts further with reactant C. The resultant mixture passes through a measurement flow cell and into a stopping syringe where the flow is stopped. Just prior to stopping, a steady state flow is achieved. As the solution fills the stopping syringe, the plunger hits a block, causing the flow to be stopped instantaneously, and an absorbance is then recorded.⁷³

2.2 MATERIALS AND METHODS

2.2.1 Chemicals

Reagent grade methimazole, 6-propyl-2-thiouracil,(PTU) reduced glutathione, N-acetylcysteine and methoxylamine, perchloric acid and sodium perchlorate, acetaminophen, reduced glutathione, acetic acid, and ammonium acetate were obtained from Sigma Aldrich and were used without further purification.. Ammonia, methanol and formic acid, ammonium acetate, acetic acid, sodium formate, acetonitrile, phosphate monobasic and phosphate dibasic were from Fischer Chemicals. Water for all experiments were purified using a Barnstead Sybron Corp. water purification unit capable of producing both distilled and deionized water (Nanopure). Solvents used for electrochemical oxidation and mass spectrometry were HPLC grade. Human liver microsomes, rat liver microsomes, NADPH regenerating system were obtained from Corning.

2.2.2 On-line EC/ESI-MS electrochemical oxidation of Analytes

Experiments were carried out in acidic, neutral and alkaline medium. The analyte was dissolved in acidic medium which consisted of 20 % methanol with 80 % 20 mM formate buffer (pH 2.75). For neutral medium, a combination of 20 % methanol with 80 % 50 mM phosphate buffer (pH 7.4) was used. Alkaline media utilized a 20 % methanol with 80% 20mM ammonium buffer solution (pH 10.2). A 500 μ L sample was

infused through the electrochemical cell at a flow rate of 10 $\mu\text{L}/\text{min}$ before the cell was turned on. With the cell turned on, species generated from oxidation in each medium were monitored on the mass spectrum generated on-line. The potential was changed manually on the front panel of control module of ESA Coulochem III Electrochemical detector from 100 mv to 1200 mv. Each scan acquisition lasted for four minutes. The optimum potential was determined first before acquiring data.

2.2.3 Experimental procedure for trapping experiment

A 100 μM sample of analyte in suitable electrolyte-solvent system was infused through the electrochemical cell at a flow rate of 10 $\mu\text{L}/\text{minute}$. A solution of containing the nucleophile (e.g. N acetyl cysteine) 500 μM from another syringe was then infused at the same rate. The effluent from both channels combined and mixed at a T-junction flowed into the cavity of mass spectrometer as shown in Figure 2.4.

2.2.4 Purification and standardization of chlorite

Commercially-available sodium chlorite varied in purity (78–88%), with the main impurities being chloride and carbonate. The sodium chlorite was recrystallized once from a (1:1:1) water/methanol/acetonitrile mixture to bring the assay value to 96%. These were stored in a desiccator in small batches of 5 g or less to avoid possible explosions.⁷⁴ The recrystallized chlorite was standardized iodometrically by adding excess acidified

potassium iodide and titrating the liberated iodine against sodium thiosulfate with freshly prepared starch as an indicator as described previously.⁷⁵ Chlorine dioxide was prepared by the standard method of reducing sodium chlorate in a sulfuric acid/oxalic acid mixture.⁷⁶ The stream was passed through a sodium carbonate solution before being collected in ice-cold water at 4 °C at a pH of ~3.5. Standardization of ClO₂ was also accomplished by iodometric techniques through the addition of excess acidified potassium iodide and back-titration of the liberated iodine against standard sodium thiosulfate. The chlorine dioxide was stored in an acidic medium in a volumetric flask wrapped in aluminum foil at 4 °C. Chlorine dioxide was also standardized jointly by its molar absorptivity coefficient (ϵ) of 1265 M⁻¹ cm⁻¹ at 360 nm on a PerkinElmer Lambda 25S UV/vis spectrophotometer.

2.2.5 Reaction Dynamics

Kinetics experiments were carried out at 25 °C and at an ionic strength of 1.0 M (sodium perchlorate). The ClO₂⁻/ClO₂/MMI reactions were monitored spectrophotometrically at $\lambda = 360$ nm, as the reactions were performed in excess chlorite in order to utilize formation of chlorine dioxide as an indicator of reaction progress. Reactions monitoring consumption of MMI were monitored at 260 nm, where MMI has its strongest absorption peak. Kinetics measurements were performed on a Hi-Tech Scientific double-mixing SF-61DX2 stopped-flow spectrophotometer. Stoichiometric determinations were carried out by mixing various ratios of chlorite and MMI (in an

acidic medium to avoid alkaline disproportionation of ClO_2) in stoppered volumetric flasks and scanning them spectrophotometrically for the formation of ClO_2 after an incubation of up to 2 days. Qualitative and quantitative analysis of the sulfate produced was performed through its precipitation as BaSO_4 . For reactions run under excess chlorite conditions, the excess oxidizing power was evaluated by the addition of excess acidified iodide, which was titrated against standard thiosulfate with freshly prepared starch as an indicator.

2.2.6 Microsomal enzymatic oxidation

Human liver microsomes were obtained from Corning. A well-established protocol for microsomal incubation (provided from Corning upon purchase of the microsomes) was followed with minor changes to suit the experiment and substrates involved. The microsomal fractions were stored at -80°C and thawed immediately before each experiment. The following quantities were used. Initially, 713 μL of purified water, 200 μL of 0.5 M potassium phosphate buffer pH 7.4, 50 μL NADPH regenerating system solution A (solution A contains NADP^+ and Glucose-6-phosphate), 10 μL NADPH Regenerating system solution B (Solution B contains Glucose-6-phosphate dehydrogenase) 2 μL substrate in solvent, making a final substrate concentration of 10 μM , were combined before adding microsomes. When combined solution A and B provide the regenerating system for all NADPH requiring oxidase assays. After warming in a 37°C water bath for five minutes, the reaction was then initiated by adding 25

μL (0.5 mg) liver microsomes and then was mixed and returned to a 37 °C water bath. After 60 minutes a 100 μL aliquot from the incubation was withdrawn and the reaction was terminated by adding 100 μL acetonitrile. This was then mixed and placed on wet ice followed by centrifuging at 10,000 Xg for three minutes. The supernatant from the protein pellets was withdrawn for analysis using LC/MS. Incubations without NADPH and microsomes were used as controls, to ensure that formation of metabolites was dependent on HLMs and NADPH.

2.2.7 LC-MS analysis.

The metabolites produced by incubation of PTU, were collected and analyzed by LC-MS. The separation of the metabolites was achieved using a reverse phase Zorbax Eclipse Plus 3.5 μm , C8 column. Column dimensions were as follows: 100 mm x 2.1 I.D. The flow rate was set at 200 $\mu\text{L}/\text{min}$ and the injection volume was 20 $\mu\text{L}/\text{min}$. The gradient separation was performed by two solvents. Mobile phase A: 0.1 % acetic acid in water and mobile phase B: 0.1 % acetic acid in methanol. The applied gradient profile was 10 % B for 5 minutes, followed by 30 % for another 5 minutes, and then 50 : 50 for two minutes and finally 90% B for the last six minutes. The column was operated at 35°C. The MS based detection was carried out in positive ion mode using both FTMS and ITMS detection

2.2.8 Structural elucidation, mass accuracy and theoretical m/z calculations

High resolution mass spectrometry allowed calculation of mass accuracy with a relative error of less than 4 ppm, providing unequivocal identification of metabolites. Hence, the exact nature of modification of the metabolites was elucidated, eliminating possibilities of false positives, which results during identification of metabolites. High resolution MS data-processing and calculation of elemental compositions were carried out using the Qual browser of Xcalibur SR2 Thermo Fisher Scientific. Xcalibur™ software was used to arrive at the proposed structures. For example, the elemental composition calculator in Xcalibur™ returns 10 possible elemental compositions within +/- 100 ppm for the measured mass at m/z 129.01143 (See figure 2.6) giving all plausible chemical compositions hence structures for that peak, within that mass tolerance. When the mass tolerance was within +/- 4 ppm (high accuracy); only one composition combination was possible, figure 2.7. In addition, even electron ions are assumed since electrospray ionization (ESI) was used for ion generation. Simulation of the proposed elemental compositions under the measured spectrum was also used in mining possible chemical formula for the major ions⁷⁷ (Figure 2.8). ChemBioDraw™ was used in obtaining exact masses for the proposed structures and calculation of mass accuracy from exact versus observed masses, with five decimal places. Mass tolerance for reported structures was within +/- 4 ppm, giving high mass accuracy and an unambiguous assignment of the peaks.⁷⁸

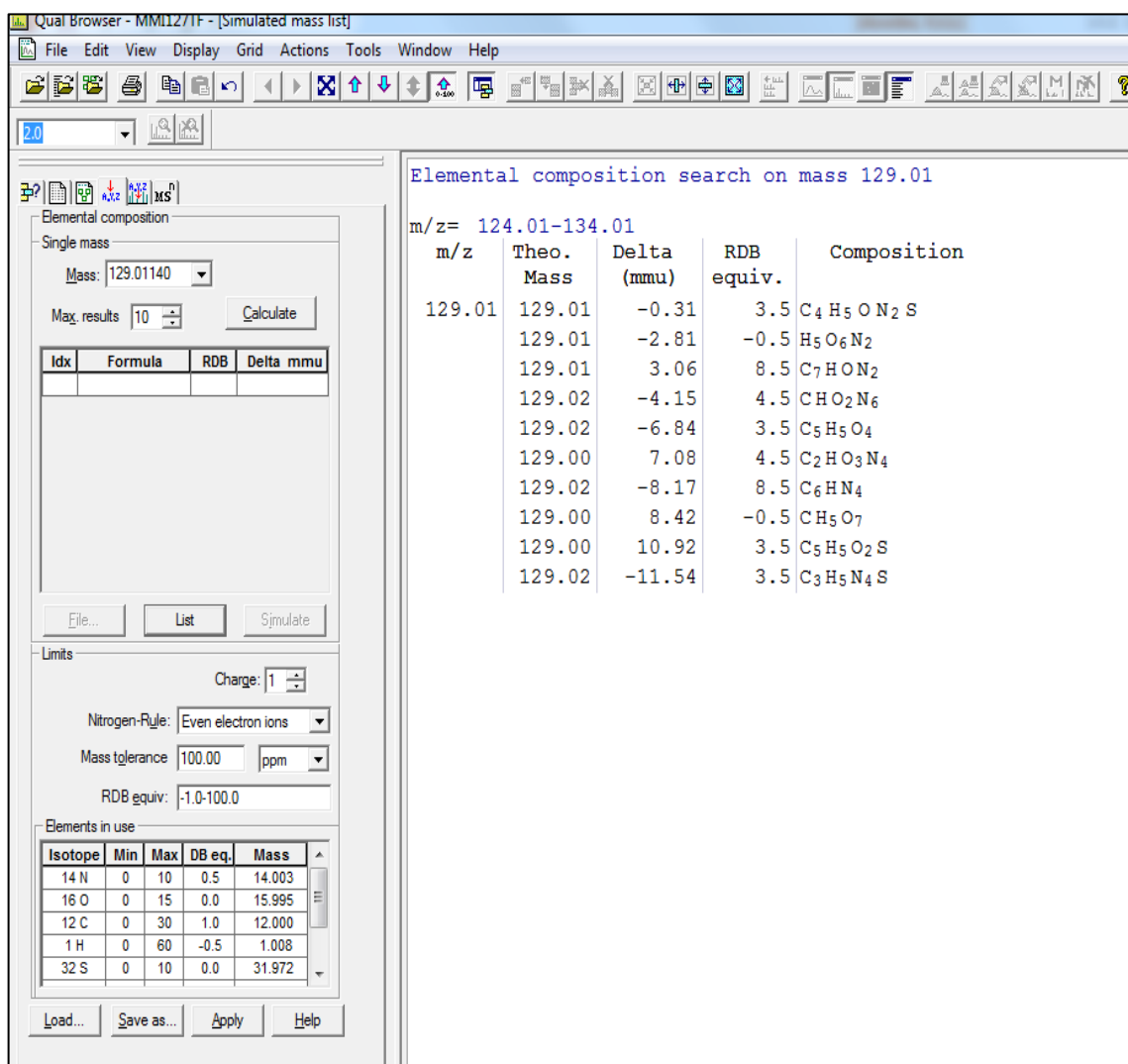


Figure 2.6: Qual Browser™ showing simulation for elemental composition using Xcalibur™, calculator, showing 10 possible composition at low accuracy of +/- 100 ppm.

Qual Browser - MMI127TF - [MMI127TF]

File Edit View Display Grid Actions Tools Window Help

2.0

Elemental composition search on mass 129.01

m/z= 124.01-134.01

m/z	Theo. Mass	Delta (mmu)	RDB equiv.	Composition
129.01	129.01	-0.31	3.5	C ₄ H ₅ O ₂ S

Elemental composition

Single mass

Mass: 129.01140

Max. results 10 Calculate

Idx	Formula	RDB	Delta mmu

File... List Simulate

Limits

Charge: 1

Nitrogen-Rule: Even electron ions

Mass tolerance 4.00 ppm

RDB equiv: -1.0-100.0

Elements in use

Isotope	Min	Max	DB eq.	Mass
14 N	0	10	0.5	14.003
16 O	0	15	0.0	15.995
12 C	0	30	1.0	12.000
1 H	0	60	-0.5	1.008
32 S	0	10	0.0	31.972

Load... Save as... Apply Help

Figure 2.7: Qual BrowserTM showing simulation for elemental composition using XcaliburTM, calculator, showing only one possible composition at high mass accuracy of +/- 4 ppm.

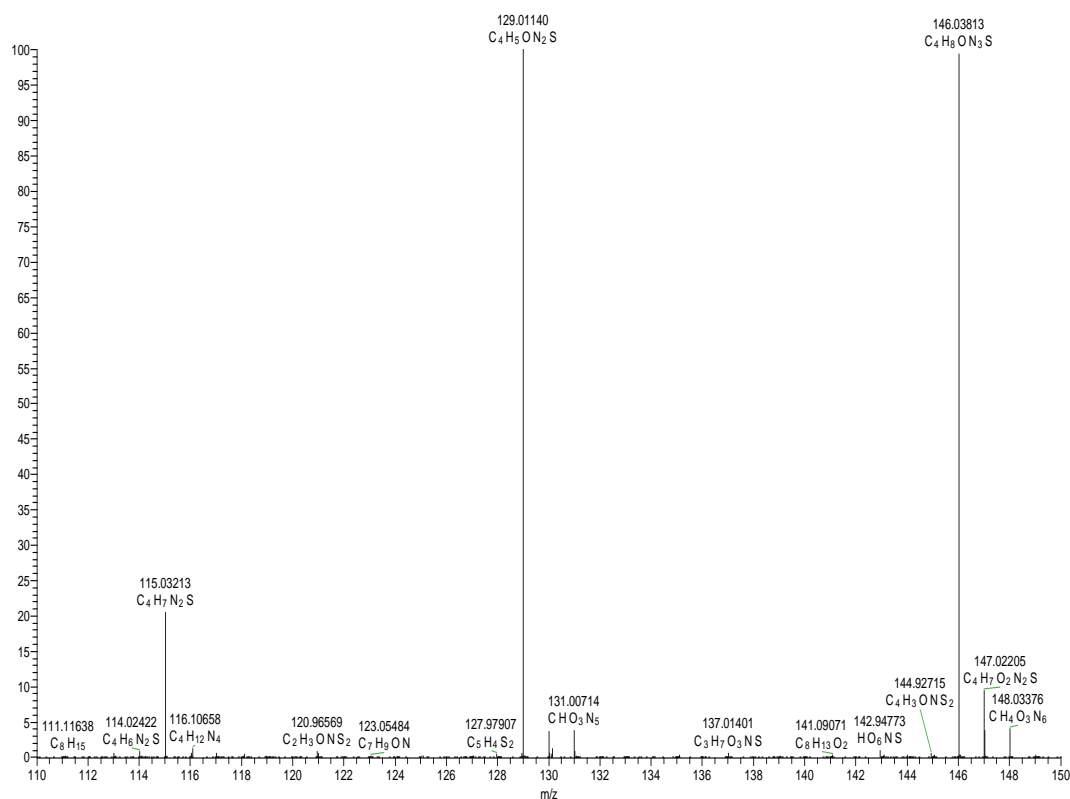


Figure 2.8: Simulation of the proposed elemental compositions under the measured spectrum confirming chemical formula for the major ions.

By exploiting the capability of LTQ-OrbitrapTM and the Qual BrowserTM software which gives exact mass measurement at high resolution,⁷⁹ it was able to identify modifications on analyses. These software allows identifications of small molecules, even in complex endogenous matrix with microsomes, this has become standard practice in drug development.⁸⁰

2.3 OPTIMIZATION OF PARAMETERS

2.3.1 Optimization of electrochemical methods

The most important part of developing this technique was to optimize it with drug whose behavior is well established. In the electrochemical cell used in these studies, the conversion rate of analytes to metabolites was affected by flow rate, pH of the electrolyte, and nature of the analyte as well as the potential applied to the electrochemical cell⁴⁸.

APAP is oxidized into well-known hepatotoxic (n-acetyl-p-benzoquinone imine) NAPQI which forms conjugates with thiols such as GSH and N-acetyl-l cysteine⁸¹.

Electrochemical properties of acetaminophen (APAP) are well characterized and documented in literature, hence APAP was chosen as the test compound in order to optimize the method.^{48,82} Getek et al, successfully coupled the coulometric cell to a mass spectrometer and were able to detect APAP conjugates with glutathione and cysteine⁸¹.

Formation of its reactive metabolites and their subsequent conjugation with glutathione is also well established. A number of studies using cyclic voltammetry reported that APAP is oxidized to the reactive metabolite N acetyl-p- benzoquinone imine (NAPQI).^{83,84}

Cyclic voltammetry was used initially to determine oxidative potential of APAP.

Potentials between 450 mV- 650 mV with respect to Pd/H₂ electrode, were established to be optimum oxidation potential for acetaminophen. Different pH conditions, solvents and potentials were tested as described in literature. The parameters described in literature were modified in order to suit the available equipment. For cyclic voltammetry the optimum pH was found to be 6.4.

2.3.2 Sample preparation and delivery

A 10 μM solution of APAP solution in 20 mM ammonium acetate, pH 6.4 in 20 % aqueous methanol, was infused into the Dionex synthesis cell model 5051 using a syringe pump at flow rate of 10 $\mu\text{L}/\text{min}$. The effluent from the cell was directed into a T-junction where it was mixed with a solution of 50 μM GSH, also pumped at a rate of 10 $\mu\text{L}/\text{min}$ from another syringe pump into the mass spectrometer. The flow-through coulometric cells used here were associated with high back-pressure and clogging, resulting in leakages in the system and breaking of the gas tight syringes, stalling experiments. Instead of using a micron filter that was connected to cell, to prevent fouling and clogging of electrodes, the solutions were filtered off-line before being introduced to the cell. Using the cell without the micron filter reduces back-pressure therefore leakages. Plastic syringes were used versus gas tight glass syringes. Although using gas tight, glass syringes sounds convenient, under compressive stress glass syringes were easily breaking as opposed to plastic syringes that would yield and bend. Thus high flow rates above 50 $\mu\text{L}/\text{min}$ resulted in high back pressure, subsequent breaking and leaking. These parameters were optimized during this phase. Optimum flow rates were found to lie below 40 $\mu\text{L}/\text{min}$. The syringe pump on the Orbitrap could only be used with flow rate of 10 $\mu\text{L}/\text{min}$ thus reducing the pressure. Despite the limitation imposed by flow injection, lower flow rates resulted in higher conversion of analytes into metabolites, due to the extended residence time in the cell. Effect of residence and ageing times of analytes in the cell were also determined during optimization stage.

2.3.3 Results and discussion from optimization

Figure 2.9 shows the mass spectrum obtained from oxidation of APAP at 650 mV vs Pd/H₂ solid state reference electrode and its reaction with GSH. The most dominant peaks at m/z 152 is due to acetaminophen [M+H⁺] and m/z 308 is GSH [M+H⁺]. The next largest peak at m/z 615 was generated by GSH disulfide (GSSG). Shayani-Jam and co-workers suggested that (N-acetyl-p-benzoquinone imine) NAPQI has a catalytic role in which it reacts with GSH rather than in formation of the APAP-GSH adduct as reported in previous publications, thus the process mimic phase I and phase II drug metabolism.^{48,81} They proposed that this reaction will result in oxidation of GSH to glutathione disulfide (GSSG) while reducing NAPQI to APAP again, without formation of the adducts as shown in Figure 2.10 implying the adduct is not the major product. This suggestion appears to agree with the low yield of adduct that was experimentally observed during the electrochemical oxidation of APAP.

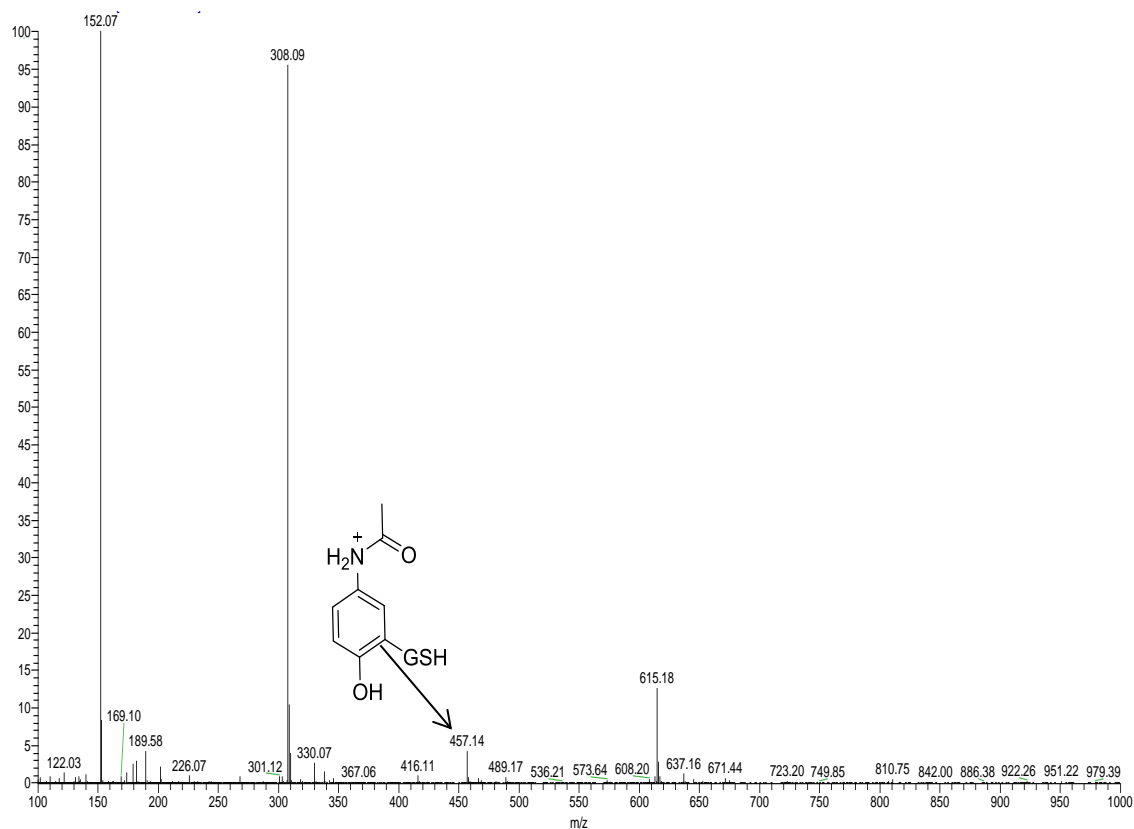


Figure 2.9: ESI (+) mass spectrum of APAP and GSH mixture, after APAP oxidation at 650mv vs Pd/H₂.

Interestingly, the mass spectrum obtained, resulting from coupling the electrochemical cell to a high resolution and high mass accuracy orbitrap had both adduct and GSSG dimer, albeit in low concentrations. This shows that these two methods are synergistic and complementary to each other. It is important to note that the GSH was not incubated with analyte that was passed through the cell. If it was passed through the cell it would have been oxidized to give its GSSG disulfide.⁴⁸ The disulfide was instead oxidized by NAPQI, and not by electrochemical oxidation.

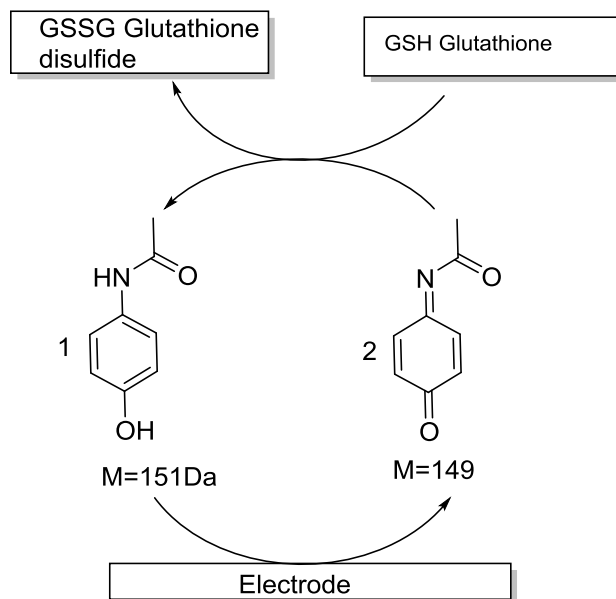
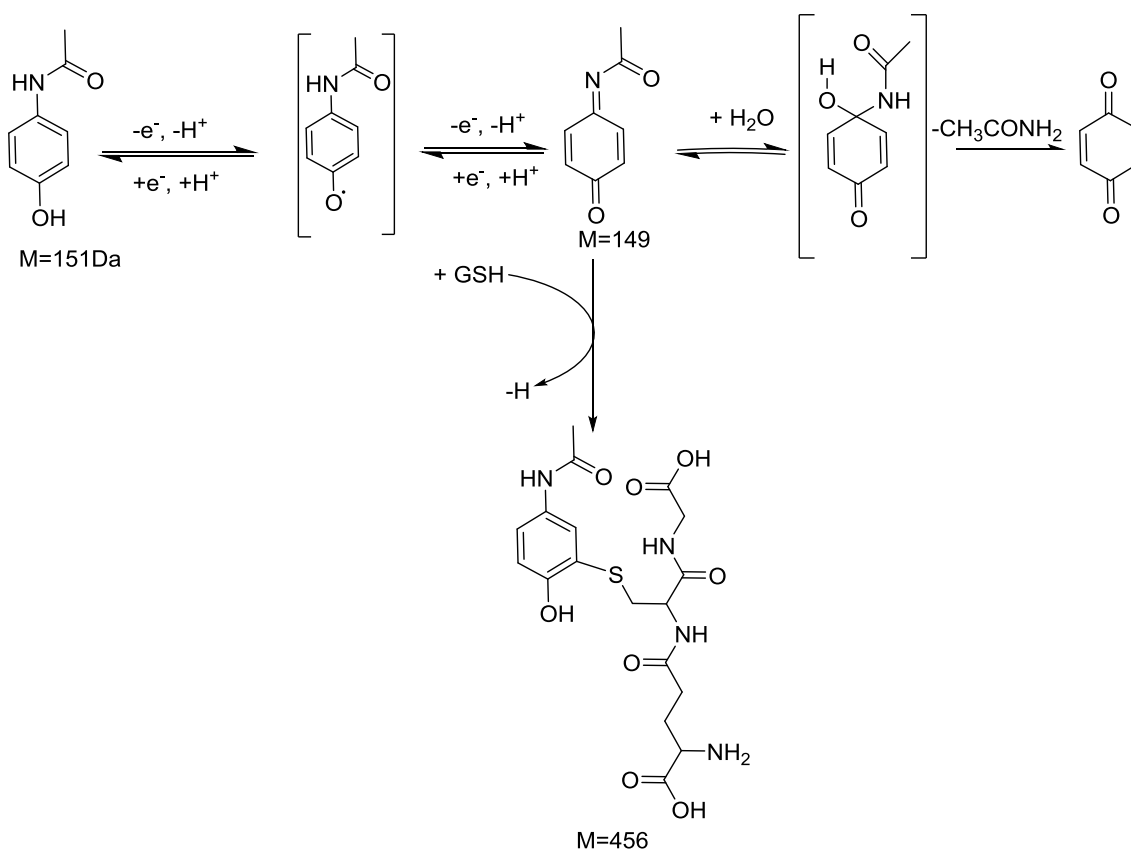


Figure 2.10 Cyclic voltammetry, catalytic oxidation of GSH to GSSG and subsequent reduction of NAPQI to APAP.⁸²

It turns out that reactive metabolites are not usually produced in large quantities; however their binding to macro cellular molecules has large impact in ADRs. These results clearly show that in addition to the GSSG, there is formation of APAP-GSH, [M+GSH+H⁺] adduct shown with m/z 457. Due to the nature of their reactivity and low concentrations, these electrophilic metabolites are difficult to detect and are often suppressed during detection of endogenous materials. The LTQ Orbitrap has an advantage of high resolution and has high mass accuracy detection allowing assessment of the exact nature of the modification that took place on the parent compound. The conjugate and disulfide were identified based on their accurate mass data, with deviations of less than 4 ppm. Due to this high sensitivity; low metabolite concentrations can be

detected using EC coupled to high resolution MS. Physiological processes are such that, the reactive metabolites are quickly detoxified; thus they will only be available in very small quantities and therefore will be difficult to detect.



Scheme 2.1: Reaction scheme for the oxidation of APAP in the presence of GSH.⁴⁸

A well-known established electrochemical reaction pathway for oxidation of APAP is a 2 electron oxidation process that is initiated by the loss of single electron and proton, resulting in formation of a radical,^{48,81} as shown in Scheme 2.1 above. This will be followed by another electron and proton loss to give the reactive NAPQI. In the presence of thiol-containing molecules such as glutathione or n-acetyl-cysteine, it will form adducts such as the APAP-GSH adduct appearing at $m/z = 457$. *In vivo*, APAP is metabolized and excreted as the nontoxic conjugates of the phase II glucuronidation reaction. However, during an overdose it saturates all the detoxification conjugation pathways and depletes intracellular reduced glutathione (GSH), hence the reactive metabolites will instead react with cellular proteins binding covalently and irreversibly (haptentation) resulting in cellular necrosis or subsequent liver-induced injury.

CHAPTER THREE

Electrochemistry-Coupled to Mass Spectrometry in Oxidation of Methimazole:

3.1 Introduction

Methimazole, an antithyroid drug used in the treatment of hyperthyroidism, has been associated with idiosyncratic toxicity, characterized by skin reactions, leucopenia, agranulocytosis, aplastic anemia, hepatitis and cholestasis.^{85,86} The relationship between idiosyncratic adverse reactions and reactive metabolites is not well established. There is circumstantial evidence, however, that reactive metabolites generated during oxidation of methimazole are involved in the onset of idiosyncratic adverse reactions associated with MMI.^{87,88} We set out to investigate formation of any unexpected or reactive intermediates/ metabolites from MMI. These metabolites are electrophilic in nature, thus reactive, and have the capacity to bind to nucleophilic cellular macromolecules which can then elicit an immune response. A range of metabolites have been suggested from biological oxidation of MMI. MMI metabolism is thought to occur through a P450-mediated process resulting in ring scission, with further S-oxidation mediated through FMO to produce the tandem of sulfenic and sulfinic acids.⁸⁹ However, some sources reported that FMO sequentially monooxygenates intact methimazole to produce unstable methimazole sulfenic and sulfinic acids without ring scission.⁹⁰

The objective of this study was to use electrochemistry and mass-spectrometry to mimic oxidative metabolism in order to generate and characterize intermediates and products using electrospray ionization. Various electrochemical methods using modified

electrodes to enhance catalytic oxidation of MMI have been developed and used for the determination of MMI at sub-micromolar detection limits using cyclic voltammetry.⁹¹⁻⁹³ While most of these studies were focusing on detection and determination of MMI using electrochemical techniques, our study is designed to explore metabolic fate of MMI. Members of the cytochromes P450 class (CYP450) of enzymes are responsible for the majority of phase I biotransformations leading to reactive electrophilic intermediates.⁹⁴ The chemical reactivity of electrophilic metabolites usually prevents their detection *in vivo* since, by definition, they are short-lived and likely to undergo one or more structural modifications to form more stable final products. Electrochemical oxidation of thiol compounds such MMI is complicated by large anodic over potential and poor voltammetric signals. In the coulometric cell used in this study, the eluent flows through the electrodes rather than by the electrodes as in convectional cells. This maximizes the contact of the electro-active compound in solution with the electrode surface, ensuring that diffusion and convection controlled process do not limit the electrochemical oxidation of the compound.⁹⁵

3.2 RESULTS AND DISCUSSION

3.2.1 Electrochemical Oxidation in basic medium

Technical limitations with respect to the spectrometer cavity could not allow for a faster flow rate of more than 10 μL per minute. Figure 3.1 shows the on-line negative mode ESI spectrum obtained, at 5 μL per minute. The residence time of the substrate in the oxidation chamber was generally long enough for full oxidation of MMI to its full oxidation products of the sulfonic acid at 600 mV. The reaction could be slowed down by running the oxidation in basic environments.

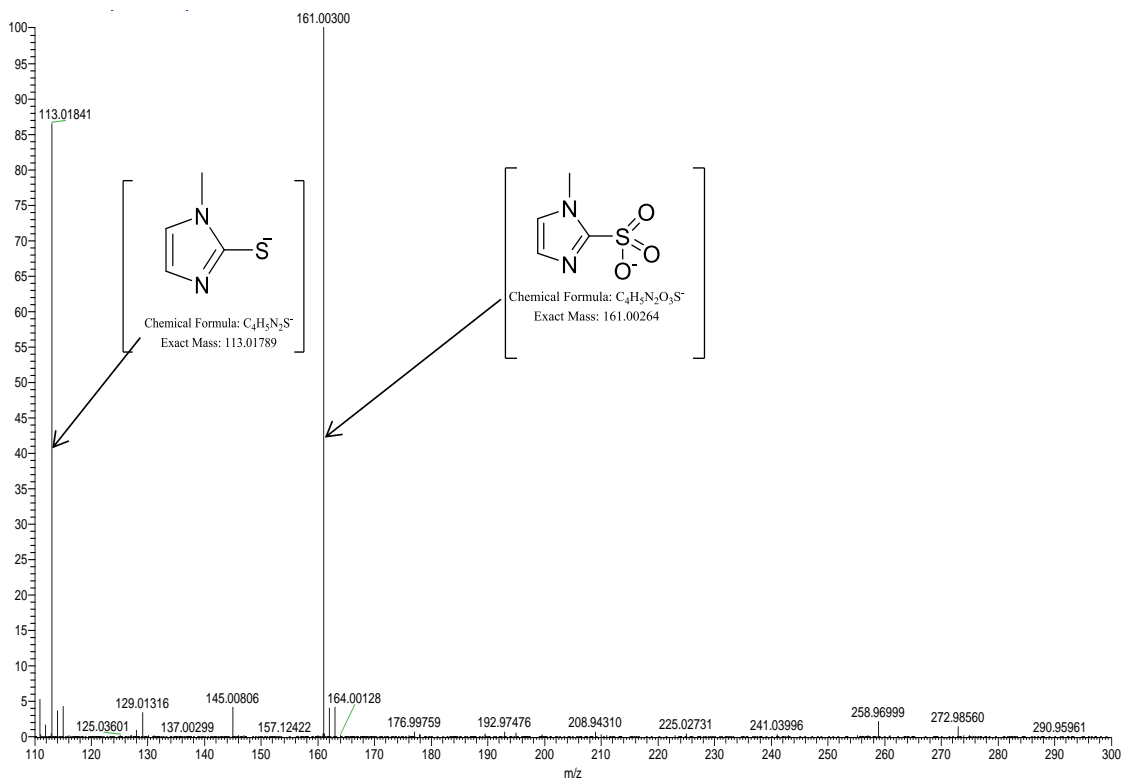


Figure 3.1: On-line negative mode ESI-MS analysis of methimazole oxidized in ammonium buffer. MMI was infused at 5 $\mu\text{L}/\text{minute}$. At this low flow rate the substrate has sufficient residence time in the cell allowing complete oxidation to sulfonic acid.

This spectrum shows a strong peak of the sulfonic acid at $m/z = 161.003$ and another for the unoxidized substrate, MMI at $m/z = 113.01$. In-between, there are smaller peaks at $m/z = 129.01$ and 145.01 . These ramp to the sulfonic acid, $m/z = 161.003$ by jumps of 16 amu's signifying these are putative the sulfenic (or S-oxide) and sulfinic acids (the dioxide). The relative abundances of the peaks indicate that the sulfenic and sulfinic acid derivatives are relatively unstable. The rate determining step for the oxidation of MMI is the formation of the S-oxide.

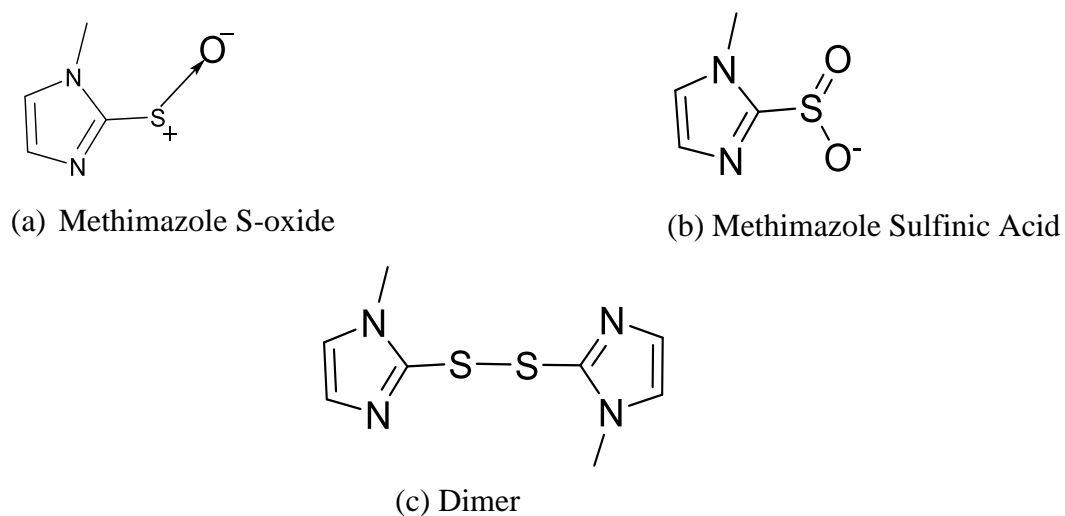


Figure 3.2: Putative metabolites from oxidation of MMI

Subsequent oxidation (after the first 2-electron oxidation) of the S-oxide is facile, hence the relative low abundance of these metabolites. Structures of the S-oxide and sulfonic acid metabolites are shown in Figures 3.2 a and b, respectively.

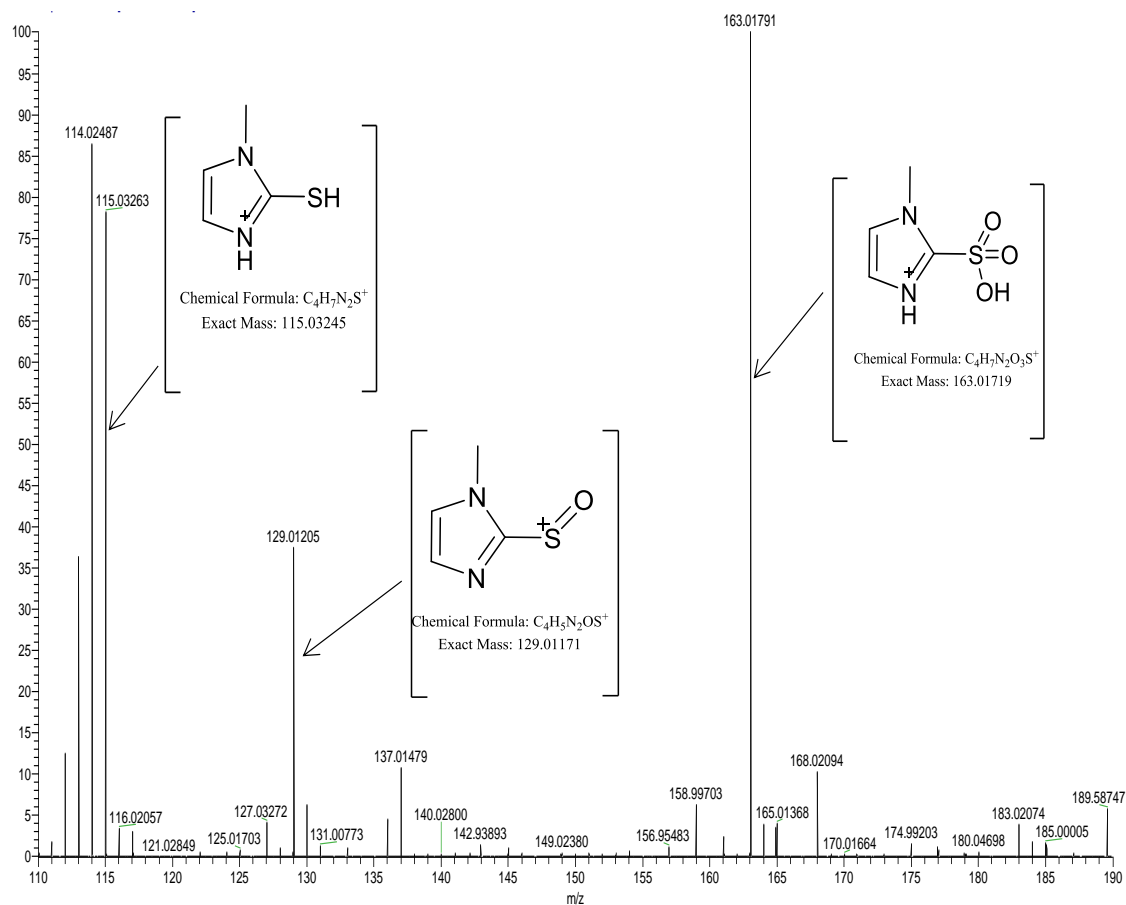


Figure 3.3: Positive mode. On-line ESI spectrum acquired in basic medium. This spectrum shows strong peaks for the dimer ($m/z = 114.025$, not labeled), the sulfenic acid, and the sulfonic acid. The sulfinic acid is not observed under these conditions.

Figure 3.3 shows spectra derived from on-line spectra in the positive mode. As expected, the substrate now shows up at $m/z = 115.03$. There is, surprisingly, a very

strong peak for the S-oxide at 129.01. There is virtually no evidence for the sulfinic acid. The major metabolite, before full oxidation to the sulfonic acid, is the doubly charged dimer, at $m/z = 114.025$ (Figure 3.2c). A slow oxidation rate will allow the electrophilic S-oxide to react with the thiol substrate in a condensation-type reaction to produce the dimer. Dimeric disulfides are not as reactive as the original thiols, and thus they accumulate. Their further oxidation rates back through the sulfenic acid are relatively slower.

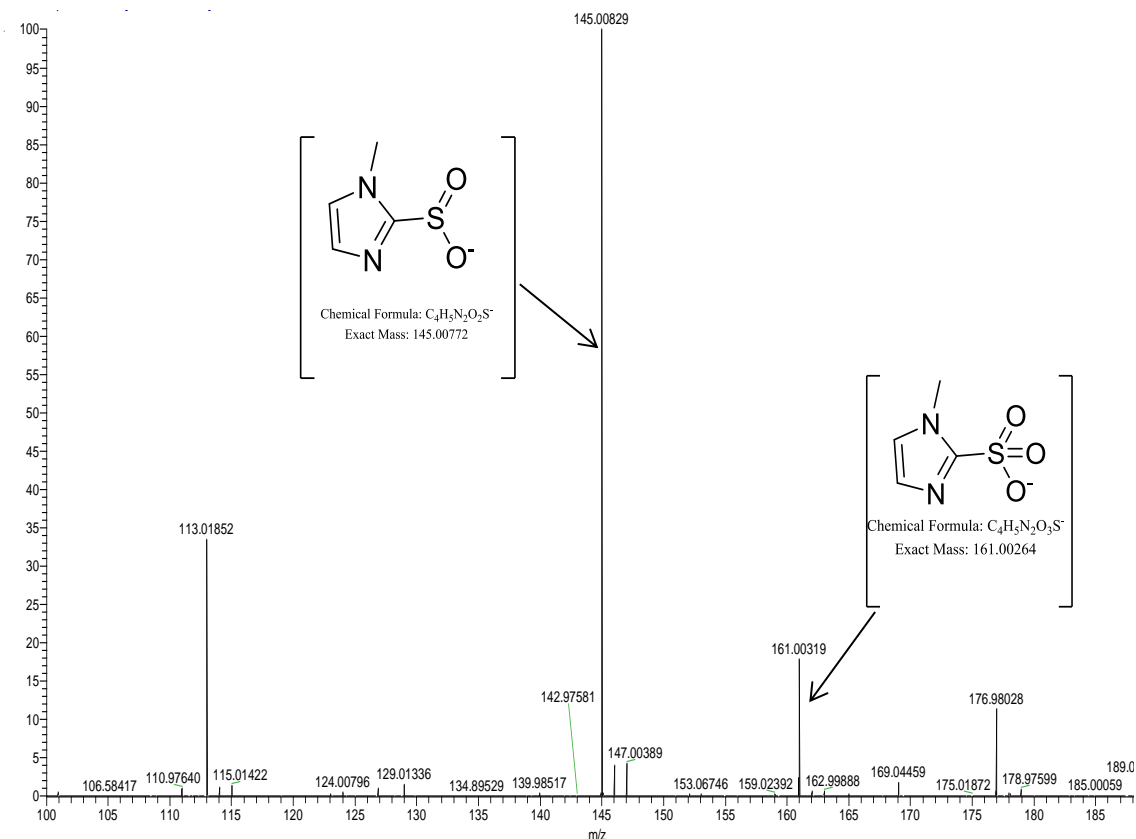


Figure 3.4. Negative mode. Off-line synthesis and analysis of MMI oxidation products. The products were identified with a mass accuracy of 3.93 ppm and 3.43 ppm, absolute values, for the methimazole sulfinic acid and Methimazole sulfonic acid respectively.

Figure 3.4 shows the batch off-line experimental spectra. Incubation period was long enough for the near-full completion of the reaction. Since this is a batch environment, with no outflow of unreacted metabolites, facile reactions were able to react to completion. In contrast, negligible amounts of S-oxide are observed; the major metabolite is the dioxide, methimazole sulfinic acid. Since the batch environment is constantly in an oxidizing environment, the highly labile sulfenic acid is not observed.

3.2.2 Electrochemical oxidation in acidic media and neutral medium.

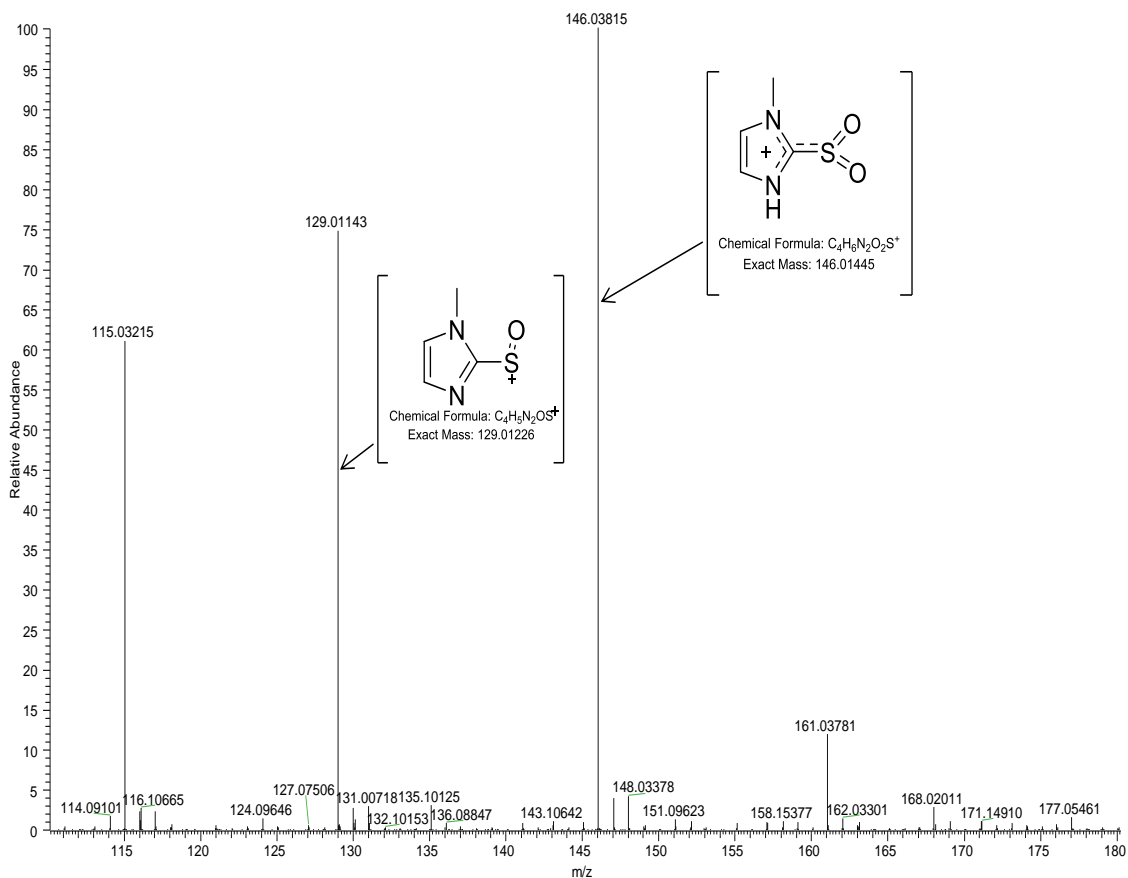


Figure 3.5. Off-line Positive mode. ESI spectrum showing the oxides of Methimazole at pH 6.75

The positive mode results of the batch process are shown in Figure 3.5. Basic environments destabilize electrophilic intermediates. However acidic and slightly acidic environments stabilize them. Thus, in Figure 3.5, the S-oxide is observed, as well as the sulfinic acid. The scale excludes the dimer. The Methimazole dimer was the predominant product in acidic medium (Figure 3.8 page 47, structure M4). Figure 3.6 shows strong peaks for the singly charged dimer at $m/z = 227.04$ and the doubly charged species at $m/z = 114.03$.

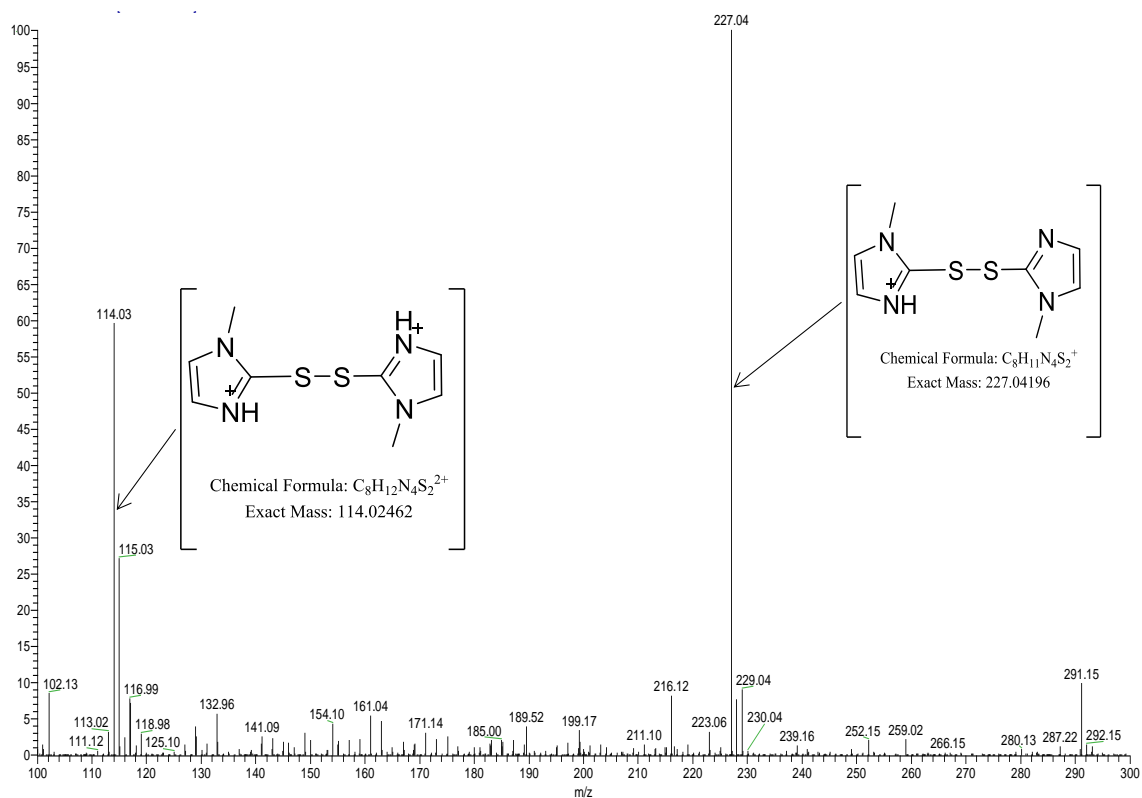


Figure 3.6. Positive mode ESI in acidic medium.

3.2.3 Choice of supporting electrolyte and effect of pH

Larger currents were attained in phosphate and in ammonium buffers. The same species obtained at pH 7.4 in phosphate were also obtained in more alkaline media of pH 10.2. Phosphate buffer, however, was not used for subsequent experiments. This was because phosphate buffers are non-volatile and can clog the MS inlet capillary, hence ammonium buffer was chosen as the suitable supporting electrolyte in subsequent experiments.

3.2.4. Assessment of stability, reactivity of metabolites and off-line synthesis

In order to perform off-line synthesis of intermediates, stability of the electrochemically generated species were monitored over a period of 30 h. To collect samples off-line, samples were infused at 40 $\mu\text{L}/\text{min}$, with potential maintained at 600 mV. The samples were then collected in vials with one batch kept at room temperature and the other batch kept at -20°C . Samples were analyzed by ESI-MS. Relative abundances of the intermediates at m/z 129 and 146 decreased significantly after 26 h. for both the samples that were kept frozen at -20°C and those maintained at room temperature. There was a 75 % decrease in abundance of these intermediates over this time duration. In addition, stability of MMI was also monitored and was found to be stable for prolonged periods in solution.

S-oxidation reactions *in vitro* had revealed that reactive intermediates are produced during oxidation of MMI and these can be eliminated by addition of nucleophiles such as glutathione to the reaction mixture.⁸⁹ In order to check reactivity of the intermediate species, samples were also incubated with a select set of nucleophiles. Conjugates were observed when the samples were incubated with N-acetylcysteine. Methoxylamine and glutathione, however did not form conjugates with MMI metabolites.

3.2.5 Experimental results derived from nucleophilic trapping.

Figure 3.7 shows the ESI spectrum derived from the use of N-acetylcysteine (NAC) as the trap. One strong peak is observed, of a 1:1 adduct of NAC with MMI. The experimental setup involved flowing NAC through a T-junction into the flow going into the spectrometer cavity (see Figure 2.4 schematic diagram)

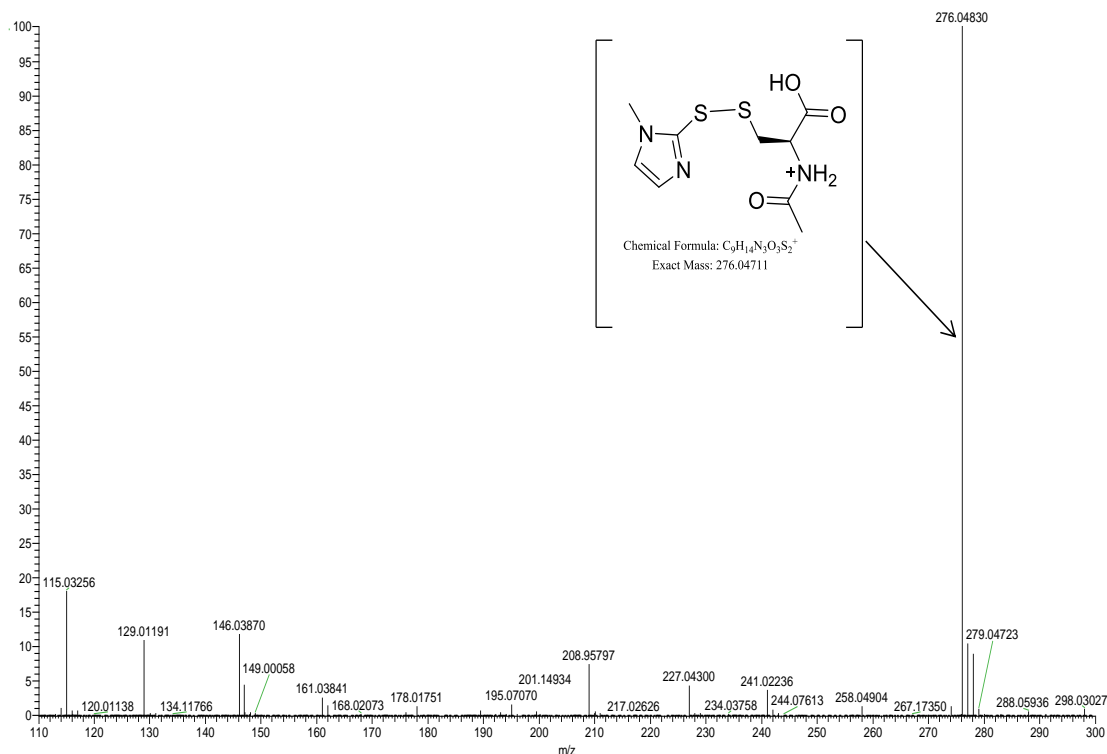
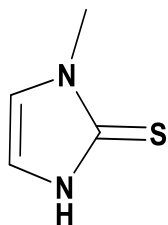


Figure 3.7 *MMI metabolite conjugate with N-acetyl cysteine. There is one dominant adduct 1:1 adduct of the N-acetylcysteine and MMI. There is a small peak for the S-oxide and an even smaller peak for the dioxide.*

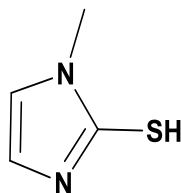
NAC was not electrochemically oxidized. It combined with the effluent from the electrochemical cell as a reducing thiol. It reacts strongly with any electrophilic species from the electrochemical cell. The absence of symmetric disulfides is important: it means no radicals are involved in this mechanism. The only electrophile present in the electrochemical oxidation cell is the S-oxide. The decrease in abundance of metabolite and formation of the conjugate strongly indicates that it is the reactive metabolite. The sulfinic and sulfonic acids are not strong electrophiles. Figure 3.7 thus shows that the

sulfenic acid is very stable in the oxidizing environment but is quickly and quantitatively deactivated in a reducing environment such as in the presence of NAC. This (reducing environment) is the expected medium in the physiological environment. The maintenance of an oxidizing environment in the electrochemical environment has allowed for the observation of those highly electrophilic intermediates that would otherwise have been quenched by the reducing physiological environment

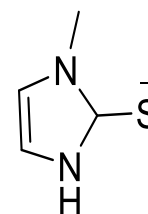
List of structures



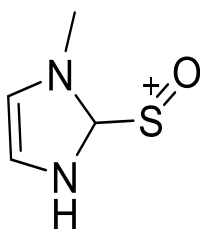
Methimazole (1-methyl-3H-imidazole-2-thione) (S1)



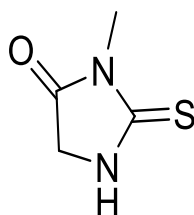
1-methyl-1H-imidazole-2-thiol (S2)



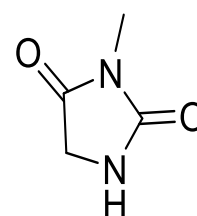
1-methyl-2,3-dihydro-1H-imidazole-2-thiolate (S3)



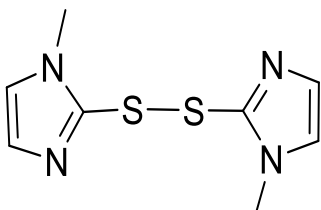
Methimazole S-oxide (M1)



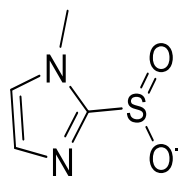
3-methyl-2-thioxoimidazolidin-4-one (M2)



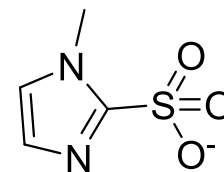
3-methylimidazolidine-2,4-dione (M3)



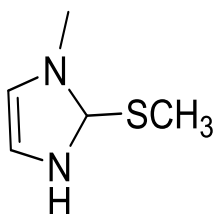
bis(1-methylimidazol-2-yl)disulfide (M4)



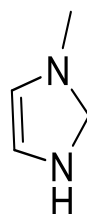
1-methyl-1H-imidazole-2-sulfinate (M5)



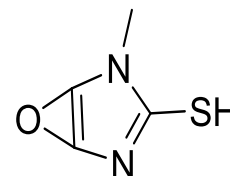
1-methyl-1H-imidazole-2-sulfonate (M6)



1-methyl-2-(methylthio)-2,3-dihydro-1H-imidazole (M7)



1-methyl-2,3-dihydro-1H-imidazole (M8)



4-methyl-6-oxa-2,4-diazabicyclo[3.1.0]hexa-1(5),2-diene-3-thiol (M9)

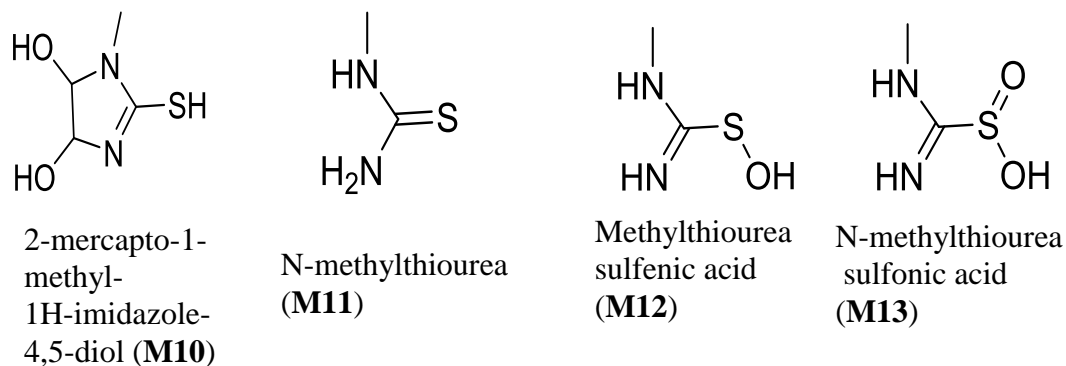


Figure 3.8 List of metabolite from MMI Those labeled with a prefix of 'S' indicate different forms of the substrate, methimazole, and those with 'M' indicate metabolites, either observed in this study or in previous studies.

3.2.6 NMR experiments

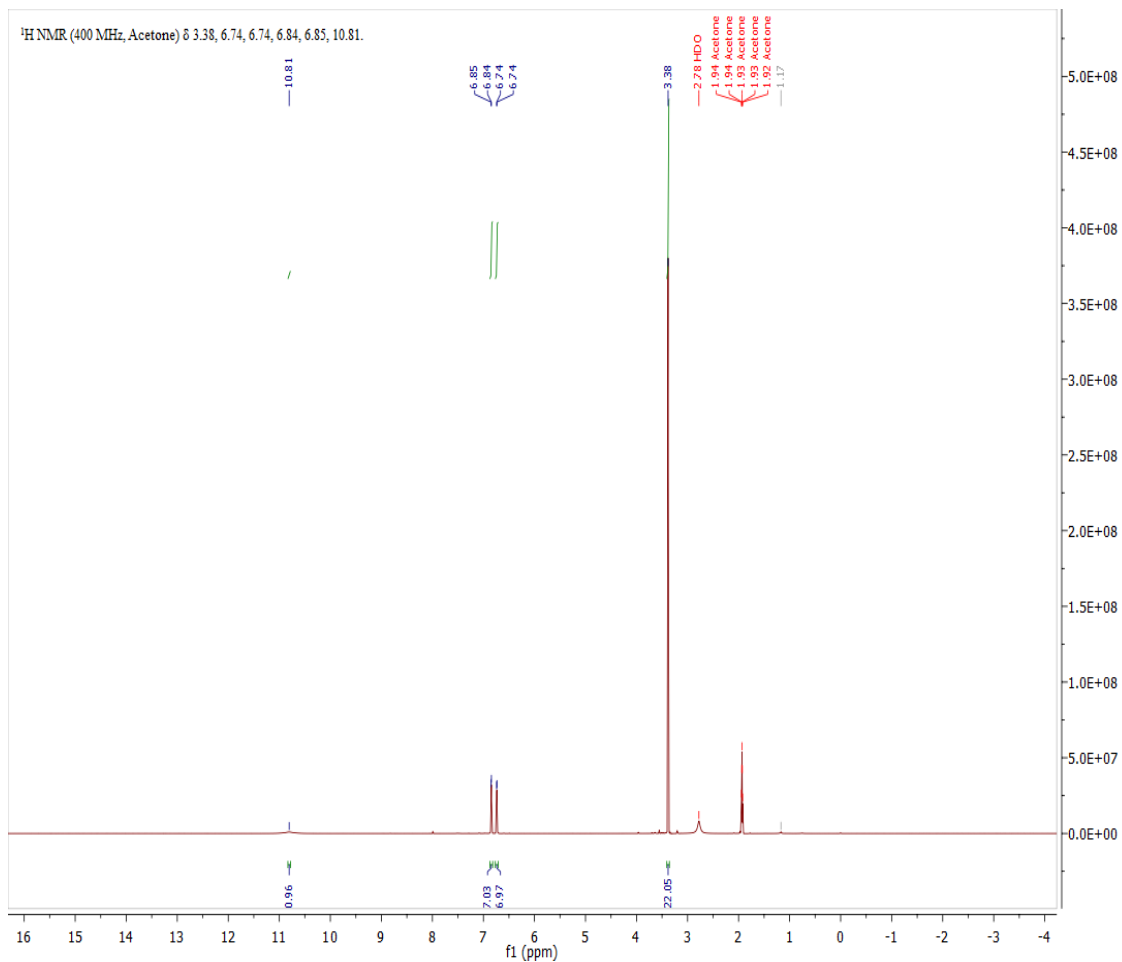


Figure 3.9: NMR spectra of the oxidized MMI products, the NMR shows the ring intact.

NMR experiments were carried out on the products/intermediates. However, stability of such intermediates is dictated by local environment, after lyophilizing and purifying the products for NMR analysis, there were changes in environment and morphology, hence no intermediates were observed. NMR results obtained showed

mostly substrate see figure 3.8 above, even after oxidation, it is as expected because the S-OH bond is unstable.

3.2.7 Mechanism.

All the data derived from electrochemical oxidations suggests a very strong case for a viable S-oxide. This has been, previously, an elusive metabolite. Very strong and stable peaks have been observed in Figures 3.3 and 3.5. Figure 3.6, though not showing a strong sulfenic acid peak, does show a peak for the dimer. This dimer is derived from a sulfenic acid (*vide supra*).

The oxidation pathway has a direct correlation with the physiological effects of MMI. The standard accepted oxidation pathway of sulfur-based drugs is through S-oxygenation, though the mechanism of this S-oxygenation differs with specific compounds based on the environment of the sulfur group. All β -amino sulfur compounds are oxidized *in vivo* and *in vitro* to as far as the sulfonic acid without cleavage of the C – S bond. Thus most biologically active molecules such as cysteine, glutathione, and cysteamine show this distinct oxidation pathway.⁹⁶⁻⁹⁸ In the presence of excess oxidant, the stoichiometry of the reaction was found to be strictly 1:3; with formation of the sulfonic acid and very little detectable sulfate by BaSO₄ precipitation:



Most deleterious effects of bioactive compounds are ascribed to the reactive metabolites produced during the first pass metabolism⁹⁹. By nature of the physiological

environment, such reactive metabolites are never observed. The first set of experiments carried out to detect possible reactive intermediates of MMI involved its reaction with aqueous bromine. This is a ‘clean’ and strong oxidant that oxidizes in 2 one-electron steps to produce only Br⁻ as its reduced product:



This affords the determination of the possible metabolites without interference from the oxidant. A 1:1 mixture of MMI and aqueous bromine imparts a 2-electron oxidation which should limit oxidation of MMI to the sulfenic acid. If the sulfenic acid is stable enough, it should be observed in the ESI spectrum. Figure 3.9 shows a spectrum of a 1:1 mixture of MMI and aqueous bromine. Even though the spectrum shows the sulfinic and sulfonic acids; the major metabolite is surprisingly, the S-oxide (Figure 3.2a, Structure M1). In the absence of the reducing physiological environment, this highly unstable, electrophilic S-oxide can be stabilized. Unstable S-oxides are known to disproportionate or to form thiosulfinates. They are also expected to react with the nucleophilic remaining thiol to produce a dimer:



Under insufficient oxidant equivalents, the substrate will partition into its most stable intermediates at those conditions. Spectrum in Figure 3.9 shows that the sulfinic acid, as expected, is not as stable as the sulfonic acid, which is the final oxidation product. This spectrum was taken after complete consumption of bromine and before full rearrangement of the sulfur compounds as evidenced by the coexistence of the S-oxide and the thiol. The spectrum obtained in Figure 3.9 was derived from unbuffered

solutions. pH of the reaction solution decreased due to formation of H^+ according to the reaction stoichiometry. Thus the m/z peak at 116.99 can be ascribed to the substrate, and the 115.03 to the dimer. After long incubation periods the substrate peak disappears completely, with a concomitant increase in the dimeric species and other unidentifiable thiosulfonates. The sulfonic and sulfinic acids still show up at the expected m/z values because of their acidity, and thus unlikely to be further protonated despite the highly acidic product environment.

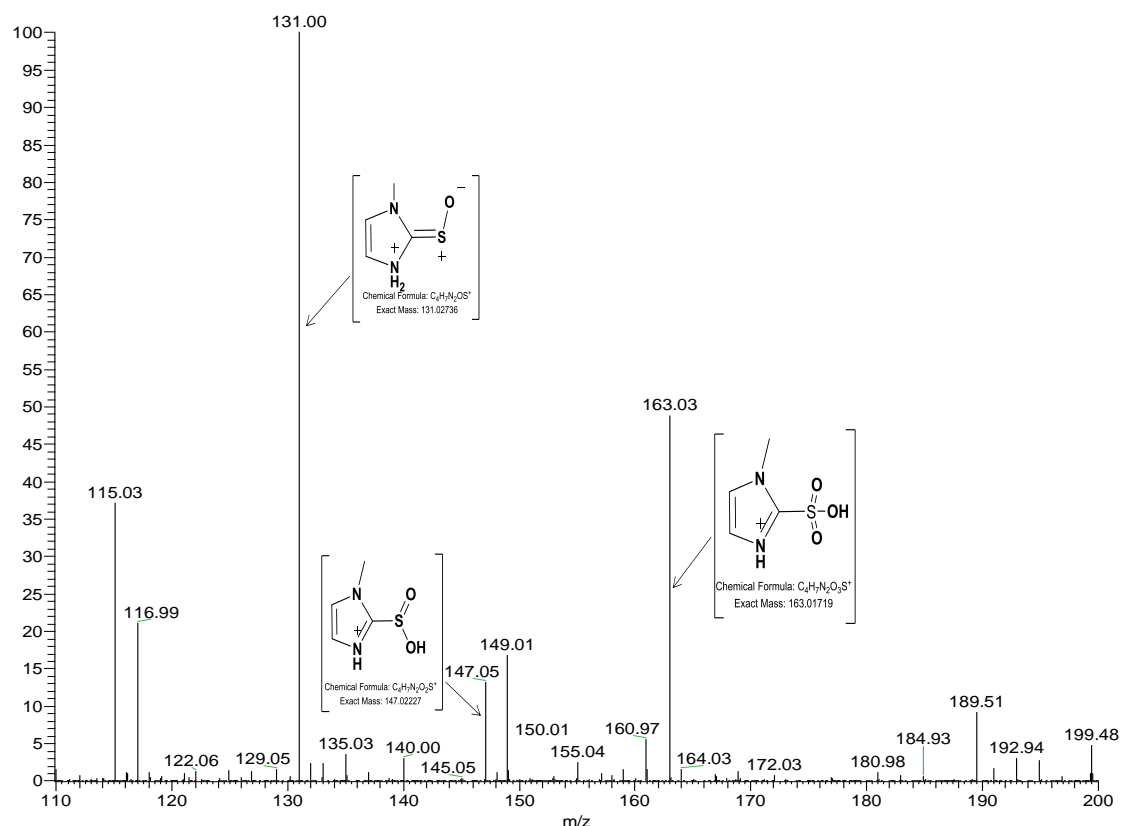
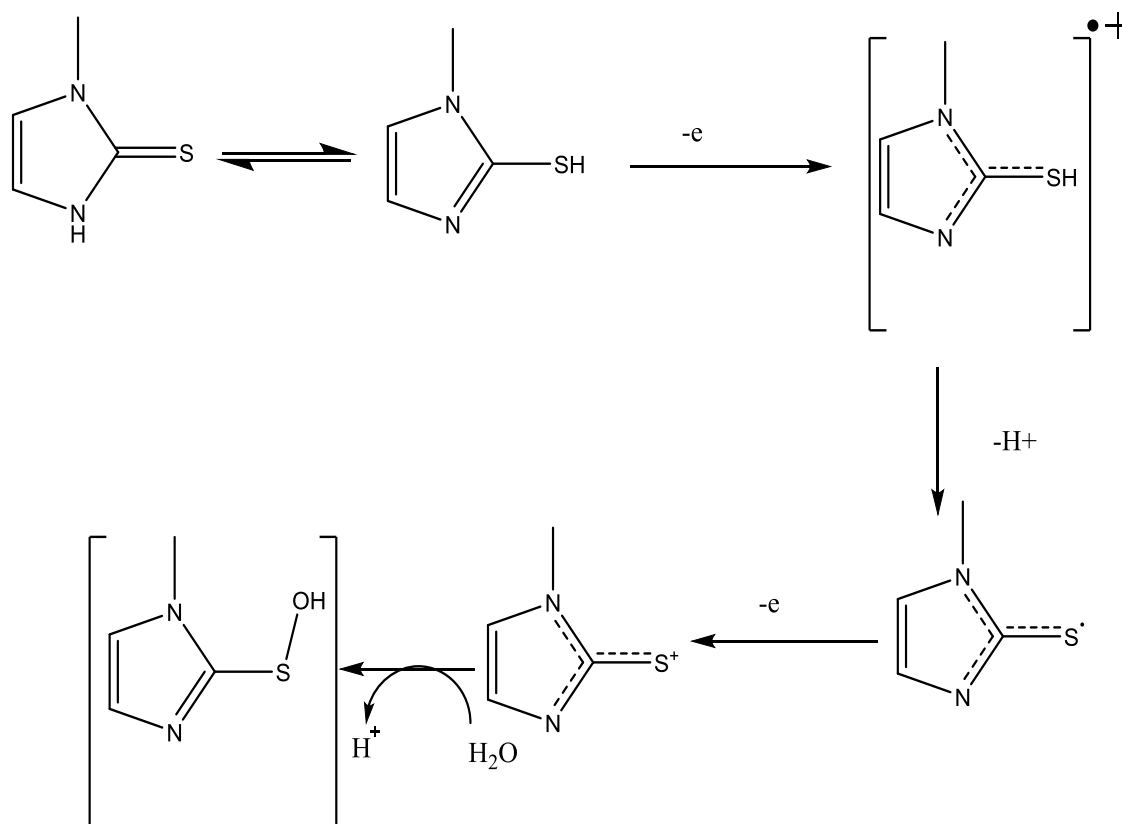


Figure 3.10: ESI spectrum of oxidation of methimazole using bromine in a 1:1 mixture ratio. As expected, the sulfinic acid is the major metabolite in these conditions of excess reductant.

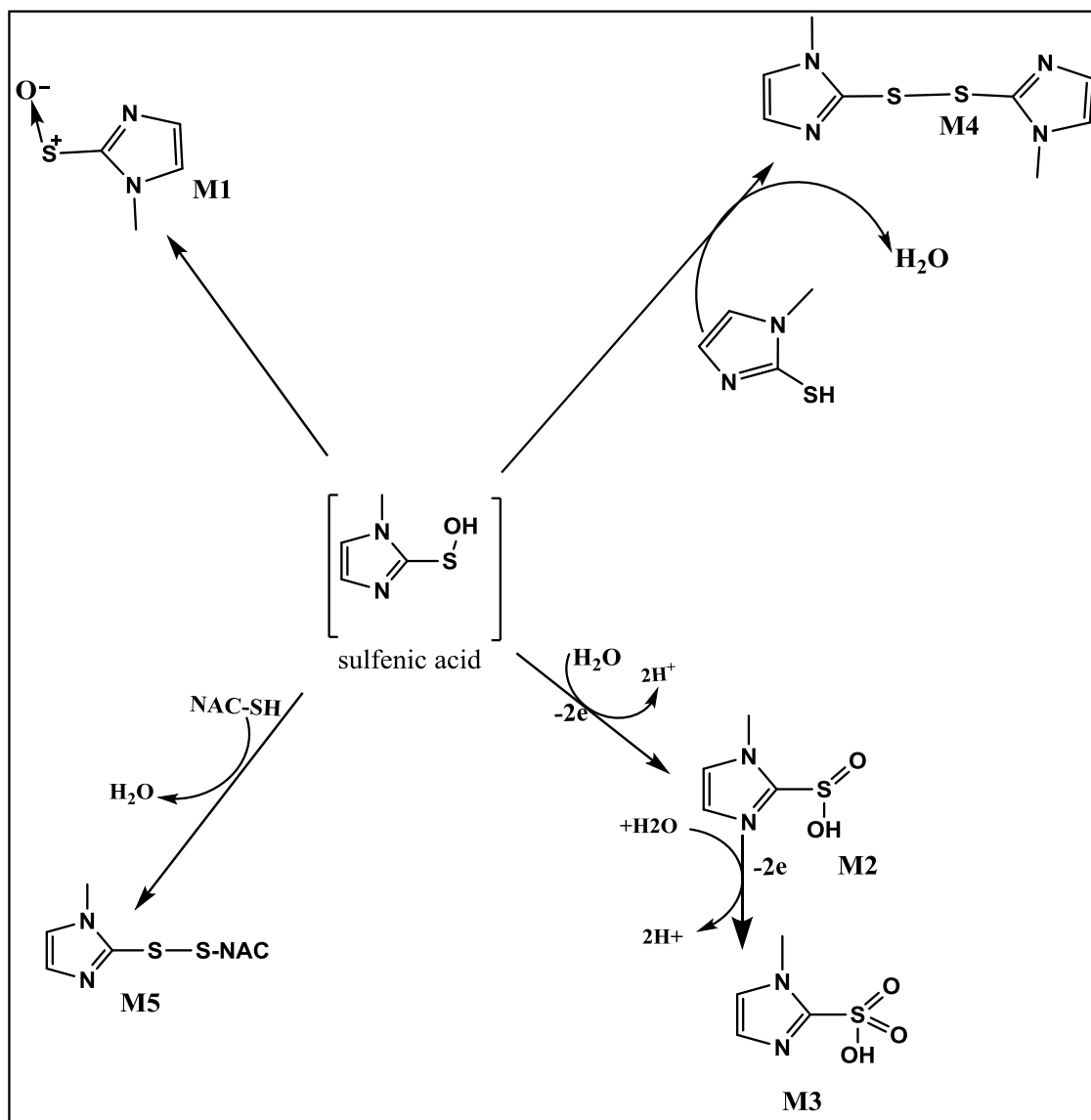
3.2.8 Proposed mechanism for electrochemical oxidation of methimazole

Our experimental results can now allow us to suggest a plausible mechanism of electrochemical oxidation of MMI. This is shown in Scheme 3.1. Electrochemical oxidation of sulfur-based drugs is complicated by the fact that sulfur centers generally oxidize via 2-electron jumps, while electrochemical abstractions generally involve a single electron transfer at a time. Starting with the thiol center would produce a sulfur-based thiyl-type radical on abstraction of the first electron. This would immediately precipitate a cascade of free radical reactions with a strong formation of the dimeric disulfide. Our results thus lead us to the conclusion that the abstraction of the first electron results in the formation of a positive charge delocalized mostly over the C-N-C network and not a sulfur-based radical. Zwitterionic forms of thioureido oxo-acids have similarly been described.¹⁰⁰



Scheme 3.1: Reaction scheme for the oxidation of MMI and subsequent formation of sulfenic acid

Scheme 3.2 below summarizes different fate of sulfenic acid. Depending on the environment, the sulfenic acid will react to give stable states. The reaction of sulfenic acid with nucleophiles such as n-acetyl cysteine may be advantageous in the physiological environment, as this is a detoxification pathway. Other pathways also leads to less reactive metabolites.



Scheme 3.2: Summary of sulfenic acid

3.2.9 Comparison with biological metabolism

Since MMI is a well-tolerated drug for hyperthyroidism, its *in vitro* and *in vivo* metabolism has been extensively studied. Human, rat and pig microsomal incubations with MMI have concluded that the major activation of MMI is performed by FMO's rather than CYP450's. Presence of FMO's however, seemed to deactivate CYP-based bioactivations, and it has since been established that MMI is a competitive inhibitor of FMO's.^{101,102} Isolation of the effect of CYP450's can be determined by heating, which deactivates FMO's or addition of N-octylamine, which inhibits FMO bioactivations. The variety of metabolites obtained which involved ring cleavage to obtain methyl thiourea and its oxo-acids (structures M11 – 13 in Figure 3.8) can be attributed to CYP450-mediated bioactivations. This can be justified through the initial epoxidation of MMI (structure M9) whose subsequent hydrolysis product of a 1,2 dihydroxy moiety can easily cleave the C-C bond by even the mildest oxidants. Thus one expects a wide variety of possible metabolism products when microsomal oxidations are utilized to metabolize MMI. The major pathway of microsomal bioactivation of MMI involves S-oxygenation, with the sulfinic acid (structure M2) as the major metabolite. While the sulfenic acid has been postulated (structure M1), microsomal incubations have never been able to isolate it; even though formation of M2 has to pass through M1. Our study has been able to isolate this formerly postulated metabolite. The deactivation of CYP450's is clearly related to formation of a highly reactive electrophilic metabolite of MMI derived from FMO's. This has been observed with the oxidation of a novel kinase

inhibitor, TG100435.^{103,104} Its bioactivation by FMO's gives an S-oxygenated S-oxide, TG100855, which not only deactivates CYP450's but is also reduced back to TG100435 during the deactivation. Thus the products, kinetics and dynamics of microsomal bioactivations are expected to be complex. Our electrochemical oxidations simplify this process. This makes evaluation of physiological effects, especially toxicities, easier to determine.

3.4 Conclusion

We have demonstrated that electrochemistry coupled to mass spectrometer can mimic oxidative metabolism of MMI, the mechanism initiated by single e- transfer process coupled to proton (H⁺) abstraction. The absence of complex endogenous material enhanced detection of an S-oxide in oxidation of MMI, this intermediate metabolite has been speculated before, but has never been isolated. The elusive sulfenic acid was captured as a conjugate with n-acetyl cysteine. Bioactivation of MMI and related molecules, to reactive metabolites has a direct physiological implication in toxicity of thionamides.

CHAPTER FOUR

Kinetics and Mechanism of Oxidation of Methimazole by Chlorite in Slightly Acidic

Media

4.1 Introduction

As indicated above, thionamides drugs, methimazole (1-methyl-3H-imidazole) MMI and 6-propyl-2-thiouracil (PTU) are two important antithyroid drugs used in treatment of hyperthyroidism and thyrotoxicosis.^{105,106} After administration, the drugs are concentrated in the thyroid gland.¹⁰⁷ Hypochlorous acid (HOCl) is the most powerful oxidant produced by human neutrophils. Peroxidases including thyroid peroxidase have been shown to contribute to oxidation of MMI, to a range of products.¹⁰⁸ Model in vitro studies, using myeloperoxidase (MPO) in H₂O₂/Cl⁻ system, show that hypohalous acids are some of potent oxidants generated during catalytic oxidation of H₂O₂ in presence of Cl⁻ or Br⁻.¹⁰⁹ Ironically MMI is an antioxidant that scavenges reactive species, and can be oxidized to potentially reactive intermediates, such as its sulfenic acid.

A number of toxicological and metabolic studies have been conducted in an attempt to identify possible reactive intermediates associated with the antithyroid drugs.¹¹⁰ Whereas there is a general consensus on the ultimate products of oxidation of MMI, as sulfate and N-methyl-imidazole,¹¹¹ there has not been a clear identification of possible intermediates. Other metabolites suggested from previous research include S-methyl imidazole, 1-methyl-2-thiohydantoic acid, methylhadantoin and methylthiourea.¹¹² However, lack of toxic profiles by most of these metabolites could not

explain the trend in observed adverse reactions associated with MMI. Here a system that employs potent oxidants hypohalous acids; HClO and HBrO which were generated in situ were used to study the rapid kinetics and mechanism of reaction of MMI oxidation. With mild oxidants such as bromine, a stable S-oxide was observed. However, in acidified chlorite the reaction was very fast and the resulting in the unstable intermediate that was short lived and was not observed in ESI.

4.2 Results and discussion

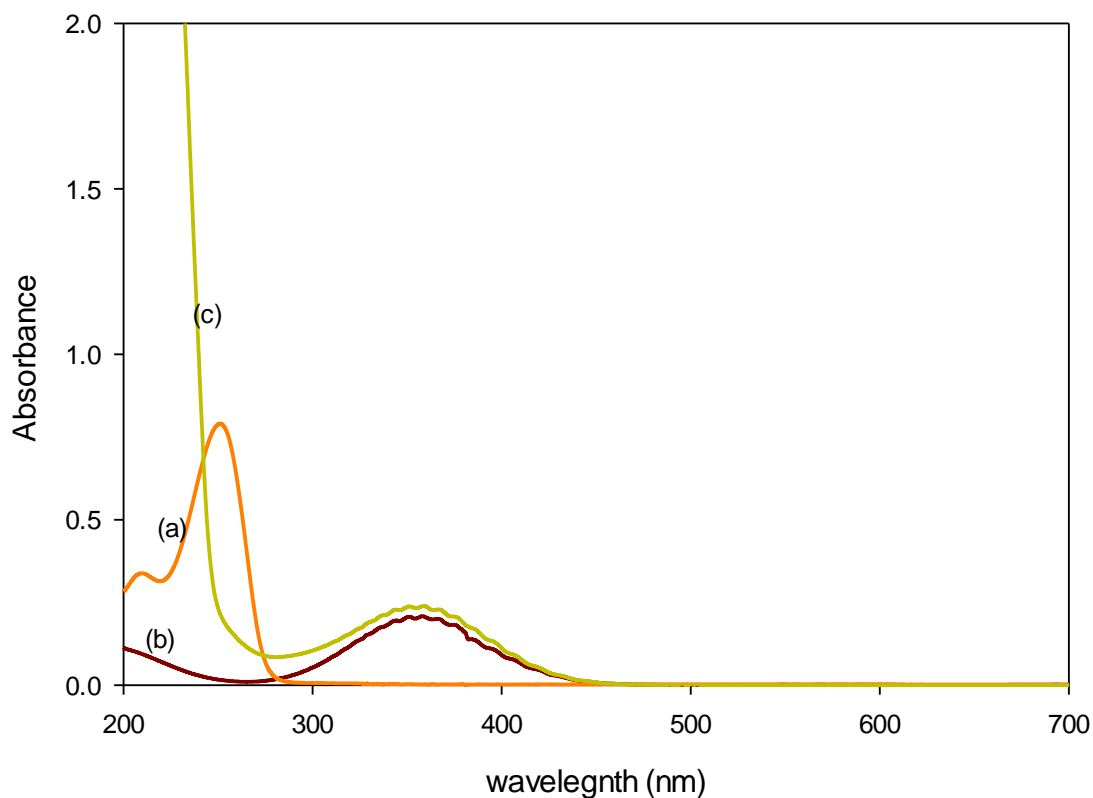


Figure 4.1. Spectral scans showing (a) $[MMI] = 1.00 \times 10^{-5} M$, (b) $ClO_2 = 1.70 \times 10^{-4} M$ and (c) product of reaction $[MMI] = 3.00 \times 10^{-4}$, $[ClO_2^-] = 3.00 \times 10^{-3}$ and $[HClO_4] = 1.00 \times 10^{-1} M$

4.2.1 Stoichiometry.

Stoichiometric determinations utilized two complementary techniques: spectrophotometric and titrimetric. The titrimetric techniques were more accurate as they relied on several readings to derive a single stoichiometry. Figure 4.2 shows a titrimetric analysis of residual oxidizing power. For the whole data set shown, MMI concentrations were fixed at 1.00 mM. Iodometric titrations gave the expected linear plot which extrapolated to 2.0 mM chlorite concentrations, showing complete consumption of 1.0 mM MMI. Each chlorite molecule gains 4 electrons to attain the Cl^- state. This suggests that the only oxidation on the MMI molecule occurs on the sulfur center which is oxidized from -2 to +6. Tests with barium chloride showed an almost quantitative formation of sulfate as expected from MMI.

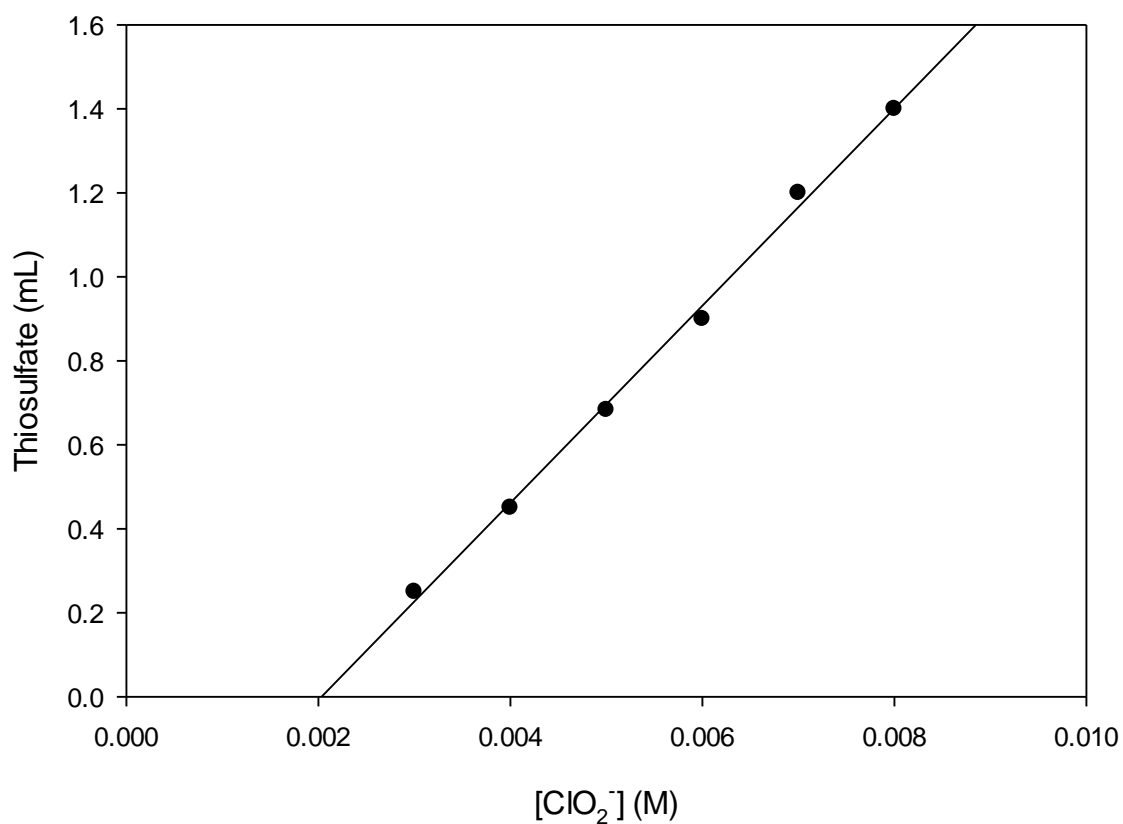


Figure 4.2. Iodometric titration to determine stoichiometry. Fixed $[MMI] = 1.00 \times 10^{-3} M$, $[H^+] = 0.20 M$, and varied $[ClO_2^-]$ from $3.00 \times 10^{-3} M$ to $8.00 \times 10^{-3} M$, X intercept = 0.002033 This suggests an oxidant to reductant stoichiometric ratio of 2:1

Despite the observed clean 2:1 stoichiometry, we could not experimentally determine the organic residue. However, the residue did not seem to involve any further oxidation, only hydrolysis and/or ring-opening. ESI spectra of the reaction were acquired in solution using slightly less than stoichiometric amounts of oxidant. Figure 4.3 shows an ESI spectrum in the positive mode. It shows, predominantly, the dimeric species at $m/z = 227.04313$ and the N-methylimidazole at $m/z = 83.0604$. N-methylimidazole would be the expected organic residue if the sulfur atom is oxidized to sulfate with a concomitant cleavage of the C-S bond. It would appear N-methylimidazole rapidly decomposes by hydrolysis to smaller fragments after ring opening.

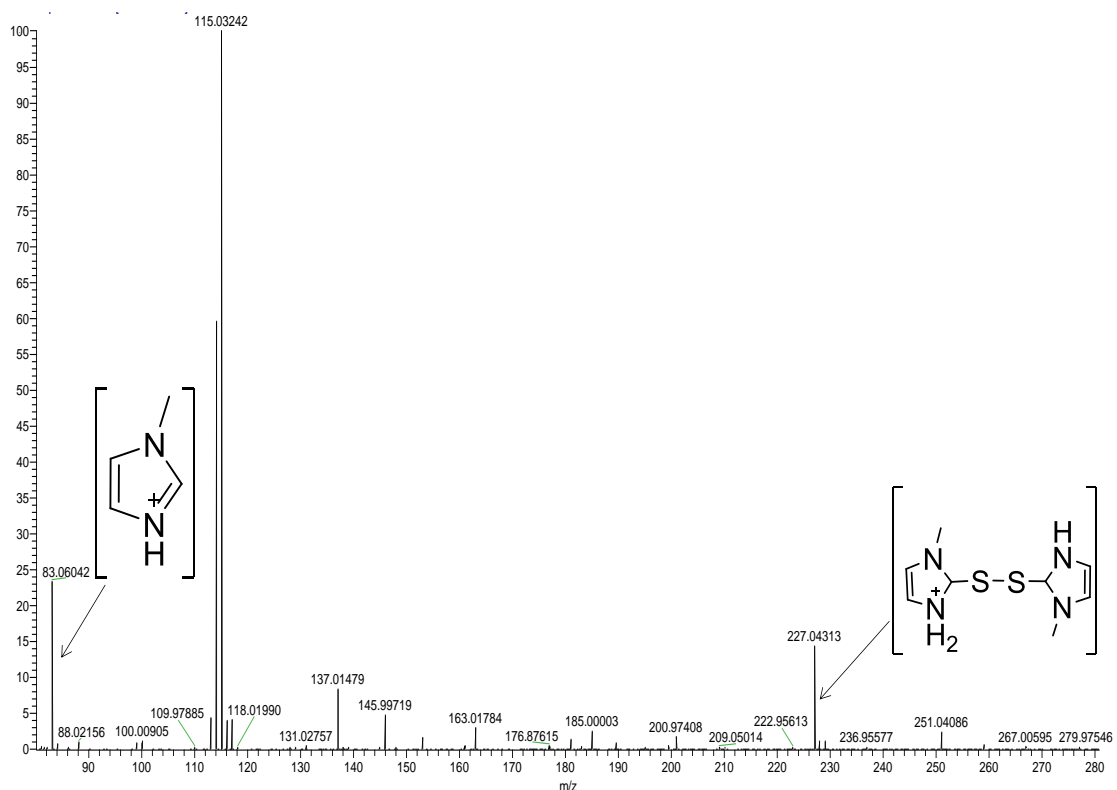


Figure 4.3: ESI spectrum in the positive mode before reaction proceeds to completion showing the predominant peak of the substrate at $m/z = 115.03242$. Two peaks for the dimeric species are observed, one at $m/z = 227.04313$. The doubly-charged dimeric species is observed as the peak just below that of the substrate. The N-methylimidazole species is at $m/z = 83.06402$.

Figure 4.4 shows the ESI spectrum of chlorite and MMI with slightly less chlorite than that needed for full oxidation of MMI. As expected, there is a predominant peak for sulfate, captured as the bisulfate at $m/z = 96.96032$. There is a large peak for the sulfonic acid of MMI at $m/z = 161.00252$. A further 2-electron oxidation of this sulfonic acid will give sulfate and N-methylimidazole. There is a very tiny peak for the sulfenic acid at 129.01273 , but, surprisingly, there is no sulfinic acid, which is supposed to be more stable than the sulfenic acid. Another stoichiometric determination was attempted for

the chlorine dioxide – methimazole reaction. From the radical nature of chlorine dioxide, the stoichiometry could not be determined with certainty. From electron balance alone, we were expecting an 8:5 ratio, oxidant to reductant, but this was never obtained. We can, however, write the following general equation for the oxidation of MMI by chlorite:

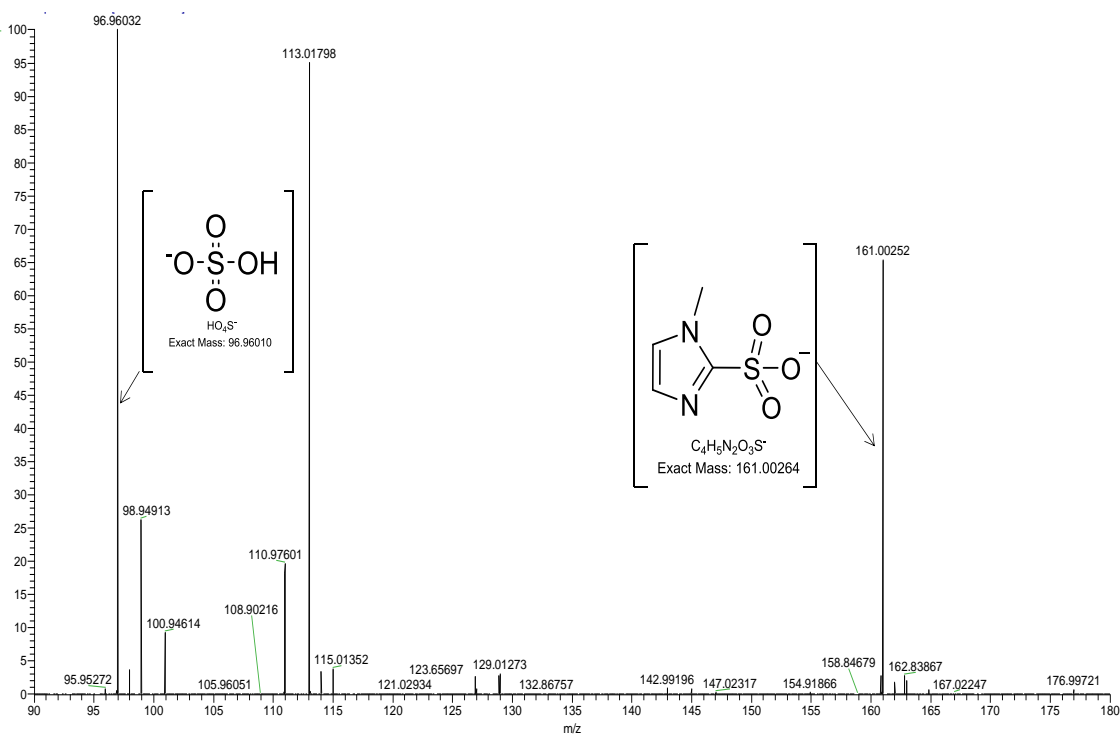


Figure 4.4: ESI spectrum in the negative mode. Sulfate is the dominant product, as expected, at $m/z = 96.96032$. The sulfonic acid can be seen at $m/z = 161.00252$. The substrate can still be seen at 113.01798 .

4.3 Reaction Kinetics.

Figure 4.5 shows rapid kinetics scans of the reaction mixture which shows activity at 260 nm and 360 nm. The peak at 260 is consistently decreasing peak at 260, This peak which is attributed to λ_{max} for methimazole, Figure 4.1 trace (a). Another peak of importance is at 360 nm, it commences after an induction period determined by initial conditions. This peak is attributed to ClO_2 . The peak at 260 nm is at its lowest when that at 360 nm reaches its peak. Chlorine dioxide color slowly faded after prolonged standing due to its decomposition and volatility. In high acid conditions, the absorbance measured at 360 nm attained a transient peak which then slowly decreases to its final value, hinting some oligooscillatory behavior.

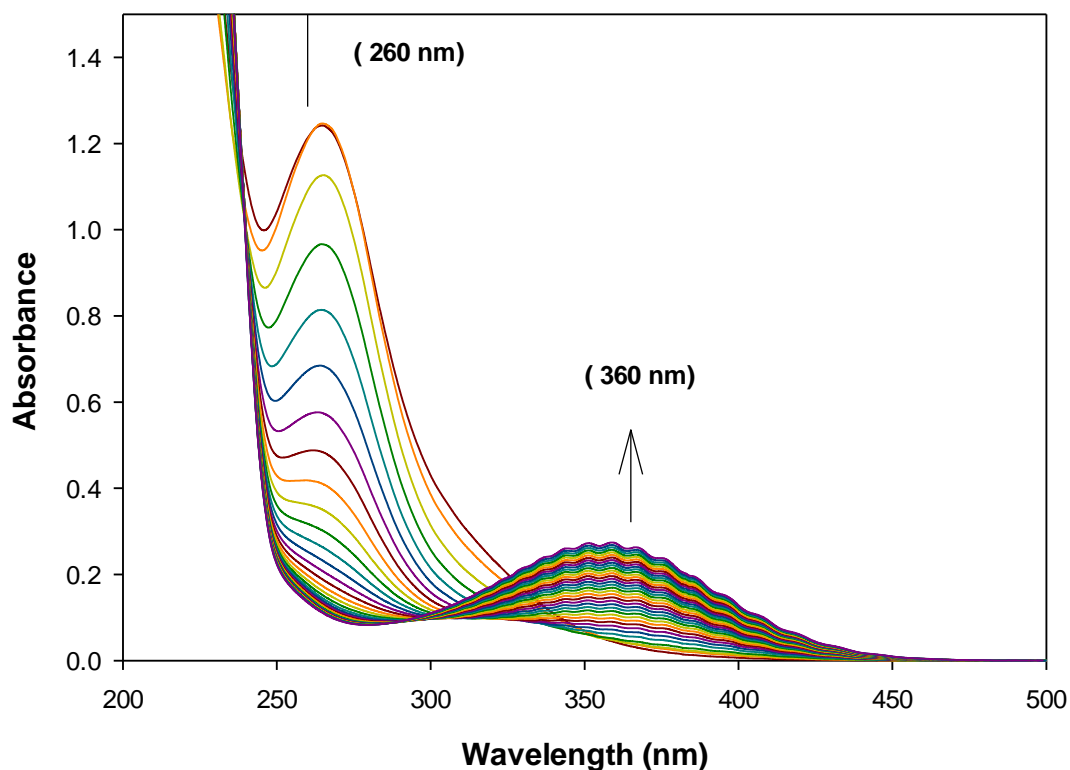


Figure 4.5: Multiple scan of MMI oxidation by chlorite in aqueous acidic medium at 60 seconds intervals. $[MMI]_0 = 3.00 \times 10^{-4} M$, $[ClO_2^-]_0 = 3.00 \times 10^{-3} M$ and $[HClO_4]_0 = 1.00 \times 10^{-1} M$

Figure 4.6 shows the effect of MMI on the chlorite-MMI reaction. Chlorine dioxide formation commences almost immediately after mixing. In all traces shown in this figure, chlorite was in stoichiometric excess over MMI, that is; the ratio was over 2:1. The transient peak in chlorine dioxide absorbance is attained within 2 seconds. If this reaction is monitored further, the chlorine dioxide will attain a minimum value which remains invariant for up to an hour. The final chlorine dioxide concentration is determined by the excess chlorite concentrations. This effectively involves the well-known disproportionation of chlorite in acidic environments.¹¹³

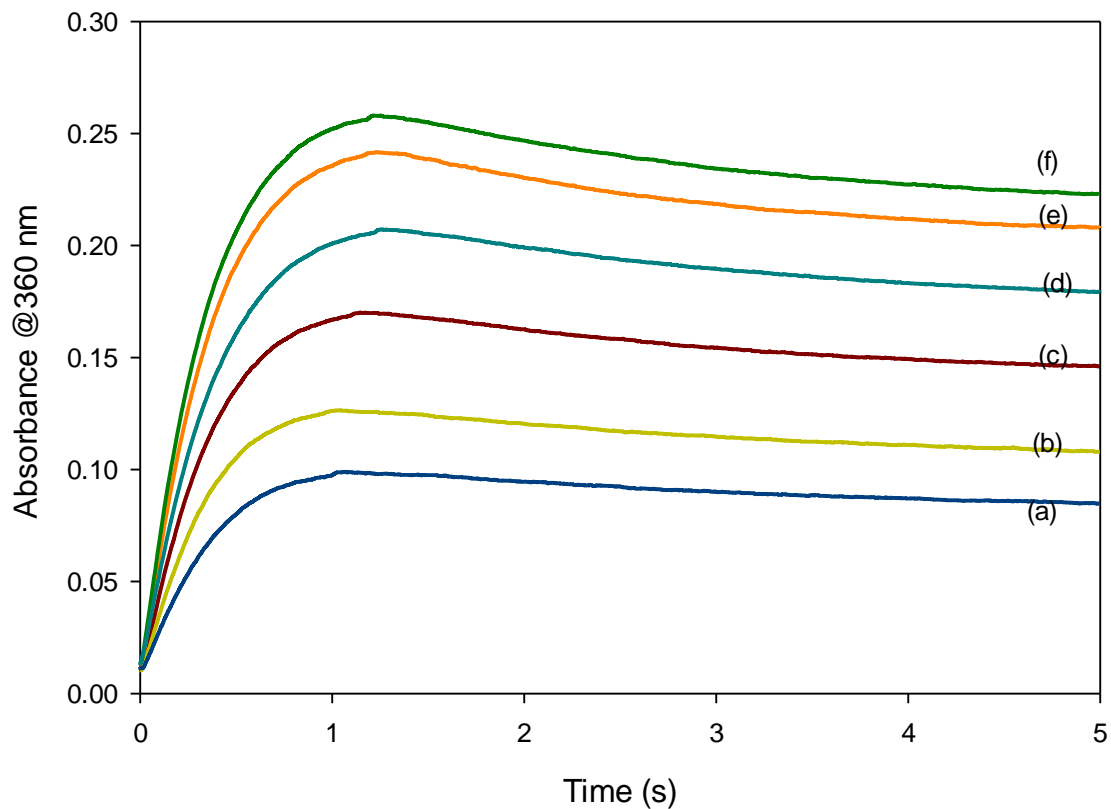
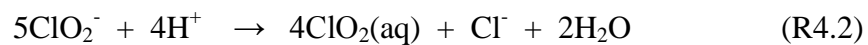


Figure 4.6. Variation of $[\text{MMI}]_o$ and its oxidation, Fixed $[\text{ClO}_2^-] = 2.50 \times 10^{-3} \text{ M}$, $[\text{H}^+] = 5.00 \times 10^{-2}$ and varied $[\text{MMI}]$ (a) $5.00 \times 10^{-4} \text{ M}$, (b) $6.00 \times 10^{-4} \text{ M}$, (c) $7.00 \times 10^{-4} \text{ M}$, (d) $8.00 \times 10^{-4} \text{ M}$ (e) $1.00 \times 10^{-1} \text{ M}$ and (f) $1.10 \times 10^{-3} \text{ M}$

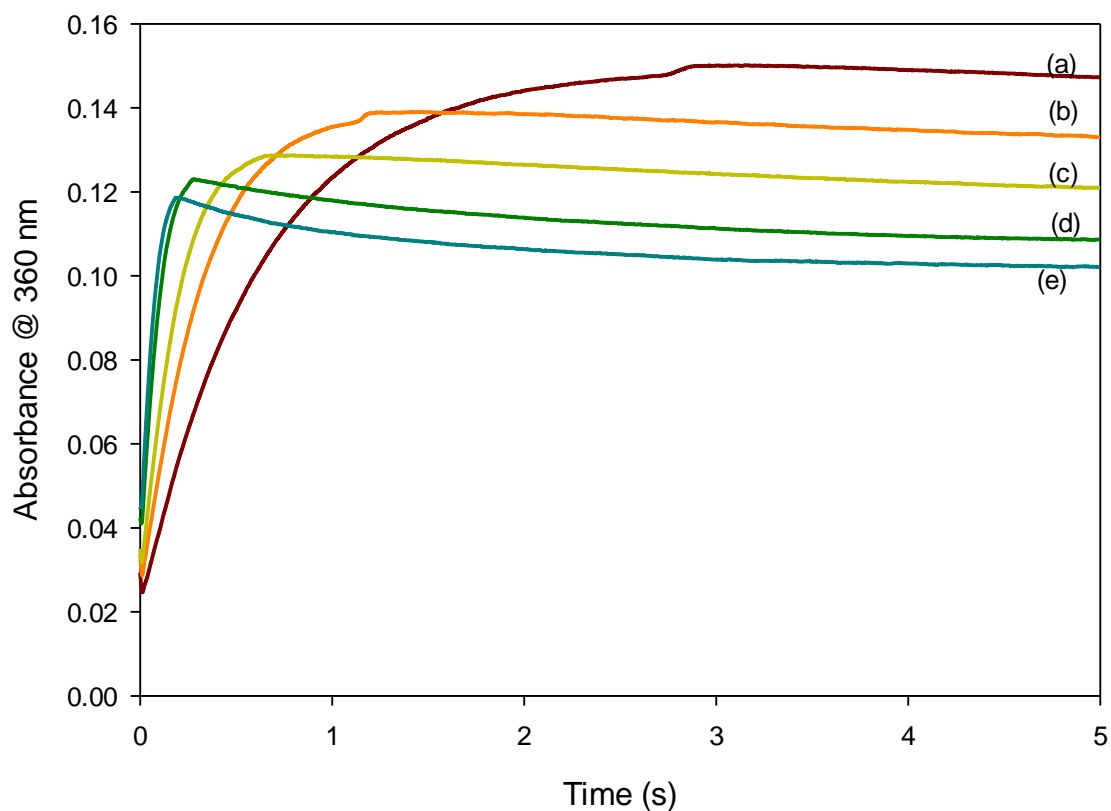


Figure 4.7. Effect of $[\text{ClO}_2^-]_o$ variation on the reaction with MMI. Fixed: $[\text{MMI}] = 1.00 \times 10^{-3} \text{ M}$, $[\text{H}^+] = 0.01 \text{ M}$ and varied $[\text{ClO}_2^-] =$ (a) $1.00 \times 10^{-2} \text{ M}$, (b) $2.00 \times 10^{-2} \text{ M}$, (c) $4.00 \times 10^{-2} \text{ M}$, (d) $6.00 \times 10^{-2} \text{ M}$ and (e) $1.00 \times 10^{-1} \text{ M}$. $I_{\text{NaClO}_4} = 1.00 \text{ M}$.

Figure 4.7 shows the variation of initial chlorite concentrations at a pH of 1.00. The reaction is much faster than those reactions run at pH 1.3 in Figure 4.6, above, and the transient peak of chlorine dioxide is attained much earlier. The peak is also much sharper. Figure 4.8 shows the complex dependence of the reaction on acid concentrations. Lower concentrations gave a monotonic increase in chlorine dioxide concentrations within the 5 seconds observation window. Higher acid concentrations gave oligooscillations. Acid catalyzed a faster initial rate of formation of chlorine

dioxide. Absorbance traces, for the range of acid concentrations studied, seemed to all converge at a specific absorbance value 1.3 seconds into the reaction. It was not possible to determine the significance of this coherence since this could not be related to an isosbestic point: nothing else absorbs at 360 nm apart from chlorine dioxide. Thus it could merely be a saturation point.

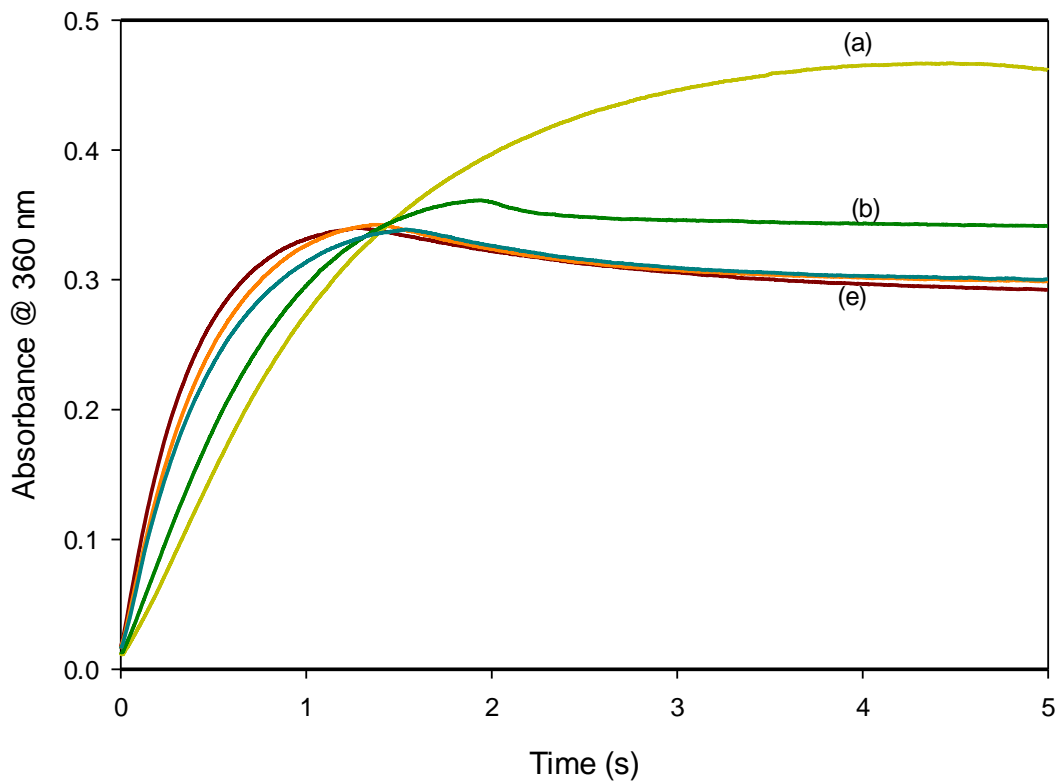


Figure 4.8. Effect of $[H^+]_o$ variation on the reaction with MMI with ClO_2^- . Fixed: $[MMI] = 1.00 \times 10^{-3} M$, $[ClO_2^-] = 2.50 \times 10^{-3} M$, varied $[H^+] =$ (a) $2.50 \times 10^{-3} M$ (b) $5.00 \times 10^{-3} M$, (c) $1.00 \times 10^{-2} M$, (d) $3.00 \times 10^{-2} M$ (e) $5.00 \times 10^{-2} M$ and $0.01 M$. $I_{NaClO_4} = 1.00 M$.

4.3.1 Chlorine dioxide-MMI reaction kinetics

The direct reaction of chlorine dioxide with MMI was also studied. With the observed oligooscillations in chlorine dioxide concentrations, it meant this reaction was directly relevant. It appears the reactions that form and consume chlorine dioxide are approximately of the same order of magnitude in rates, with the dominance of each being determined by the presence of the relevant reagents. If the chlorine dioxide – MMI reaction was much faster than the chlorite – MMI reaction, then one would observe an induction period followed by formation of chlorine dioxide, and in the opposite case, one would observe a monotonic increase in chlorine dioxide formation up to its final absorbance. However, what we see here is non-linear behavior. Figure 4.9 shows the effect of varying chlorine dioxide concentrations. Of note, traces, a to e, apart from trace f, all contain stoichiometric excess of MMI such that, at the end of the reaction, all chlorine dioxide would have been expended. The observed residual absorbance of 0.02 units is derived from the other products in the reaction mixture. Thus the reaction will appear to be rapidly shutting down due to contribution to the absorbance from the product.

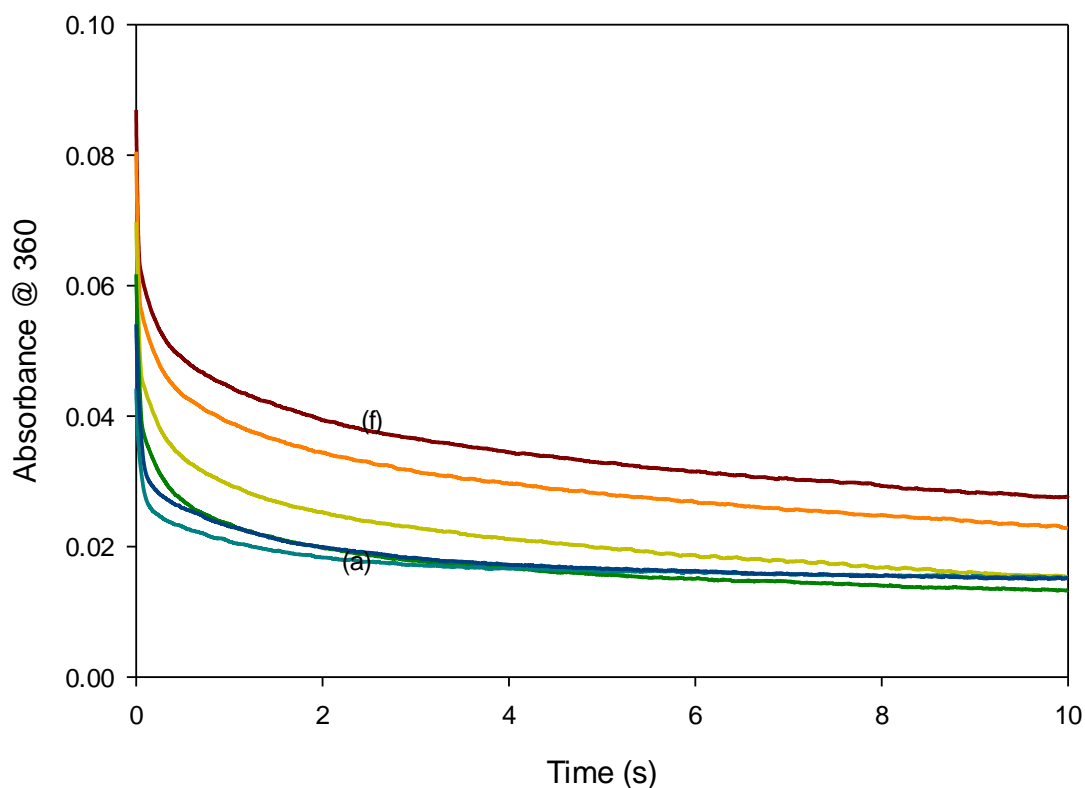
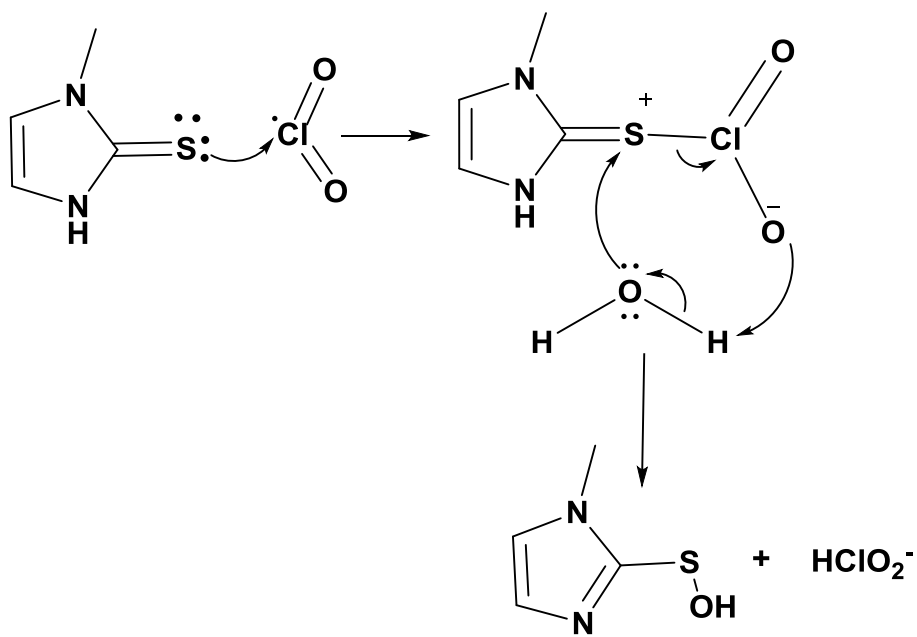


Figure 4.9. Variation of $[ClO_2]_0$ concentration and its effect on rate of reaction, Fixed $[MMI] = 5.00 \times 10^{-5} M$, and varied $[ClO_2]$ (a) $5.00 \times 10^{-5} M$, (b) $6.00 \times 10^{-5} M$, (c) $7.00 \times 10^{-5} M$, (d) $8.00 \times 10^{-5} M$ (e) $9.00 \times 10^{-5} M$ and (f) $1.00 \times 10^{-4} M$

The direct reaction of chlorine dioxide and MMI appears to be very rapid in this unbuffered environment; essentially over in 200 msec. Our stopped-flow instrument has a mixing time of 1.0 msec, and from the experimental traces observed in Figure 4.9, it appears the first electron transfer is too rapid to be observed. For example, for trace f, we expect an initial absorbance of 0.110, and our observed initial absorbance is 0.088. Thus the initial step of this reaction will involve a rapid adduct formation between the radical chlorine dioxide and the nucleophilic sulfur center of MMI, as shown below.



Scheme 4.1 Proposed MMI-Chlorite adduct formation and concomitant formation of sulfenic acid

Figure 4.10 shows the variation of MMI concentrations. MMI is in stoichiometric excess in all these traces. There is, progressively a decrease in observed initial absorbance of chlorine dioxide as initial MMI concentrations are increased, indicating the presence of an initial rapid step which is beyond the capabilities of our stopped-flow spectrophotometer.

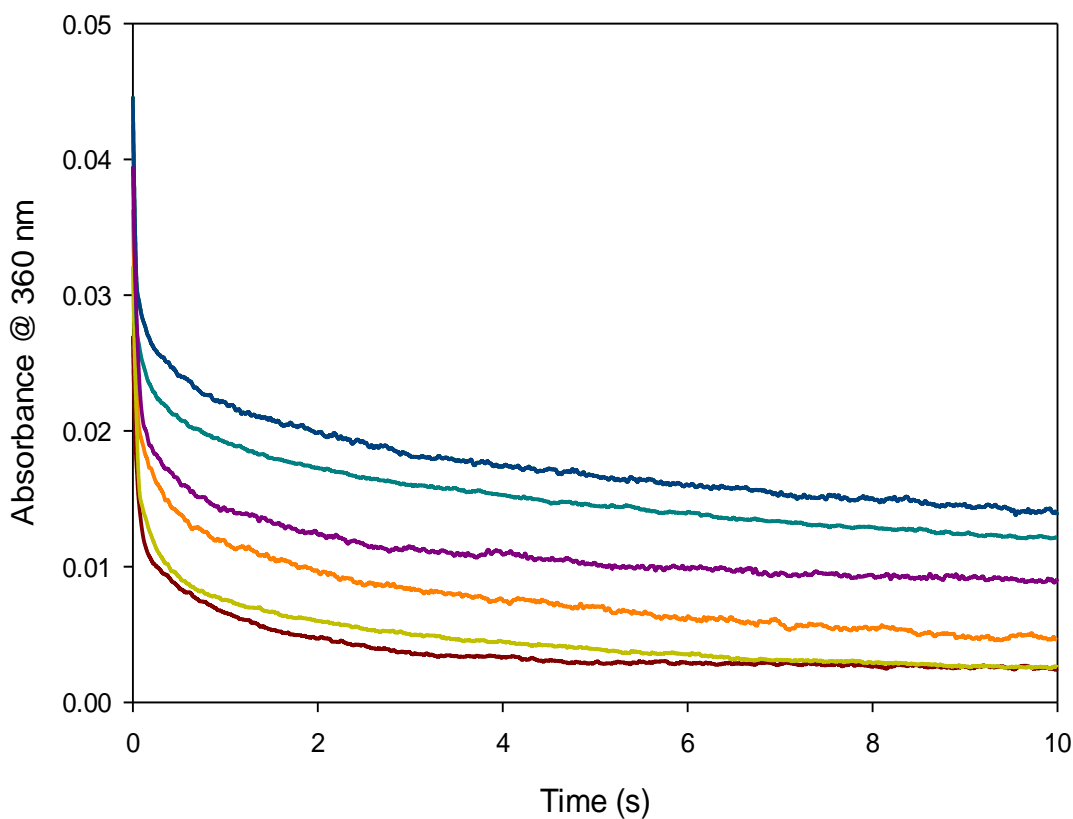


Figure 4.10: Variation of $[MMI]_0$ and their effect on rate of reaction, Fixed $[ClO_2] = 5.00 \times 10^{-5} M$, and varied $[MMI]$ (a) $2.50 \times 10^{-5} M$, (b) $2.60 \times 10^{-5} M$, (c) $2.70 \times 10^{-5} M$, (d) $2.80 \times 10^{-5} M$ (e) $2.90 \times 10^{-5} M$ (f) $5.00 \times 10^{-5} M$

Thus it becomes very difficult to determine an initial rate of reaction, except a lower limit rate constant with no statistical analysis nor error bars. Both Figures 4.9 and 4.10 suggest bimolecular kinetics with the reaction first order in both chlorine dioxide and MMI.

4.3.2 Chlorite-MMI reactions at λ_{max} 260 nm.

Absorbance traces at 360 nm show formation of chlorine dioxide due to the MMI – Chlorite reaction. Spectral scans in Figure 4.1 show an initially isolated peak for MMI at 260 nm. Absorbance observations at this wavelength could show us the initial dependence of the reaction on MMI and chlorite, as well as the requisite initial rate. We had initially evaluated an absorptivity of MMI at 260 nm of $11412 \text{ M}^{-1} \text{ s}^{-1}$. Figure 4.11 shows the dependence of MMI on the MMI – Chlorite reaction. The reaction was run at 0.25 M acid, and was over in about 2 s. It was first order in MMI.

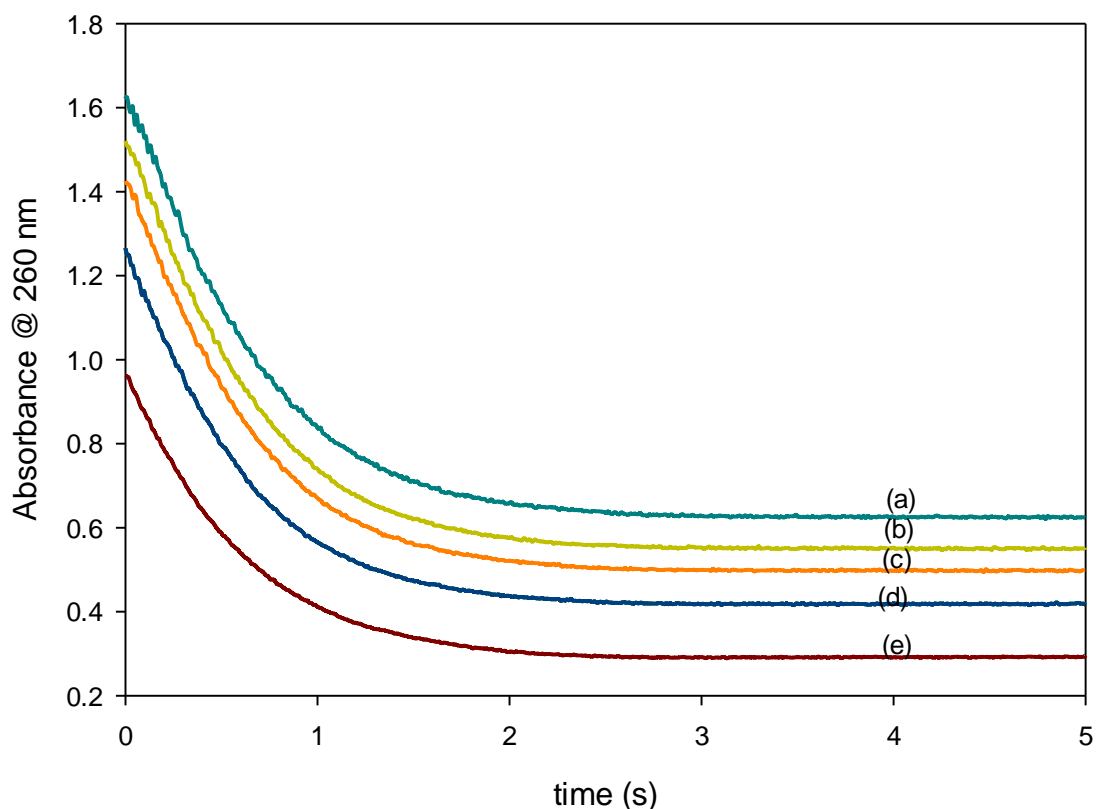


Figure 4.11: Effect of $[MMI]_o$ variation on its oxidation by chlorite at 260 nm. $[ClO_2^-] = 2.50 \times 10^{-3} M$, $[H^+] = 0.25 M$ and varied $[MMI] =$ (a) $1.40 \times 10^{-4} M$, (b) $1.30 \times 10^{-4} M$, (c) $1.20 \times 10^{-4} M$, (d) $1.10 \times 10^{-4} M$, (e) $1.00 \times 10^{-4} M$

Figure 4.12 shows absorbance traces taken at 260 nm while varying chlorine dioxide. These plots are significant: With MMI maintained at a constant initial concentration, one notices that the starting absorbance readings are invariant over the series of experiments undertaken. This implies that our stopped-flow instrument is able to capture the whole reaction sequence, i.e. there is not initial rapid section of the reaction that is not within the mixing time limitations of the instrument.

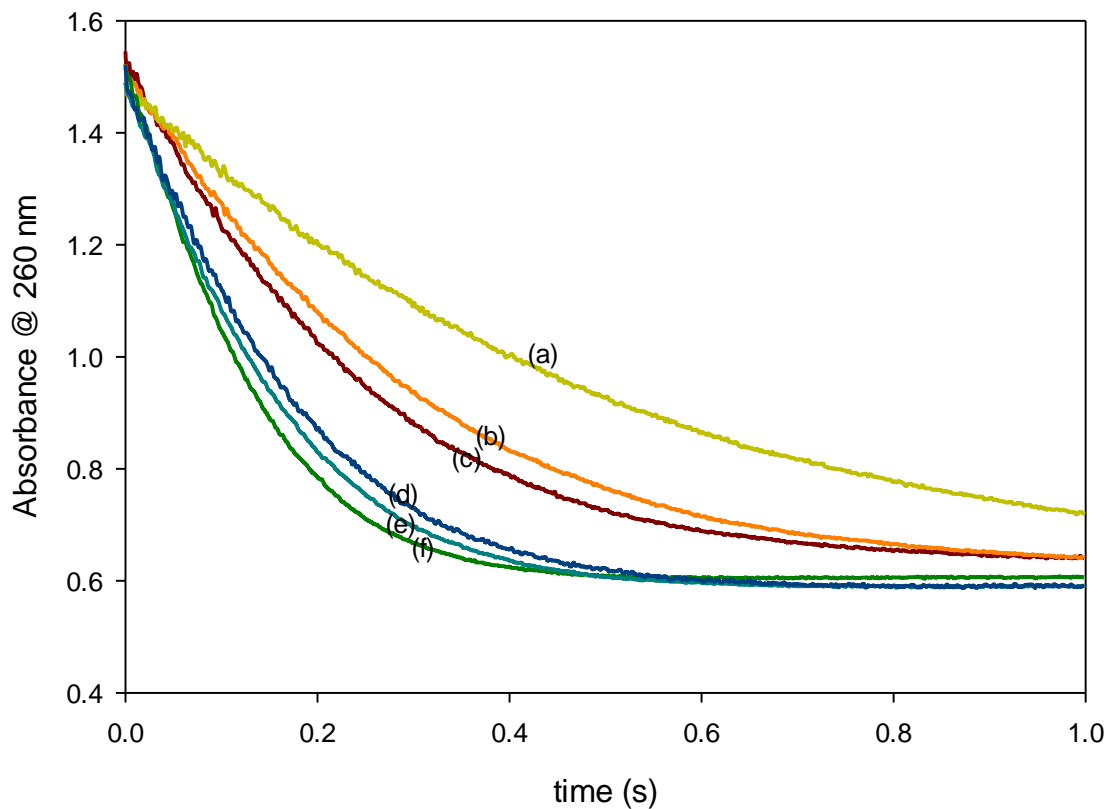


Figure 4.12: *Effect of varying $[ClO_2^-]_o$ on oxidation of MMI at 260 nm Fixed $[MMI] = 1.2 \times 10^{-4} M$, $[H^+] = 0.25 M$ and varied $[ClO_2^-] =$ (a) $1.0 \times 10^{-3} M$, (b) 1.5×10^{-3} , (c) 1.8×10^{-3} , (d) $2 \times 10^{-3} M$, (e) $2.5 \times 10^{-3} M$ (f) $3.0 \times 10^{-3} M$*

Although chlorite was in overwhelming excess over MMI, no pseudo-first-order kinetics are observed. This is as a result of the residual absorbance derived from the products.

Both Figures 4.11 and 4.12 delivered a bimolecular rate constant for the MMI – chlorite reaction of $3.02 \pm 0.42 \times 10^2 M^{-1} s^{-1}$.

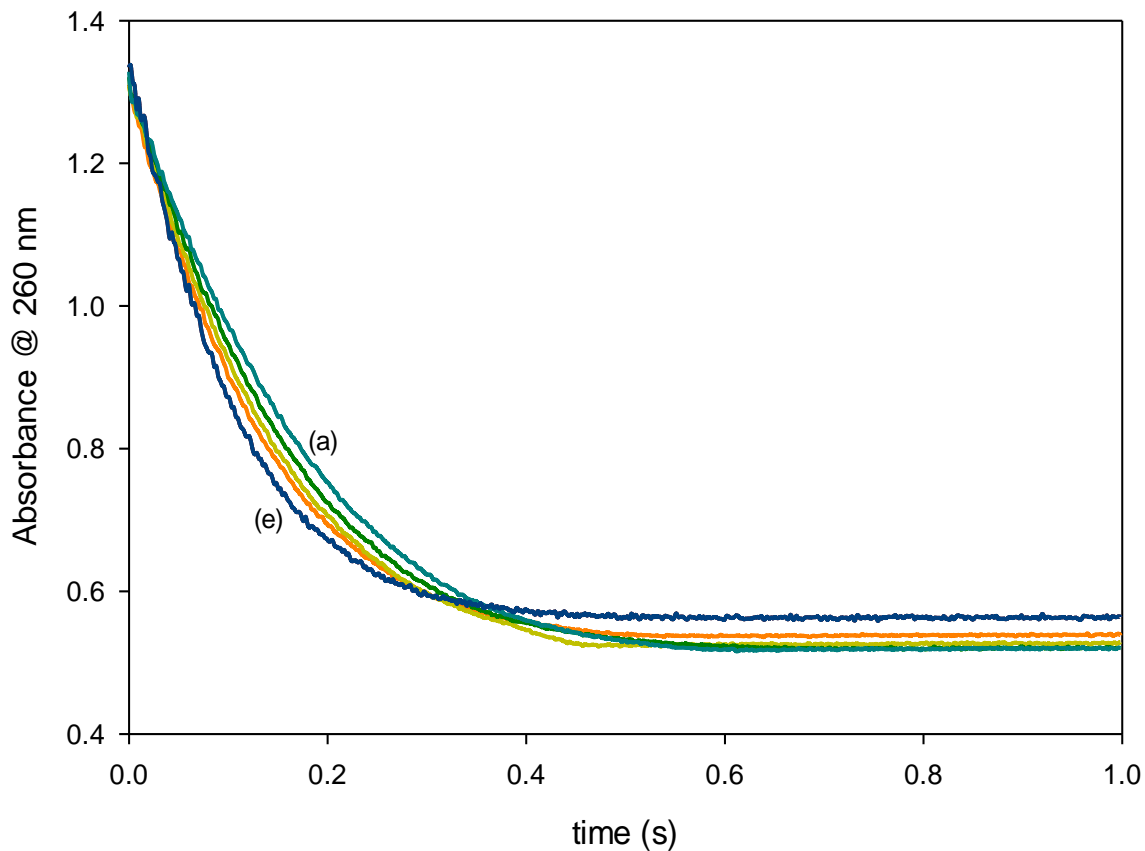


Figure 4.13: Effect of acid variation on oxidation of MMI. Fixed $[MMI] = 1.30 \times 10^{-4} M$, $[ClO_2^-] = 0.25 M$ and varied $[H^+] = (a) 0.10 M$, $(b) 0.20 M$, $(c) 0.30 M$, $(d) 0.40 M$, $(e) 0.50 M$

Figure 4.13 shows the acid dependence of the reaction. Acid seems to have very little effect on the reaction. Higher acid concentrations marginally increase the rate of reaction, however, it gives a higher residual absorbance at the end of the reaction.

4.4 Mechanism

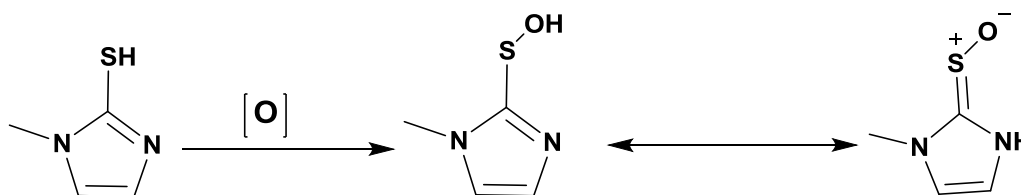
The almost instantaneous formation of chlorine dioxide implies that there is a rapid formation of HOCl in the initial phase of the reaction. Hypochlorous acid is known to rapidly react with chlorite in acidic medium to form chlorine dioxide¹¹⁴:



Thus it would appear that the initial oxidation/reduction involved 2-electrons to produce HOCl and the oxidized form of methimazole, the sulfenic acid. Assuming that methimazole can be represented as RSH, the enol form; the sulfenic acid can be represented as RSOH as represented in the



Scheme 4.2: *The keto and enol forms of MMI*



Scheme 4.3: *The initial oxidation scheme of MMI to form the sulfenic and S-oxide*



The sulfenic acid is known to be unstable and can either be further oxidized to the sulfinic acid in excess oxidant, or to the dimeric species in excess reductant.



This has been confirmed by an experiment in which MMI is reacted with one equivalent of aqueous bromine.⁶² This will impart a 2-electron oxidation on MMI. This should halt the oxidation at the sulfenic acid if the sulfenic acid is stable. If the sulfenic acid is not stable, we would expect a series of sulfur oxo-acids. This has been thoroughly described in section 3.2.7.

4.4.1 Oxychlorine chemistry:

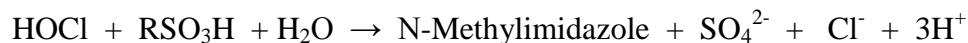
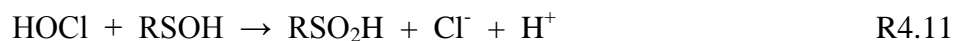
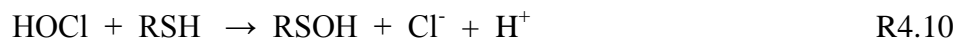
Chlorine dioxide formation is so rapid. Its formation is enhanced by the formation of a reactive species, HOCl. There is however another intermediate species involved in the sequence. This was identified as the asymmetric intermediate Cl₂O₂ species.^{115,116}



Addition of R4.7 and R4.8 gives quadratic autocatalysis in HOCl in excess ClO₂⁻.

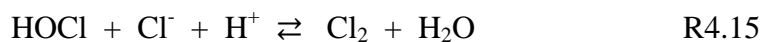


Formation of HOCl thus exponentially increases the formation of more HOCl. One can assume, then, that the major oxidizing species in the reaction medium is HOCl:



R4.14

As Cl⁻ builds up, the hydrolysis reaction of Cl₂ becomes relevant:



The lack of gaseous chlorine observation indicates that the Cl_2 – MMI is very rapid.

4.4.2 Effect of chloride:

There has been some debate in oxychlorine kinetics on the reaction of chlorite and chloride:^{117,118}

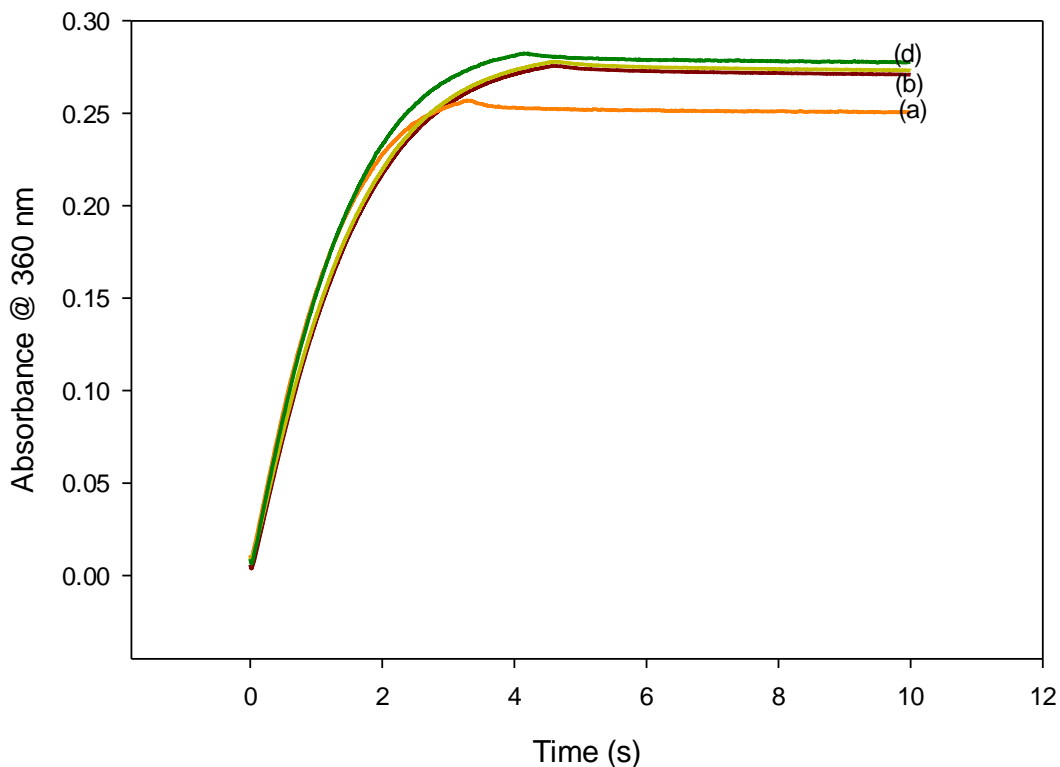
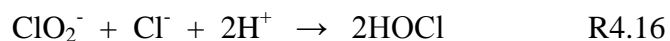


Figure 4. 14. Effect of chloride ions on the oxidation of MMI. Fixed $[\text{MMI}] = 1.0 \times 10^{-3} \text{ M}$, $[\text{H}^+] = 2.5 \times 10^{-3} \text{ M}$, $[\text{ClO}_2^-] = 2.5 \times 10^{-3}$ and (a) No Cl^- , (b) $[\text{Cl}^-] = 1.0 \times 10^{-3} \text{ M}$ (c) $2.0 \times 10^{-3} \text{ M}$, (d) $3.0 \times 10^{-3} \text{ M}$, (e) $5.0 \times 10^{-3} \text{ M}$. There is minimal effect of chloride on the overall reaction.

It is clear from above experiment that, there is minimal effect of chloride on the overall reaction.

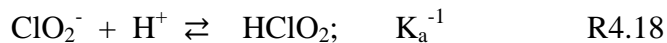
There is a very viable and well-known analogue of reaction R4.16 involving bromous acid:



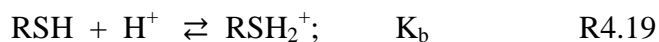
Equilibrium of reaction R4.17 lies more to the right, with formation of HOBr enhancing the rate of reaction since, in all bromate oxidations, HOBr is the major oxidizing species. Thus bromate oxidations are catalyzed by addition of bromide. Figure 4.14, however, shows that chlorite has little effect on the reaction, thus conforming that Reaction R18 is essentially inert.

4.4.3 Effect of acid:

Both chlorite – MMI and chlorine dioxide – MMI reactions show complex dependence on acid. This is due to effectively two acid-base equilibria that are relevant in the reaction mixture. The first is the dissociation constant of chlorous acid:



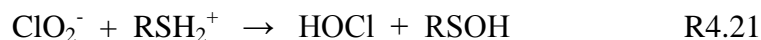
And the second involves protonation of the thiol center:



The protonation can also occur with the keto-form of MMI in which the 5-membered imidazole ring can be represented as R_1R_2 :



The ideal situation for the fastest initiation, reaction R4.4-type reaction would involve the protonated thiol with the unprotonated Cl(III) species:



Reaction R4.21, however, is an unlikely combination, given that pK_a of chlorous acid is 1.72. Low pH conditions will have negligible concentrations of ClO_2^- and high pH conditions will have negligible concentrations of protonated MMI. Thus from the combination of reaction R4 with equilibria R4.18 and R4.19:



The experimentally observed acid dependence can be explained as following. At pH conditions less than 1.0; virtually all Cl(III) species will be in $HClO_2$. The thiol protonation scheme is very rapid in either direction. Thus there is only minimal acid catalysis in the chlorite – MMI reaction between pH 1.0 and 0.301; as is shown in Figure 4.12. However, all oxychlorine reactions proceed faster with acid, especially the composite reaction for the formation of chlorine dioxide, reaction R4.3. Thus, at the initial part of the reaction, high acid would catalyze formation of chlorine dioxide. After the initiation reaction(s) that form $HOCl$, the $HOCl$ can proceed to oxidize MMI and its

sulfur oxo-acids, R4.10 to R4.11, or proceed to oxidize chlorite to chlorine dioxide. Kinetics data suggests that these two sets of reactions, those that form and consume HOCl are of approximately equal magnitude, hence the oligooscillatory behavior observed in chlorine dioxide formation. Acid will catalyze formation of HOCl much more rapidly than the oxidation of MMI by HOCl. HOCl, being an electrophile, reacts faster with the unprotonated thiol.

4.4.4 Reaction of chlorine dioxide and MMI.

The direct reaction of chlorine dioxide is initially slower than reactions that produce chlorine dioxide; hence there is the immediate and almost instantaneous production of chlorine dioxide in the chlorite – MMI reaction. Acid has a minimal effect on this reaction. Bimolecular kinetics suggest the first step of the reaction is an initial adduct formation between chlorine dioxide and MMI. Chlorine dioxide is a radical species, and the first step is the addition of an electron to the odd-electron deficient chlorine center to a more stable species; the Cl(III) chlorite:



Chlorite will then continue with the oxidation of the substrate.



This reaction is solvent assisted; with the reaction faster in protic solvents and sluggish in solvents such as acetonitrile.¹¹⁹ Thus for bimolecular kinetics to prevail, the solvent dissociates the adduct in reaction R4.24 first before addition of the second chlorine dioxide molecule. If the order was reversed, third order kinetics would have been observed. The adduct will have a partial positive charge, which can be attacked by a nucleophile. This would give an unstable Cl(II) intermediate which can rapidly react, in a non-rate-determining manner, with chlorine dioxide, to form chlorite.



The $[\text{R}_1\text{R}_2\text{C}=\text{SOH}]^+$ intermediate can lose a proton to give an S-oxide or a sulfenic acid.

4.4.5 Oligooscillations

Figures 4.6 and 4.7 all show that chlorine dioxide attains a transient maximum before decaying to its final value. Rate of chlorine dioxide production is dependent on the rate of formation of HOCl since subsequent formation of chlorine dioxide is autocatalytic in HOCl. Figure 4.7 reflects this logic. Higher acid concentrations display a higher rate of formation of chlorine dioxide. Lower acid concentrations display a lower chlorine dioxide production rate such that the concentrations of chlorine dioxide do not ‘over-shoot’ its expected stoichiometric concentration and a monotonic rate of formation is observed as in trace (a) in Figure 4.7. Figure 4.6 echoes the same logic. Lower chlorite

concentrations display a monotonic rate of chlorine dioxide formation (trace (a) in Figure 4.6) due to the lower rate of formation of HOCl and subsequently chlorine dioxide.

4.5. Overall reaction scheme.

Table 5.1 shows the full set of reactions involved in this reaction mixture. There are three oxidizing species in the reaction mixture: Cl(III), ClO₂ and HOCl. There are 4 possible reducing species: MMI, the sulfenic, sulfinic and sulfonic acids, sulfite and Cl(III). Chlorite, Cl(III), whether in the protonated or unprotonated forms, acts as either an oxidizing agent (for the substrate), or a reductant (for HOCl to form chlorine dioxide). Table 5.1 encompasses all three possible reactions: ClO₂⁻ - MMI; ClO₂ - MMI and ClO₂⁻ - HOCl reactions. The table assumes all oxidation reactions, except those involving purely only oxychlorine species among themselves, are irreversible. Most of the kinetics of the oxychlorine species are well known. Those involving MMI oxidations were estimated in this study. The initiation reactions that produce the reactive species HOCl are represented by reactions M4 to M6. The highly unlikely combination of unprotonated ClO₂⁻ and the protonated MMI was not included in this scheme. The autocatalysis involves reaction M7 in combination with any of reactions M9, M10 and M11. With establishment of HOCl as the autocatalytic species, after the initiation reactions, one can use HOCl as the sole oxidizing species with very little loss in accuracy. This implies addition of reactions M17 to M21 does not improve the model except when there is overwhelming excess of chlorite. Oxidation of the sulfonic acid could be through the entropy-driven composite reaction M19, or through the 2-step process M22 and M23.

HSO_3^- is labile and easily oxidized to sulfate even by the mildest oxidizing agents; thus just the use of reaction M17. Chlorine dioxide reactions are represented by reactions M24 to M28. The activities of aqueous chlorine dioxide, at various low pH conditions, however, were not known. Some of the wavy traces observed, e.g. Figure 4.6 and 4.7 were derived from formation of gaseous ClO_2 . This precluded a successful modeling of the reaction scheme.

Table 4.1. Chlorite – Chlorine Dioxide – MMI reaction.

No.	Reaction
M1	$\text{ClO}_2^- + \text{H}^+ \rightleftharpoons \text{HClO}_2$
M3	$\text{R}_1\text{R}_2\text{C}=\text{S} + \text{H}^+ \rightarrow [\text{R}_1\text{R}_2\text{C}=\text{S}-\text{H}]^+$
M4	$\text{ClO}_2^- + \text{R}_1\text{R}_2\text{C}=\text{S} + \text{H}^+ \rightarrow \text{R}_1\text{R}_2\text{CSOH} + \text{HOCl}$
M5	$\text{HClO}_2 + \text{R}_1\text{R}_2\text{C}=\text{S} \rightarrow \text{R}_1\text{R}_2\text{CSOH} + \text{HOCl}$
M6	$\text{HClO}_2 + [\text{R}_1\text{R}_2\text{C}=\text{S}-\text{H}]^+ \rightarrow \text{R}_1\text{R}_2\text{CSOH} + \text{HOCl} + \text{H}^+$
M7	$\text{ClO}_2^- + \text{HOCl} + \text{H}^+ \rightleftharpoons \text{Cl}_2\text{O}_2 + \text{H}_2\text{O}$
M8	$\text{Cl}_2\text{O}_2 + \text{ClO}_2^- \rightleftharpoons 2\text{ClO}_2(\text{aq}) + \text{Cl}^-$
M9	$\text{Cl}_2\text{O}_2 + \text{R}_1\text{R}_2\text{C}=\text{S} + \text{H}_2\text{O} \rightarrow \text{R}_1\text{R}_2\text{CSOH} + 2\text{HOCl}$
M10	$\text{Cl}_2\text{O}_2 + \text{R}_1\text{R}_2\text{CSOH} + \text{H}_2\text{O} \rightarrow \text{R}_1\text{R}_2\text{CSO}_2\text{H} + 2\text{HOCl}$
M11	$\text{Cl}_2\text{O}_2 + \text{R}_1\text{R}_2\text{CSO}_2\text{H} + \text{H}_2\text{O} \rightarrow \text{R}_1\text{R}_2\text{CSO}_3\text{H} + 2\text{HOCl}$
M12	$\text{Cl}_2\text{O}_2 + \text{R}_1\text{R}_2\text{CSO}_3\text{H} + \text{H}_2\text{O} \rightarrow \text{R}_1\text{R}_2\text{C}=\text{O} + \text{SO}_4^{2-} + 2\text{HOCl} + 2\text{H}^+$
M13	$\text{HOCl} + \text{R}_1\text{R}_2\text{C}=\text{S} \rightarrow \text{R}_1\text{R}_2\text{CSOH} + \text{H}^+ + \text{Cl}^-$
M14	$\text{HOCl} + \text{R}_1\text{R}_2\text{CSOH} \rightarrow \text{R}_1\text{R}_2\text{CSO}_2\text{H} + \text{H}^+ + \text{Cl}^-$
M15	$\text{HOCl} + \text{R}_1\text{R}_2\text{CSO}_2\text{H} \rightarrow \text{R}_1\text{R}_2\text{CSO}_3\text{H} + \text{H}^+ + \text{Cl}^-$
M16	$\text{HOCl} + \text{R}_1\text{R}_2\text{CSO}_3\text{H} + \text{H}_2\text{O} \rightarrow \text{R}_1\text{R}_2\text{C}=\text{O} + \text{SO}_4^{2-} + 3\text{H}^+ + \text{Cl}^-$
M17	$\text{ClO}_2^- + \text{R}_1\text{R}_2\text{CSOH} + \text{H}^+ \rightarrow \text{R}_1\text{R}_2\text{CSO}_2\text{H} + \text{OCl}^-$
M18	$\text{ClO}_2^- + \text{R}_1\text{R}_2\text{CSO}_2\text{H} \rightarrow \text{R}_1\text{R}_2\text{CSO}_3\text{H} + \text{OCl}^-$
M19	$\text{ClO}_2^- + \text{R}_1\text{R}_2\text{CSO}_3\text{H} + \text{H}_2\text{O} \rightarrow \text{R}_1\text{R}_2\text{C}=\text{O} + \text{SO}_4^{2-} + \text{OCl}^- + 2\text{H}^+$
M20	$\text{HClO}_2 + \text{R}_1\text{R}_2\text{CSOH} \rightarrow \text{R}_1\text{R}_2\text{CSO}_2\text{H} + \text{HOCl}$
M21	$\text{HClO}_2 + \text{R}_1\text{R}_2\text{CSO}_2\text{H} \rightarrow \text{R}_1\text{R}_2\text{CSO}_3\text{H} + \text{HOCl}$
M22	$\text{R}_1\text{R}_2\text{CSO}_3\text{H} + \text{H}_2\text{O} \rightarrow \text{R}_1\text{R}_2\text{C}=\text{O} + \text{HSO}_3^- + \text{H}^+$
M23	$\text{HSO}_3^- + \text{HOCl} \rightarrow \text{SO}_4^{2-} + 2\text{H}^+ + \text{Cl}^-$
M24	$\text{ClO}_2(\text{aq}) + \text{R}_1\text{R}_2\text{C}=\text{S} \rightleftharpoons [\text{R}_1\text{R}_2\text{C}=\text{S}:\text{ClO}_2]$
M25	$[\text{R}_1\text{R}_2\text{C}=\text{S}:\text{ClO}_2] + \text{ClO}_2(\text{aq}) + \text{H}_2\text{O} \rightleftharpoons 6 \text{R}_1\text{R}_2\text{CSOH} + 2\text{H}^+ + 2\text{ClO}_2^-$
M26	$\text{ClO}_2(\text{aq}) + \text{R}_1\text{R}_2\text{CSO}_2\text{H} \rightleftharpoons [\text{R}_1\text{R}_2\text{CSO}_2\text{H}:\text{ClO}_2]$
M27	$[\text{R}_1\text{R}_2\text{CSO}_2\text{H}:\text{ClO}_2] + \text{ClO}_2(\text{aq}) \rightleftharpoons \text{R}_1\text{R}_2\text{CSO}_3\text{H} + 2\text{H}^+ + 2\text{ClO}_2^-$
M28	$\text{ClO}_2 + \text{HSO}_3^- \rightleftharpoons [\text{O}_2\text{ClSO}_3\text{H}]$
M29	$2 \text{R}_1\text{R}_2\text{CSOH} \rightleftharpoons \text{R}_1\text{R}_2\text{CSO}_2\text{H} + \text{R}_1\text{R}_2\text{C}=\text{S}$

4.6. Conclusion

MMI is oxidized by chlorite and chlorine dioxide all the way through to desulfurization. Chlorite oxidation of MMI produces negligible amounts of the S-oxide (see Figure 4.4) and no evidence of the sulfinic acid. The sulfonic acid is a major pathway of oxidation before formation of sulfate and N-methylimidazole. The lack of observation of substantial amounts of the sulfenic and sulfinic acids in the ESI spectrum does not preclude their presence in the pathway and mechanism: it just means that these oxoacids are very unstable and are easily oxidized further.

CHAPTER FIVE

Electrochemical and Enzymatic in Vitro Studies, of 6-propyl-2-thiouracil

5.1. Introduction

6-propyl-2-thiouracil (PTU) is an antithyroid drug that was introduced close to seventy years ago.⁸⁶ This drug is effective in the treatment and management of Grave's disease, an autoimmune diseases mediated by thyroid stimulating immunoglobulins; resulting in hyperthyroidism, which is over production of thyroid hormones.¹²⁰ It works by inhibiting the activity of thyroid peroxidase and blocks the conversion of thyroxine (T4) to triiodothyronine (T3). The action of PTU may partly depend on its ability to function as a thiol as shown by tautomer forms below.¹²¹

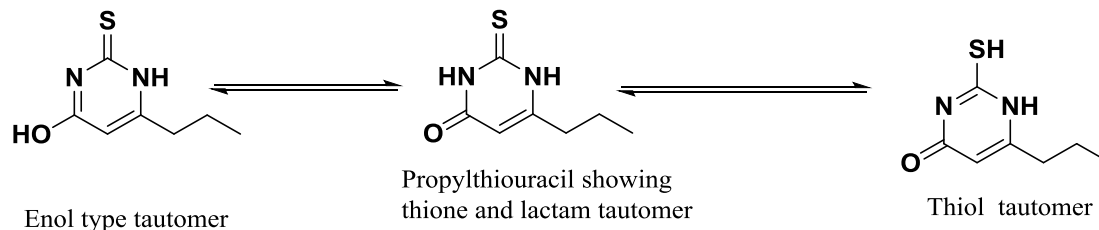


Figure 5.1 *Tautomers of PTU*

Although effective, PTU has been associated with rare but severe idiosyncratic toxicity, characterized by; skin reactions, agranulocytosis, aplastic anemia, hepatitis and cholestasis.^{85,86} PTU is identified as being the third most frequent cause of drug-induced liver transplant in the United States.¹²² In 2008, a panel of experts extensively reviewed adverse events reports and case reports of PTU-induced liver failure and deaths. They

recommended that PTU should not be used as first line of therapy in Grave's disease.¹²³ In 2010 the Food and Drug Administration (FDA) issued a black box warning about severe liver injury associated with treatment using PTU. Hepatotoxicity of therapeutic drugs is not a new phenomenon in drug therapy.

A number of drugs have already been withdrawn from market after cases of severe toxicity were noted. Bioactivation of drugs resulting in reactive metabolites is considered as the initial step towards drug induced organ damage.¹²⁴ Presumably the hepatotoxicity associated with PTU is due to its reactive metabolites in the liver, these could be radicals or electrophiles. However, as of now, there are no reports on the PTU reactive metabolite(s) formation in liver, and the role of the formed intermediates in the hepatotoxicity induced by this drug is ambiguous.¹²⁵ There has been a variety of metabolites observed from PTU metabolism. Two oxidation systems were examined for the oxidation of PTU. Metabolites generated by electrochemical oxidation were compared to those that were identified from microsomal oxidation. Slight differences were noted in the identity of the metabolites.

5.2 Results and discussion

5.2.1 Electrochemical oxidation of PTU in basic medium

Electrochemical oxidation of PTU was carried out using the arrangement shown in figure 2.4. Initial experiments were carried out in the absence of trapping agents. Control experiments were initiated with the cell turned off at 0 potential. Figure 5.2 clearly

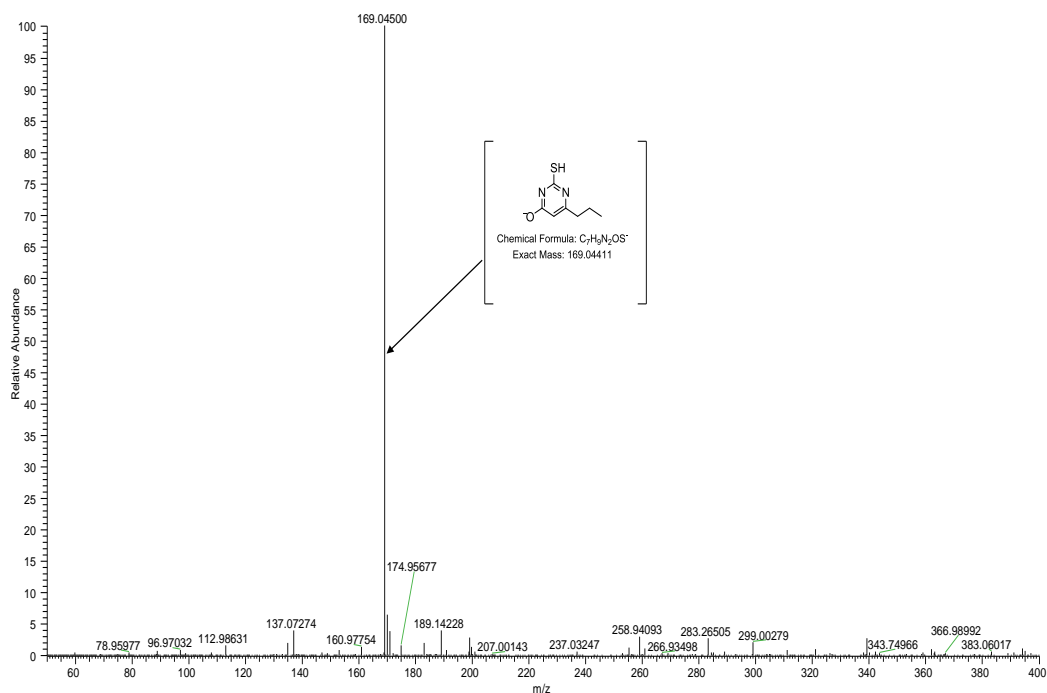


Figure 5.2 ESI (-) MS, with cell turned off 0 mv obtained for 0.1 mM PTU in ammonium in 20 mM ammonia, 20% MeOH, pH 10, Flow rate 10 μ L/min.

shows a clean ESI-spectrum of PTU that was obtained in the negative mode. The only peak that is evident from the spectra above is the substrate PTU with m/z 169.04

The presence of a single peak from the solvent-electrolyte mixtures shows that there were no any other reactions or contaminants prior to the electrochemical oxidation.

Contaminants as well as other reactions in the electrolyte mixture, are usually confused for modifications that might take place on the compound of interest. As such, any products that emerged when the reaction was initiated by applying potential could thus be attributed to transformations due to oxidation of PTU in the electrochemical cell.

When the cell was turned on, the voltage was gradually increased with a ramp of 100 mV each time. There was emergence of additional peaks at 400 mV. This potential was enough to initiate oxidation of PTU to a disulfide and sulfinic acid, as shown in figure 5.3 below. PTU disulfide was the dominant peak in both acidic and alkaline medium.

However, in acidic medium there were many spurious peaks that could not be easily assigned to anything.

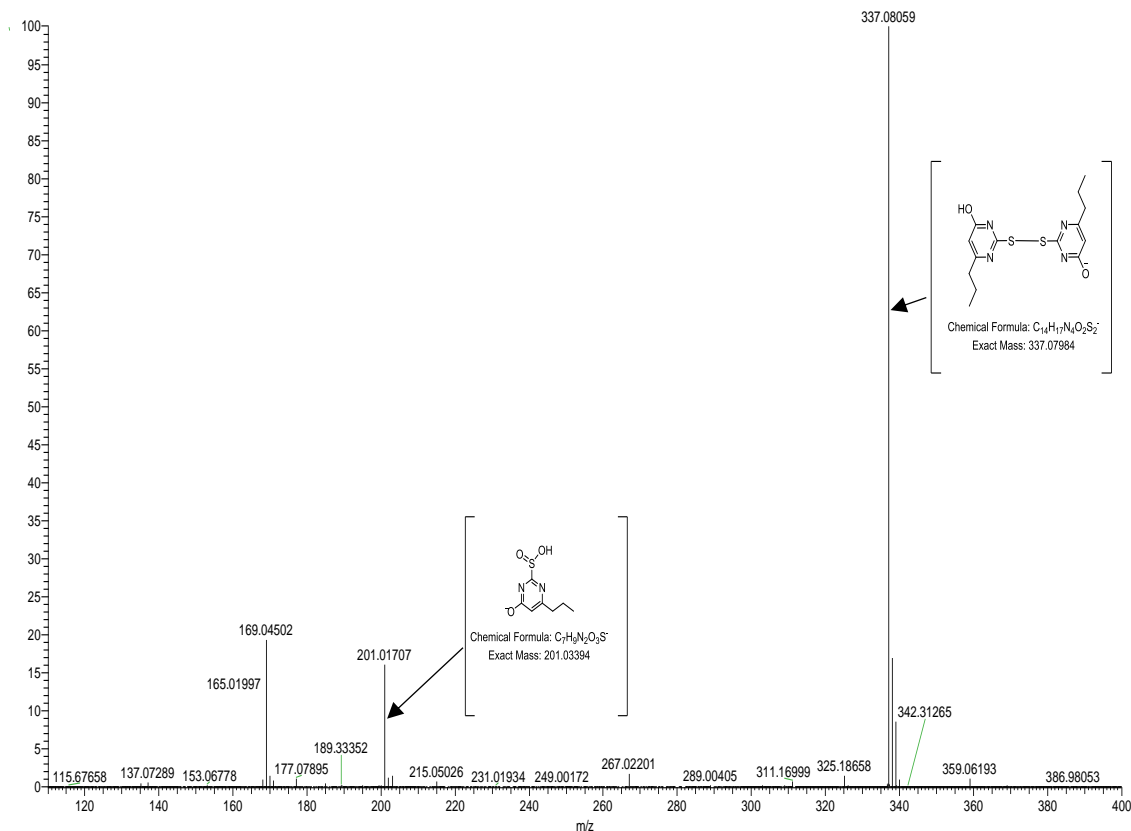
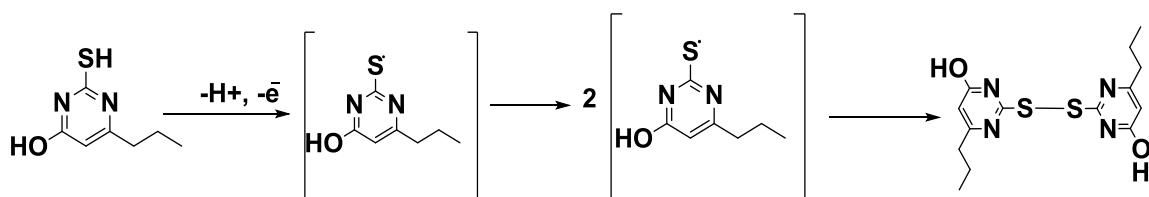


Figure 5.3. ESI-MS spectra generated with the cell potential at 400 mV.

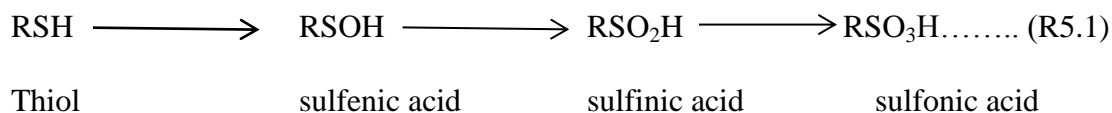
Figure 5.3 shows a strong peak of PTU-disulfide, which is the major product of oxidation at the given potential of 400 mV. Dimeric species from thiols are usually unreactive compared to parent thiols, hence they accumulate. Surprisingly, the electrochemical oxidation of PTU was achieved at very low potentials, compared to what has been reported previously in literature. Sartori *et al*, reported higher electrode potentials of 1.42 V for oxidation of PTU to its dimer using cyclic voltammetry.¹²⁶

Electrode potential (E_m) is pH-dependent, it has been shown that it decreases with approximately 0.06 V/pH, for a simple thiol such as glutathione. Therefore, as the pH is increased, the potential required to effect oxidation decreases.¹²⁷ The data below points out the possibility of two competing reaction pathways. Thiol oxidation can proceed through two competing pathways. Abstraction of a single electron is relatively easy leading to a thiyl radical. The two electron pathway, results in formation of sulfenic acid. These two intermediates participate in further reactions resulting in metastable products.¹²⁸ Thus the thiyl radical might initiate chain reactions that results in a disulfide. This is a coupled-proton electron transfer process resulting in a radical that dimerizes to a disulfide as shown in scheme 5.1 below.

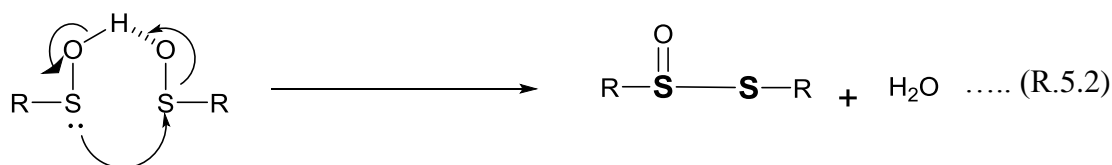


Scheme 5.1 Proposed oxidation scheme for PTU and its dimerization to a disulfide compound.

There is a relatively weak peak at m/z 201 which shows a sulfenic acid. In theory one would expect to observe the S-oxides of PTU in the mass spectrum. Thiols are known to undergo oxidation to sulfenic acid which further oxidizes to more stable sulfenic and sulfonic acids respectively,^{129,130} as seen in the equation below.



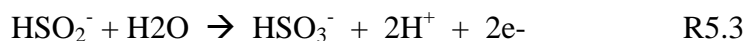
There is no evidence of formation of sulfenic acid, or the S-oxide in the spectrum. The sulfenic acid may transform to its more stable form of an S-oxide.⁶² However, sulfenic acids exhibit potent electrophilic and relative weak nucleophilic reactivity.¹³¹ Thus in small molecules such as PTU, this dual behavior can lead to self-condensation in which one sulfur atom functions as a nucleophile and the second as an electrophile to yield a thiosulfinate ester shown below



The self-condensation reaction is facilitated by intermolecular hydrogen bonding. At a pH > 8, which is the case in this series experiments, the thiosulfinate esters disproportionate to form salts of sulfinic acid and disulfide.¹³² This reaction can thus explain both the presence of sulfinate and the dimer observed in figure 5.3. Trapping experiments were also conducted in PTU oxidations. Unlike in oxidation of methimazole, there were no conjugates that formed between PTU and nucleophiles. Presumably the reaction proceeds through formation of the dimer. This dimer then would further be oxidized to sulfinic acid. Regardless of which pathway dominates, both mechanisms have potential to result in reactive intermediates

5.2.2 Effect of oxidation potential

An analysis of the ESI spectrum collected at higher oxidative potentials of 800 mV shows two additional peaks that were observed on the mass spectrum. Figure 5.4 show that sulfur was fully oxidized, from -2 to +6, to yield sulfate (SO_4^{2-}) shown, with m/z 96. Effluent from the cell was reacted with barium chloride, resulting in formation of BaSO_4 . There was no evidence of formation of PTU-sulfonic acid from the ESI mass spectra. Hydrolysis of sulfinic acid, should result in the cleavage of the C=S bond to give a urea-type residue, $\text{R}_1\text{R}_2\text{C}=\text{O}$ and an unstable sulfur species HSO_2^- . HSO_2^- is readily oxidized to bisulfite (HSO_3^-).



HSO_3^- is in turn easily hydrolyzed to sulfate. One would expect a significant amount of the urea type organic residue if hydrolysis was the major pathway. However, only traces (propyl uracil) at m/z 153 and an unidentified metabolite with m/z 135 were observed. If this organic residue is not stable; it would further hydrolyze through ring opening giving small fragments. A decrease of 32 amu, is apparent from the initial mass of substrate. The exact mechanism from the sulfinic acid to sulfate and an organic residue can only be speculative, but involves no further oxidation past the formation of sulfate. Non-solvent assisted cleavage of C-S bond, which is either heterolytic or homolytic cleavage, should result in loss of sulfur as sulfite and sulfite radical anion respectively from sulfinic acid.¹³³ The organic residue observed is shown with the peak at m/z of 137, thus this is

6-propyl-2, 3-dihydropyrimidin-4(1H)-one. The spectrum below still shows the dimer
 m/z 168 is the symmetrical PTU dimer.

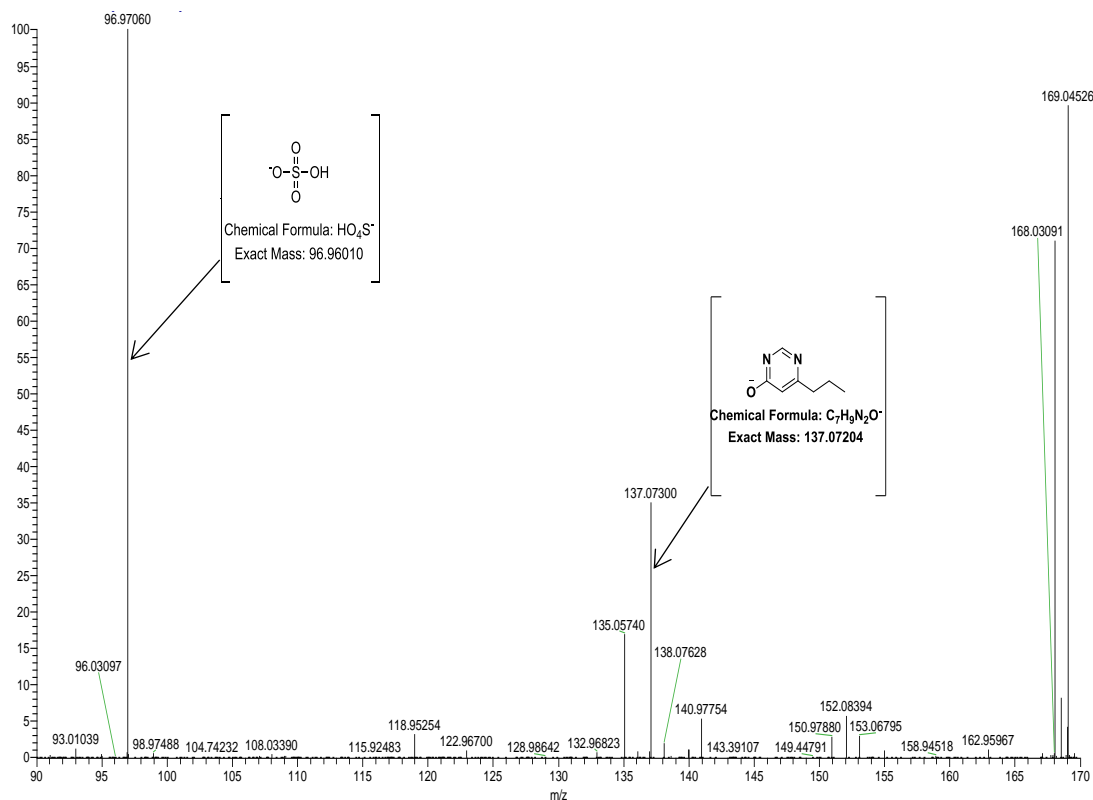


Figure 5.4. ESI-MS spectra generated with the cell potential at 800 mV.

The one-electron pathway, resulting in thiyl radicals appears to be the most dominant mechanism here. Radicals play a very important role in induced oxidative stress and subsequent liver injury. Waldhauser and co-workers investigated the oxidation of PTU in activated neutrophils. PTU was observed to be oxidized by myeloperoxidase,¹¹⁰

resulting in sulfite as one of the products, as indicated above, this can be further oxidized to sulfate. If PTU desulfurization involve forming sulfite radical, one would expect it to undergo further reactions which may or may not lead to reactive metabolites.

It has been shown that sulfite and sulfite radicals are oxidized by myeloperoxidase to free radicals. These prooxidant radicals, such as the reactive sulfur trioxide ($\text{SO}_3^{\cdot-}$), peroxymonosulfate ($-\text{O}_3\text{SOO}^{\cdot}$), and sulfate ($\text{SO}_4^{\cdot-}$) anion radicals have capacity to damage proteins and oxidize them to protein radicals, with consequences of allergic reactions.¹³⁴ Whereas some studies reported that there have been no reactive metabolites formation in the liver. Some intermediates e.g., 6-propyl-2,3-dihydropyrimidin-4(1H)-one, (propyluracil) and other unidentified metabolites, with prooxidant radicals were echoed in electrochemical system. Some of the intermediates have been proposed but have not been observed in previous *in vivo* and *in vitro* studies. Radicals can also generate toxic effects through oxidative stress without forming covalent adducts with biomolecules.¹³⁵ This forms the basic framework for the danger hypothesis that leads to idiosyncratic toxicities.

5.3 In vitro enzymatic oxidation of PTU

The metabolism of PTU was studied based on standard *in vitro* technique, involving incubation of the target compound with liver microsomes. The experiments here were performed using human microsomes. The results obtained from the liquid chromatography separation with mass spectrometry detection are shown in Figure 4.5.

The oxidation of PTU with microsomes was complex. Identification of the products from metabolism was complicated by the presence of biological matrix and a range of possible metabolites.

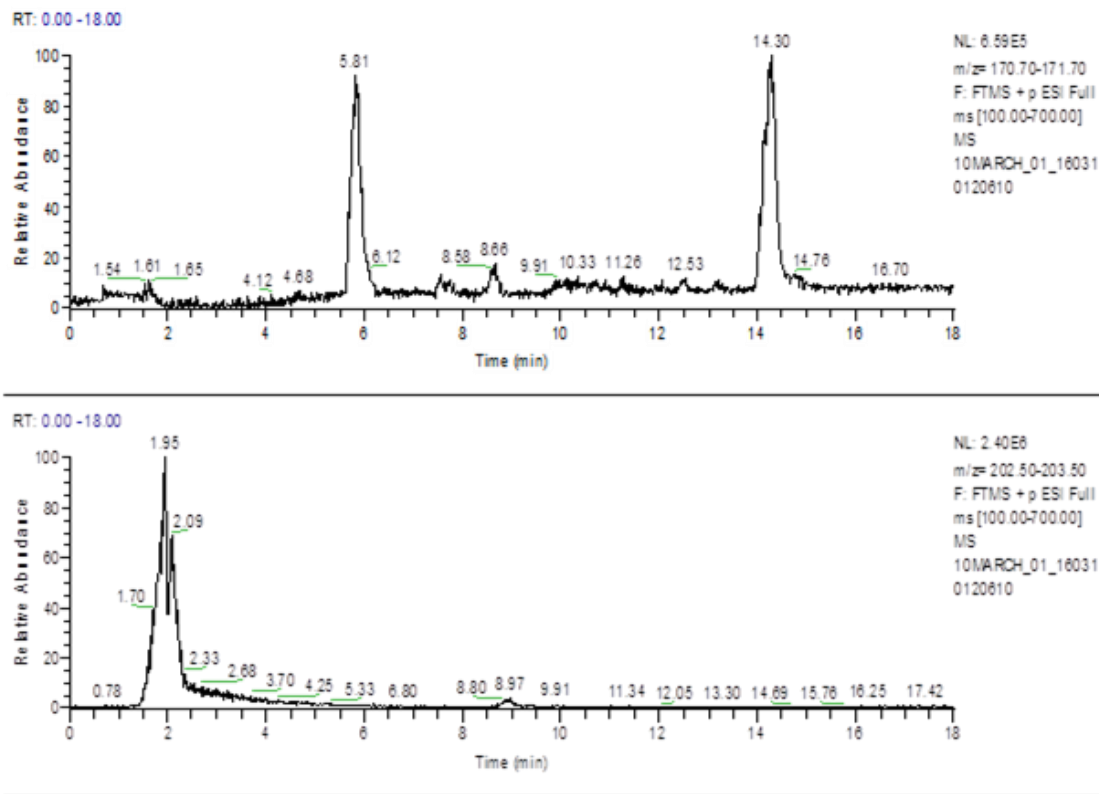


Figure 5.5. LC-MS chromatograms from metabolites generated by incubation with human liver microsomes (HLM)

Although not quite abundant figure 5.6 shows spurious peaks on the ESI-spectra, some of them were unidentified. However, this observation does not really point to an inferior technique. Instead it does show that a variety of metabolites are possible from

biological oxidations versus EC-MS. Figure 5.5 shows the chromatogram, extracted from ion filtering using Xcalibur software. Retention time of the 14.30 peak shows the unconverted substrate PTU, with m/z 171.13 shown in figure 5.6 below. Another peak on the chromatogram, with retention time of 5.81 was associated with the unconverted substrate; this could be due to tautomer of PTU, resulting in a more polar ion form of PTU. This analysis is further complicated by the appearance of another small peak that co-eluted at this same retention time. The peak had a jump of 16 amu from the substrate, thus $[M + O + H]$ with at m/z 186.22, a putative PTU S-oxide. The relatively low abundance of the peak, appears to show a transient molecule that is derived from unstable sulfenic, moreover it is fleeting towards sulfinic and sulfonic acids. In this biological matrix, the reactive sulfenic acid can react with the protein components of microsomes. Usually after centrifugation, the protein pellet will sediment and is not analyzed in LC-MS analysis, hence a diminished peak of the remaining metastable S-oxide can be observed. Its polarity also fits very well to the assigned retention time.

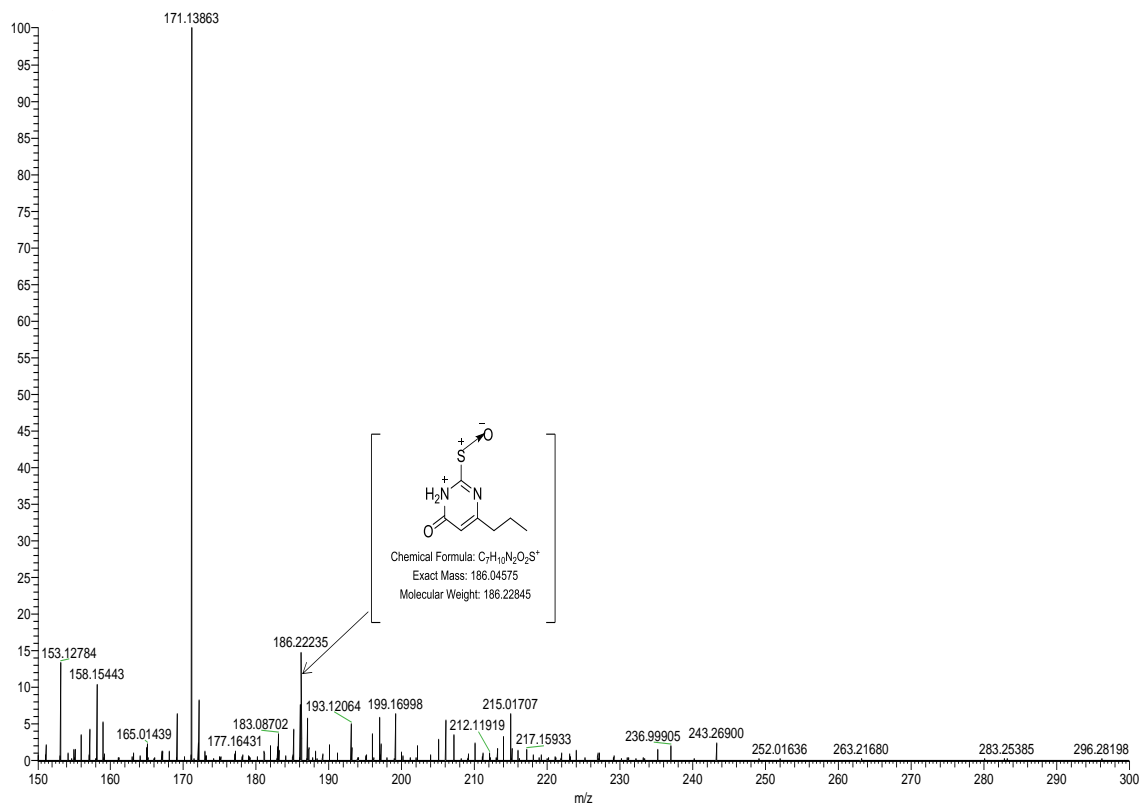


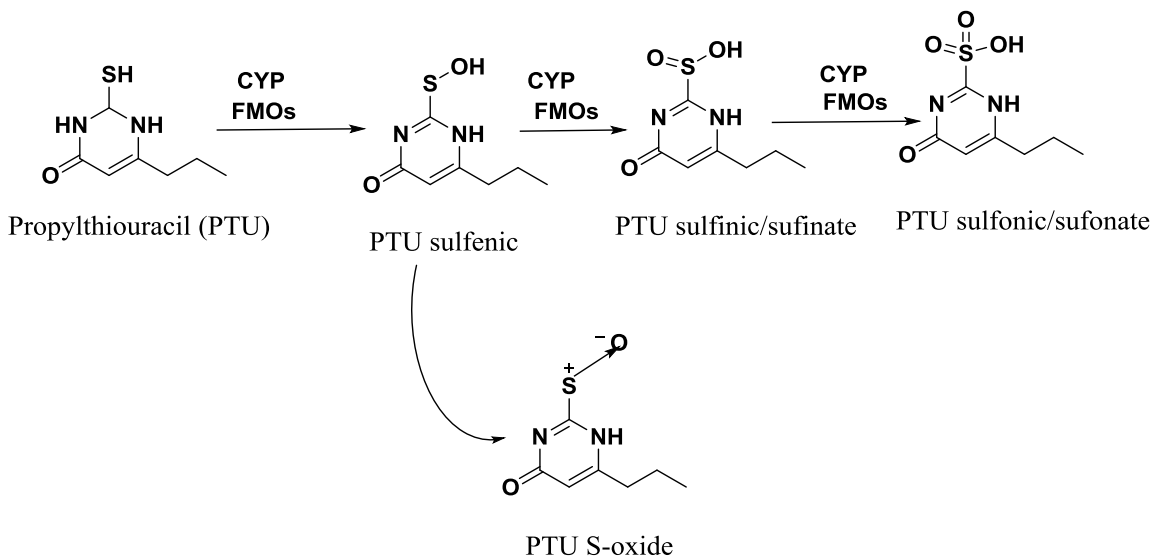
Figure 5.6 ESI (+) mass spectrum showing product of oxidation from microsomal incubation.

Interestingly, hepatotoxicity due to PTU has been known, but it is surprising that, there have not been a lot of studies dedicated to the oxidation of PTU using microsomes. Most of the studies conducted used peroxidases as oxidants, and as such, there have not been known reactive metabolites produced from microsomes. Studies on the oxidation of PTU with activated neutrophils showed that PTU-disulfide, PTU-sulfite/sulfinic acid, and PTU-sulfate/sulfonic acid were the major products of oxidation.¹¹⁰ The toxicity of thionamides, such as ethionamide has been associated with their bioactivation to reactive S-oxides.^{136,137} Therefore, hepatotoxicity due to PTU may also arise from the observed S-

oxide; this electrophilic metabolite has the capacity to bind to liver cellular macromolecules resulting in drug damage to cells.

5.3.1 Oxidation mechanism

Metabolism by microsomes involves primarily the flavin-containing monooxygenases (FMO's) and the CYP450 group of enzymes. FMO's are a family of drug-metabolizing enzymes that use FAD, NADPH and molecular oxygen to catalyze the oxygenation of a large number of xenobiotics containing 'soft' nucleophiles such as sulfur, phosphorus and nitrogen.^{138,139}



Scheme 5.2 Proposed reaction scheme for PTU metabolism in microsomes.

The scheme above shows a simple mechanism for oxidation of PTU in microsomes. FMOs convert xenobiotics into polar metabolites by adding oxygen so that they can subsequently be easily eluted through the kidneys.¹⁴⁰ While initially thought to be a single enzyme; FMO's are now known to contain at least 11 isoforms, with 5 of them having been characterized to date.^{141,142} It has been reported that FMOs oxidize thionamides and thiourea functional groups to intermediate metabolites of sulfenic (RSOH) and sulfinic (RSO₂H) acid which are responsible for deactivating CYP450 enzymes.^{143,144} As mentioned earlier on, sulfenic acid is a very unstable intermediate, giving rise to metastable S-oxide. In presence of excess oxidative power, the S-oxide and sulfinic acid will further be oxidized to sulfonic acid, as shown in scheme 5.2.

The standard procedure for trapping reactive metabolites was also carried out using glutathione and n-acetyl cysteine as trapping agents. There were no detectable conjugates, in reactions of PTU. Sulfenic acid precedes formation of S-oxide and is very reactive to be able to react with thiol. However, even if the intermediates were formed, their conjugation with nucleophiles is not always spontaneous as in the case of MMI-acetylcysteine, sometimes it requires enzymes, such as glutathione transferase which can facilitate conjugation.

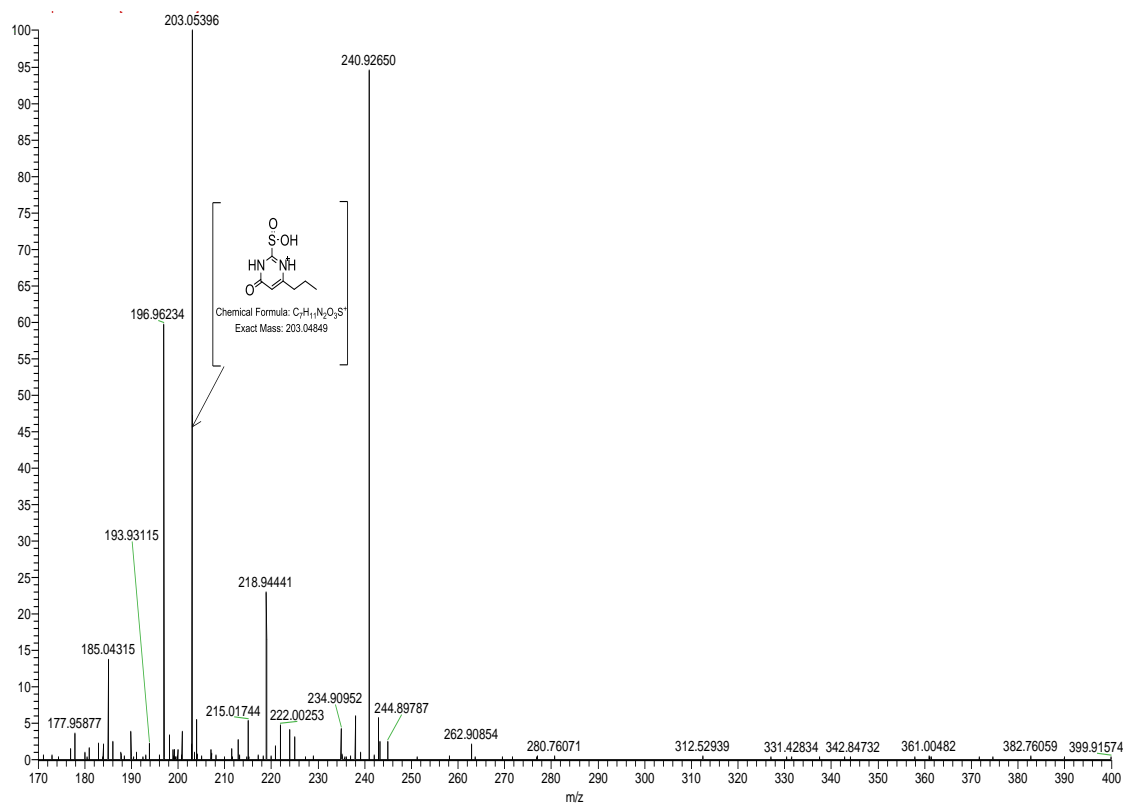


Figure 5.7 ESI (+) MS spectra showing sulfinic acid and sulfonic acid as products of oxidation of PTU.

PTU is less polar as compared to its products of oxidation, which co-eluted within 1.95 and 2.06 minutes. Figure 5.7 shows 6-propyl-2-thiouracil sulfinic acid (PTU-SO₂H) m/z 203.04, 6-propyl thiouracil sulfonic acid (PTU-SO₃H) m/z 218.94, and its sodium adduct m/z 240.09 as the major products of microsomal oxidation. These are stable oxides for oxidation of PTU. PTU-sulfonic acid/sulfonate, at m/z 218.94, [M +3O +H⁺] and 240.09, [M +3O +Na⁺] exist as a zwitterion form before adducted to a proton or

sodium respectively. Microsomal oxidations were carried out in a pH of 7.4, close to neutral pH, and thus it can afford such neutral structures. Molecules with such structure have been observed from X-ray data. Chigwada *et al*,⁷⁵ showed the existence of this putative sulfonic acid zwitterion for tetra methyl thiourea sulfonic acid (TTTU-SO₃⁻), figure 5.8 a. Figure 5.8 b shows putative the molecular ion as observed in ESI spectrum at m/z 240.02.

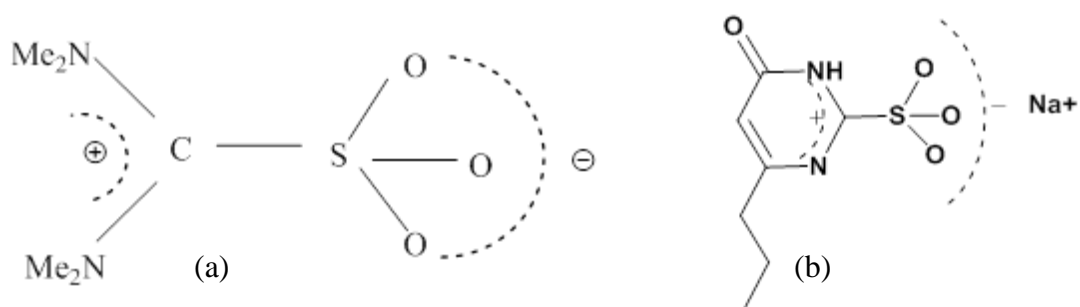


Figure 5.8 Putative zwitterion structures

Figure 5.7 shows undefined metabolite at m/z 196.96. This shows some of problems that arise from microsomal oxidations. The matrix contains different endogenous material which can co-elute with compounds of interests. Contrary to this, it also shows the diversity of metabolites that can be obtained from microsomal oxidations.

5.3.2 Comparison of electrochemical and biological metabolism.

There were variations in the nature and type of metabolites that have been observed from electrochemical oxidation of the PTU compared to what has been observed and reported in biological studies.¹⁴⁵ Both Figures 5.6 and 5.7 shows some unidentified peaks e.g., the peak with m/z 196 could not be assigned to any metabolite in the mixture. The electrochemical process is a 'cleaner' oxidation environment than that afforded by microsomes. Thus the electrochemical oxidation platform involves the most easily oxidizable part of the molecule without any regard to other parameters present in bimolecular activations such as stereochemistry.

Oxidation of thiols through formation of their disulfides is relatively easy, compared to two electron process for the formation of S-oxide. Contrary to the EC-MS system, microsomal oxidations show non competing reaction pathways. Successive formation of sulfo-oxo acids is through a two electron transfer mechanism by FMO S-oxygenation. Microsomes contain CYPs as well, which participates in functionalization reactions; as such one would expect a variety of metabolites. However, there are some other factors that might prevent this e.g., thionamides are known to be enzyme inhibitors,¹⁴⁶ this has large bearing on the nature of products that can be obtained from their biological oxidation using microsomes. The kinetics for the EC-MS two electron mechanism are quite sluggish. Electron-withdrawing groups such as oxygen in the ring for PTU may reduce the nucleophilicity nature of S atom on the thiolate ion, making it difficult to abstract a second electron. A comparison of EC-MS oxidations to microsomal

oxidations shows there is a physiological gap between the isolated microsomes and electrochemical cells. Nevertheless, there were similarities in type of metabolites obtained from EC-MS with those obtained using peroxidase enzymes as indicated earlier on. Differences in metabolites may be attributed to experimental conditions.

5.5 Conclusion

Bioactivations of sulfur-based drugs have always been difficult to determine. PTU oxidation is generally complex, characterized by free radical and two electron process mechanism in electrochemistry and microsomal oxidations respectively. PTU oxidation resulted in a range of metabolites, the absence of conjugates in either system, does not preclude formation of reactive metabolites. The kinetics of that step was much faster, such that the metabolites were not captured. However, results show that an S-oxide which is electrophilic and hepatotoxic is produced in liver microsomes. Toxicity of PTU may be attributed to this reactive metabolite. Moreover, the mechanism entails two pathways which might be involved in toxicity due to PTU. EC-MS techniques complement the microsomes and is quite informative in evaluation of toxicities from drugs, as it gives an alternative explanation to observed phenomena.

Reference List

1. Zamek-Gliszczyński, M. J.; Hoffmaster, K. A.; Nezasa, K.; Tallman, M. N.; Brouwer, K. L. R. Integration of hepatic drug transporters and phase II metabolizing enzymes: Mechanisms of hepatic excretion of sulfate, glucuronide, and glutathione metabolites. *European Journal of Pharmaceutical Sciences* **2006**, *27* (5), 447-486.
2. Delaforge, M.; Pruvost, A.; Perrin, L.; Andre, F. Cytochrome P450-mediated oxidation of glucuronide derivatives: Example of estradiol-17 beta-glucuronide oxidation to 2-hydroxyestradiol-17 beta-glucuronide by CYP2C8. *Drug Metabolism and Disposition* **2005**, *33* (3), 466-473.
3. Meunier, B.; de Visser, S. P.; Shaik, S. Mechanism of oxidation reactions catalyzed by cytochrome P450 enzymes. *Chemical Reviews* **2004**, *104* (9), 3947-3980.
4. Meyer, U. A. Overview of enzymes of drug metabolism. *Journal of Pharmacokinetics and Biopharmaceutics* **1996**, *24* (5), 449-459.
5. Yan, Z. Y.; Maher, N.; Torres, R.; Caldwell, G. W.; Huebert, N. Rapid detection and characterization of minor reactive metabolites using stable-isotope trapping in combination with tandem mass spectrometry. *Rapid Communications in Mass Spectrometry* **2005**, *19* (22), 3322-3330.
6. Park, B. K.; Kitteringham, N. R.; Maggs, J. L.; Pirmohamed, M.; Williams, D. P. The role of metabolic activation in drug-induced hepatotoxicity. *Annual Review of Pharmacology and Toxicology* **2005**, *45*, 177-202.
7. Kalgutkar, A. S.; Gardner, I.; Obach, R. S.; Shaffer, C. L.; Callegari, E.; Henne, K. R.; Mutlib, A. E.; Dalvie, D. K.; Lee, J. S.; Nakai, Y.; O'Donnell, J. P.; Boer, J.; Harriman, S. P. A comprehensive listing of bioactivation pathways of organic functional groups. *Current Drug Metabolism* **2005**, *6* (3), 161-225.
8. Leung, L.; Kalgutkar, A. S.; Obach, R. S. Metabolic activation in drug-induced liver injury. *Drug Metabolism Reviews* **2012**, *44* (1), 18-33.
9. Williams, D. P.; Shipley, R.; Ellis, M. J.; Webb, S.; Ward, J.; Gardner, I.; Creton, S. Novel in vitro and mathematical models for the prediction of chemical toxicity. *Toxicology Research* **2013**, *2* (1), 40-59.
10. Stachulski, A. V.; Baillie, T. A.; Park, B. K.; Obach, R. S.; Dalvie, D. K.; Williams, D. P.; Srivastava, A.; Regan, S. L.; Antoine, D. J.; Goldring, C. E. P.; Chia, A. J. L.; Kitteringham, N. R.; Randle, L. E.; Callan, H.; Castrejon, J. L.; Farrell, J.; Naisbitt, D. J.; Lennard, M. S. The Generation,

Detection, and Effects of Reactive Drug Metabolites. *Medicinal Research Reviews* **2013**, *33* (5), 985-1080.

11. Prakash, C.; Sharma, R.; Gleave, M.; Nedderman, A. In Vitro Screening Techniques for Reactive Metabolites for Minimizing Bioactivation Potential in Drug Discovery. *Current Drug Metabolism* **2008**, *9* (9), 952-964.
12. Roth, R. A.; Ganey, P. E. Intrinsic versus Idiosyncratic Drug-Induced Hepatotoxicity-Two Villains or One? *Journal of Pharmacology and Experimental Therapeutics* **2010**, *332* (3), 692-697.
13. Leise, M. D.; Poterucha, J. J.; Talwalkar, J. A. Drug-Induced Liver Injury. *Mayo Clinic Proceedings* **2014**, *89* (1), 95-106.
14. Utrecht, J. Idiosyncratic drug reactions: Current understanding. *Annual Review of Pharmacology and Toxicology* **2007**, *47*, 513-539.
15. Thompson, R. A.; Isin, E. M.; Li, Y.; Weidolf, L.; Page, K.; Wilson, I.; Swallow, S.; Middleton, B.; Stahl, S.; Foster, A. J.; Dolgos, H.; Weaver, R.; Kenna, J. G. In Vitro Approach to Assess the Potential for Risk of Idiosyncratic Adverse Reactions Caused by Candidate Drugs. *Chemical Research in Toxicology* **2012**, *25* (8), 1616-1632.
16. Thompson, R. A.; Isin, E. M.; Li, Y.; Weaver, R.; Weidolf, L.; Wilson, I.; Claesson, A.; Page, K.; Dolgos, H.; Kenna, J. G. Risk assessment and mitigation strategies for reactive metabolites in drug discovery and development. *Chemico-Biological Interactions* **2011**, *192* (1-2), 65-71.
17. Williams, D. P.; Naisbitt, D. J. Toxicophores: Groups and metabolic routes associated with increased safety risk. *Current Opinion in Drug Discovery & Development* **2002**, *5* (1), 104-115.
18. Stepan, A. F.; Walker, D. P.; Bauman, J.; Price, D. A.; Baillie, T. A.; Kalgutkar, A. S.; Aleo, M. D. Structural Alert/Reactive Metabolite Concept as Applied in Medicinal Chemistry to Mitigate the Risk of Idiosyncratic Drug Toxicity: A Perspective Based on the Critical Examination of Trends in the Top 200 Drugs Marketed in the United States. *Chemical Research in Toxicology* **2011**, *24* (9), 1345-1410.
19. Henney, J. E. Withdrawal of troglitazone and cisapride. *Jama-Journal of the American Medical Association* **2000**, *283* (17), 2228.
20. Fung, M. Evaluation of the characteristics of safety withdrawal of prescription drugs from worldwide pharmaceutical markets-1960 to 1999. *Drug Information Journal* **2001**, *35* (1), 293-317.

21. Obach, R. S.; Kalgutkar, A. S.; Ryder, T. F.; Walker, G. S. In vitro metabolism and covalent binding of enol-carboxamide derivatives and anti-inflammatory agents sudoxicam and meloxicam: Insights into the hepatotoxicity of sudoxicam. *Chemical Research in Toxicology* **2008**, *21* (9), 1890-1899.
22. Stepan, A. F.; Walker, D. P.; Bauman, J.; Price, D. A.; Baillie, T. A.; Kalgutkar, A. S.; Aleo, M. D. Structural Alert/Reactive Metabolite Concept as Applied in Medicinal Chemistry to Mitigate the Risk of Idiosyncratic Drug Toxicity: A Perspective Based on the Critical Examination of Trends in the Top 200 Drugs Marketed in the United States. *Chemical Research in Toxicology* **2011**, *24* (9), 1345-1410.
23. Pichler, W. J. Direct T-cell stimulations by drugs-bypassing the innate immune system. *Toxicology* **2005**, *209* (2), 95-100.
24. Pichler, W. J. Consequences of drug binding to immune receptors: Immune stimulation following pharmacological interaction with immune receptors (T-cell receptor for antigen or human leukocyte antigen) with altered peptide-human leukocyte antigen or peptide. *Dermatologica Sinica* **2013**, *31* (4), 181-190.
25. Deng, X. M.; Luyendyk, J. P.; Ganey, P. E.; Roth, R. A. Inflammatory Stress and Idiosyncratic Hepatotoxicity: Hints from Animal Models. *Pharmacological Reviews* **2009**, *61* (3), 262-282.
26. Uetrecht, J. Idiosyncratic drug reactions: Past, present, and future. *Chemical Research in Toxicology* **2008**, *21* (1), 84-92.
27. Uetrecht, J. Idiosyncratic drug reactions: Current understanding. *Annual Review of Pharmacology and Toxicology* **2007**, *47*, 513-539.
28. Uetrecht, J.; Naisbitt, D. J. Idiosyncratic Adverse Drug Reactions: Current Concepts. *Pharmacological Reviews* **2013**, *65* (2), 779-808.
29. Uetrecht, J. P. Reactive metabolites and idiosyncratic toxicity. *Drug Metabolism Reviews* **2006**, *38*, 35-36.
30. Reese, M.; Sakatis, M.; Ambroso, J.; Harrell, A.; Yang, E.; Chen, L. F.; Taylor, M.; Baines, I.; Zhu, L.; Ayrton, A.; Clarke, S. An integrated reactive metabolite evaluation approach to assess and reduce safety risk during drug discovery and development. *Chemico-Biological Interactions* **2011**, *192* (1-2), 60-64.
31. Kola, I.; Landis, J. Can the pharmaceutical industry reduce attrition rates? *Nature Reviews Drug Discovery* **2004**, *3* (8), 711-715.

32. Williams, D. P.; Shipley, R.; Ellis, M. J.; Webb, S.; Ward, J.; Gardner, I.; Creton, S. Novel in vitro and mathematical models for the prediction of chemical toxicity. *Toxicology Research* **2013**, *2* (1), 40-59.
33. Korfmacher, W. A. *Using mass spectrometry for drug metabolism studies*; 6 ed.; 2004; Vol. 4.
34. Ramanathan, R.; Korfmacher, W. The emergence of high-resolution MS as the premier analytical tool in the pharmaceutical bioanalysis arena. *Bioanalysis* **2012**, *4* (5), 467-469.
35. Thomas L.Lemke; David A.Williams Foye's Principles of Medicinal Chemistry. 99 ed.; 1995; pp 1-6.
36. Kalgutkar, A. S.; Didiuk, M. T. Structural Alerts, Reactive Metabolites, and Protein Covalent Binding: How Reliable Are These Attributes as Predictors of Drug Toxicity? *Chemistry & Biodiversity* **2009**, *6* (11), 2115-2137.
37. Lenz, E. M.; Martin, S.; Schmidt, R.; Morin, P. E.; Smith, R.; Weston, D. J.; Bayrakdarian, M. Reactive Metabolite Trapping Screens and Potential Pitfalls: Bioactivation of a Homomorpholine and Formation of an Unstable Thiazolidine Adduct. *Chemical Research in Toxicology* **2014**, *27* (6), 968-980.
38. Inoue, K.; Shibata, Y.; Takahashi, H.; Ohe, T.; Chiba, M.; Ishii, Y. A Trapping Method for Semi-quantitative Assessment of Reactive Metabolite Formation Using [S-35]Cysteine and [C-14]Cyanide. *Drug Metabolism and Pharmacokinetics* **2009**, *24* (3), 245-254.
39. Nakayama, S.; Takakusa, H.; Watanabe, A.; Miyaji, Y.; Suzuki, W.; Sugiyama, D.; Shiosakai, K.; Honda, K.; Okudaira, N.; Izumi, T.; Okazaki, O. Combination of GSH Trapping and Time-Dependent Inhibition Assays as a Predictive Method of Drugs Generating Highly Reactive Metabolites. *Drug Metabolism and Disposition* **2011**, *39* (7), 1247-1254.
40. Kalgutkar, A. S.; Didiuk, M. T. Structural Alerts, Reactive Metabolites, and Protein Covalent Binding: How Reliable Are These Attributes as Predictors of Drug Toxicity? *Chemistry & Biodiversity* **2009**, *6* (11), 2115-2137.
41. Zhanga, D.; Luo, G.; Dingc, X.; Lud, G.; Lu.C Preclinical experimental models of drug metabolism and disposition in drug discovery and development. *Acta Pharmaceutica Sinica B* **2012**, *2* (6), 549-561.

42. Arora, T.; Mehta, A. K.; Joshi, V.; Mehta, K. D.; Rathor, N.; Mediratta, P. K.; Sharma, K. K. Substitute of Animals in Drug Research: An Approach Towards Fulfillment of 4R's. *Indian Journal of Pharmaceutical Sciences* **2011**, *73* (1), 1-6.
43. Gamache, P.; Smith, R.; McCarthy, R.; Waraska, J.; Acworth, I.; Williams, D. A. Redox profiling of pharmaceuticals using on-line electrochemistry-mass spectrometry. *Drug Metabolism Reviews* **2003**, *35*, 84.
44. Bussy, U.; Tea, I.; Ferchaud-Roucher, V.; Krempf, M.; Silvestre, V.; Galland, N.; Jacquemin, D.; Andresen-Bergstrom, M.; Jurva, U.; Boujtita, M. Voltammetry coupled to mass spectrometry in the presence of isotope O-18 labeled water for the prediction of oxidative transformation pathways of activated aromatic ethers: Acebutolol. *Analytica Chimica Acta* **2013**, *762*, 39-46.
45. Lohmann, W.; Karst, U. Generation and identification of reactive metabolites by electrochemistry and immobilized enzymes coupled on-line to liquid chromatography/mass spectrometry. *Analytical Chemistry* **2007**, *79* (17), 6831-6839.
46. Lohmann, W.; Karst, U. Biomimetic modeling of oxidative drug metabolism. *Analytical and Bioanalytical Chemistry* **2008**, *391* (1), 79-96.
47. Baumann, A.; Lohmann, W.; Schubert, B.; Oberacher, H.; Karst, U. Metabolic studies of tetrazepam based on electrochemical simulation in comparison to in vivo and in vitro methods. *Journal of Chromatography A* **2009**, *1216* (15), 3192-3198.
48. Lohmann, W.; Karst, U. Simulation of the detoxification of paracetamol using on-line electrochemistry/liquid chromatography/mass spectrometry. *Analytical and Bioanalytical Chemistry* **2006**, *386* (6), 1701-1708.
49. Jurva, U.; Holmen, A.; Gronberg, G.; Masimirembwa, C.; Weidolf, L. Electrochemical generation of electrophilic drug metabolites: Characterization of amodiaquine quinoneimine and cysteinyl conjugates by MS, IR, and NMR. *Chemical Research in Toxicology* **2008**, *21* (4), 928-935.
50. Johansson, T.; Jurva, U.; Gronberg, G.; Weidolf, L.; Masimirembwa, C. Novel Metabolites of Amodiaquine Formed by CYP1A1 and CYP1B1: Structure Elucidation Using Electrochemistry, Mass Spectrometry, and NMR. *Drug Metabolism and Disposition* **2009**, *37* (3), 571-579.
51. Madsen, K. G.; Skonberg, C.; Jurva, U.; Cornett, C.; Hansen, S. H.; Johansen, T. N.; Olsen, J. Bioactivation of diclofenac in vitro and in vivo: Correlation

- to electrochemical studies. *Chemical Research in Toxicology* **2008**, *21* (5), 1107-1119.
52. Jurva, U.; Wikstrom, H. V.; Weidolf, L.; Bruins, A. P. Comparison between electrochemistry/mass spectrometry and cytochrome P450 catalyzed oxidation reactions. *Rapid Communications in Mass Spectrometry* **2003**, *17* (8), 800-810.
 53. Lahoz, A.; Vila, M. R.; Fabre, M.; Miquel, J. M.; Rivas, M.; Maines, J.; Castell, J. V.; Gomez-Lechon, M. J. An in vitro tool to assess cytochrome P450 drug biotransformation-dependent cytotoxicity in engineered HepG2 cells generated by using adenoviral vectors. *Toxicology in Vitro* **2013**, *27* (4), 1410-1415.
 54. Chipiso, K.; Mbiya, W.; Morakinyo, M. K.; Simoyi, R. H. Oxyhalogen-Sulfur Chemistry: Kinetics and Mechanism of Oxidation of N-Acetyl-L-methionine by Aqueous Iodine and Acidified Iodate. *Australian Journal of Chemistry* **2014**, *67* (4), 626-635.
 55. Chigwada, T.; Mbiya, W.; Chipiso, K.; Simoyi, R. H. S-oxygenation of thiocarbamides V: oxidation of tetramethylthiourea by chlorite in slightly acidic media. *J. Phys. Chem. A* **2014**, *118* (31), 5903-5914.
 56. Zuniga, F. I.; Loi, D.; Ling, K. H. J.; Tang-Liu, D. D. S. Idiosyncratic reactions and metabolism of sulfur-containing drugs. *Expert Opinion on Drug Metabolism & Toxicology* **2012**, *8* (4), 467-485.
 57. Israeli, A.; Or, R.; Leitersdorf, E. Captopril-associated transient aplastic anemia. *Acta Haematol.* **1985**, *73* (2), 106-107.
 58. Jaffe, I. A. Adverse effects profile of sulfhydryl compounds in man. *Am. J. Med.* **1986**, *80* (3), 471-476.
 59. Kim, C. R.; Maley, M. B.; Mohler, E. R., Jr. Captopril and aplastic anemia. *Ann. Intern. Med.* **1989**, *111* (2), 187-188.
 60. Rivkees, S. A.; Szarfman, A. Dissimilar Hepatotoxicity Profiles of Propylthiouracil and Methimazole in Children. *Journal of Clinical Endocrinology & Metabolism* **2010**, *95* (7), 3260-3267.
 61. Pommier, J.; Sokoloff, L.; Nunez, J. Enzymatic Iodination of Protein - Kinetics of Iodine Formation and Protein Iodination Catalyzed by Horseradish-Peroxidase. *European Journal of Biochemistry* **1973**, *38* (3), 497-506.
 62. Chipiso, K.; Simoyi, R. H. Electrochemistry-coupled to mass spectrometry in simulation of metabolic oxidation of methimazole: Identification and

- characterization of metabolites. *Journal of Electroanalytical Chemistry* **2016**, *761*, 131-140.
63. Wang, W. S.; Kuo, W. T.; Huang, H. Y.; Luo, C. H. Wide Dynamic Range CMOS Potentiostat for Amperometric Chemical Sensor. *Sensors* **2010**, *10* (3), 1782-1797.
 64. ESA Inc Coulochem III : User's Guide Manual. 9 ed.; 2004; pp 1205-1210.
 65. Makarov, A. A.; Grechnikov, A. A.; Nikiforov, S. M.; Tyutyunnik, O. A.; Denisov, E. V. The Orbitrap mass analyzer with direct ion injection interfaced to a laser desorption/ionization ion source. *Journal of Analytical Chemistry* **2013**, *68* (14), 1165-1169.
 66. Makarov, A. A. Orbitrap mass spectrometry in proteomics: past, present and future. *Febs Journal* **2013**, *280*, 632.
 67. Cody, R. B.; Tamura, J.; Musselman, B. D. Electrospray Ionization Magnetic-Sector Mass-Spectrometry - Calibration, Resolution, and Accurate Mass Measurements. *Analytical Chemistry* **1992**, *64* (14), 1561-1570.
 68. Banerjee, S.; Mazumdar, S. Electrospray Ionization Mass Spectrometry: A Technique to Access the Information beyond the Molecular Weight of the Analyte. *International Journal of Analytical Chemistry* **2012**.
 69. Makarov, A.; Denisov, E.; Lange, O.; Horning, S. Dynamic range of mass accuracy in LTQ orbitrap hybrid mass spectrometer (vol 17, pg 977, 2006). *Journal of the American Society for Mass Spectrometry* **2006**, *17* (12), 1758.
 70. Perry, R. H.; Cooks, R. G.; Noll, R. J. Orbitrap Mass Spectrometry: Instrumentation, Ion Motion and Applications. *Mass Spectrometry Reviews* **2008**, *27* (6), 661-699.
 71. Gunther, H. *NMR Spectroscopy: Basic Principles, Concepts and Applications in Chemistry*; 24 ed.; British Library of Congress: 2013; Vol. 4.
 72. Wawer, I.; Iehl, B.; Holzgrabe, U. *NMR Spectroscopy in Pharmaceutical Analysis*; Elsevier Science: 2011.
 73. Hi-Tech Scientific Operator's Manual for the SF-61 DX2 Double Mixing Stopped-Flow Spectrofluorimeter. Salisbury, UK, Hi-Tech Limited. 1997.
 74. Simoyi, R. H. Explosion with Sodium-Chlorite. *Chemical & Engineering News* **1993**, *71* (12), 4.

75. Chigwada, T. R.; Mbiya, W.; Chipiso, K.; Simoyi, R. H. S-Oxygenation of thiocarbamides V: Oxidation of trimethylthiourea by chlorite and chlorine dioxide. *Journal of Physical Chemistry A* **2014**.
76. Darkwa, J.; Olojo, R.; Chikwana, E.; Simoyi, R. H. Antioxidant chemistry: Oxidation of L-cysteine and its metabolites by chlorite and chlorine dioxide. *Journal of Physical Chemistry A* **2004**, *108* (26), 5576-5587.
77. Ruan, Q.; Peterman, S.; Szewc, M. A.; Ma, L.; Cui, D.; Humphreys, W. G.; Zhu, M. S. An integrated method for metabolite detection and identification using a linear ion trap/Orbitrap mass spectrometer and multiple data processing techniques: application to indinavir metabolite detection. *Journal of Mass Spectrometry* **2008**, *43* (2), 251-261.
78. Lim, H. K.; Chen, J.; Sensenhauser, C.; Cook, K.; Subrahmanyam, V. Metabolite identification by data-dependent accurate mass spectrometric analysis at resolving power of 60,000 in external calibration mode using an LTQ/Orbitrap. *Rapid Communications in Mass Spectrometry* **2007**, *21* (12), 1821-1832.
79. Zhu, M. S.; Ma, L.; Zhang, H. Y.; Humphreys, W. G. Detection and structural characterization of glutathione-trapped reactive metabolites using liquid chromatography-high-resolution mass Spectrometry and mass defect filtering. *Analytical Chemistry* **2007**, *79* (21), 8333-8341.
80. Peterman, S. M.; Duczak, N.; Kalgutkar, A. S.; Lame, M. E.; Soglia, J. R. Application of a linear ion trap/orbitrap mass spectrometer in metabolite characterization studies: Examination of the human liver microsomal metabolism of the non-tricyclic anti-depressant nefazodone using data-dependent accurate mass measurements. *Journal of the American Society for Mass Spectrometry* **2006**, *17* (3), 363-375.
81. Getek, T. A.; Korfmacher, W. A.; Mcrae, T. A.; Hinson, J. A. Utility of Solution Electrochemistry Mass-Spectrometry for Investigating the Formation and Detection of Biologically Important Conjugates of Acetaminophen. *Journal of Chromatography* **1989**, *474* (1), 245-256.
82. Shayani-Jam, H.; Nematollahi, D. Electrochemical evidences in oxidation of acetaminophen in the presence of glutathione and N-acetylcysteine. *Chemical Communications* **2010**, *46* (3), 409-411.
83. Su, W. Y.; Cheng, S. H. Electrochemical Oxidation and Sensitive Determination of Acetaminophen in Pharmaceuticals at Poly(3,4-ethylenedioxythiophene)-Modified Screen-Printed Electrodes. *Electroanalysis* **2010**, *22* (6), 707-714.

84. Li, Y.; Chen, S. M. The Electrochemical Properties of Acetaminophen on Bare Glassy Carbon Electrode. *International Journal of Electrochemical Science* **2012**, *7* (3), 2175-2187.
85. Otsuka, F.; Noh, J. Y.; Chino, T.; Shimizu, T.; Mukasa, K.; Ito, K.; Ito, K.; Taniyama, M. Hepatotoxicity and cutaneous reactions after antithyroid drug administration. *Clinical Endocrinology* **2012**, *77* (2), 310-315.
86. Rivkees, S. A.; Szarfman, A. Dissimilar Hepatotoxicity Profiles of Propylthiouracil and Methimazole in Children. *Journal of Clinical Endocrinology & Metabolism* **2010**, *95* (7), 3260-3267.
87. Uetrecht, J. P. Reactive metabolites and idiosyncratic toxicity. *Drug Metabolism Reviews* **2006**, *38*, 35-36.
88. Uetrecht, J. Idiosyncratic drug reactions: Past, present, and future. *Chemical Research in Toxicology* **2008**, *21* (1), 84-92.
89. Mizutani, T.; Yoshida, K.; Murakami, M.; Shirai, M.; Kawazoe, S. Evidence for the involvement of N-methylthiourea, a ring cleavage metabolite, in the hepatotoxicity of methimazole in glutathione-depleted mice: Structure-toxicity and metabolic studies. *Chemical Research in Toxicology* **2000**, *13* (3), 170-176.
90. Kedderis, G. L.; Rickert, D. E. Loss of Rat-Liver Microsomal Cytochrome-P-450 During Methimazole Metabolism - Role of Flavin-Containing Monooxygenase. *Drug Metabolism and Disposition* **1985**, *13* (1), 58-61.
91. Aslanoglu, M.; Peker, N. Potentiometric and voltammetric determination of methimazole. *Journal of Pharmaceutical and Biomedical Analysis* **2003**, *33* (5), 1143-1147.
92. Sun, J. Y.; Zheng, C. Y.; Xiao, X. L.; Niu, L.; You, T. Y.; Wang, E. K. Electrochemical detection of methimazole by capillary electrophoresis at a carbon fiber microdisk electrode. *Electroanalysis* **2005**, *17* (18), 1675-1680.
93. Wang, Y. Z. Electrochemical determination of methimazole based on the acetylene black/chitosan film electrode and its application to rat serum samples. *Bioelectrochemistry* **2011**, *81* (2), 86-90.
94. Kalgutkar, A. S.; Gardner, I.; Obach, R. S.; Shaffer, C. L.; Callegari, E.; Henne, K. R.; Mutlib, A. E.; Dalvie, D. K.; Lee, J. S.; Nakai, Y.; O'Donnell, J. P.; Boer, J.; Harriman, S. P. A comprehensive listing of bioactivation pathways of organic functional groups. *Curr. Drug Metab* **2005**, *6* (3), 161-225.

95. ESA Inc Coulochem III (50W) Reference Manual: Chapter 4. 2004; pp 5-7.
96. Darkwa, J.; Mundoma, C.; Simoyi, R. H. Antioxidant chemistry - Reactivity and oxidation of DL-cysteine by some common oxidants. *Journal of the Chemical Society-Faraday Transactions* **1998**, *94* (14), 1971-1978.
97. Darkwa, J.; Olojo, R.; Chikwana, E.; Simoyi, R. H. Antioxidant chemistry: Oxidation of L-cysteine and its metabolites by chlorite and chlorine dioxide. *Journal of Physical Chemistry A* **2004**, *108* (26), 5576-5587.
98. Darkwa, J.; Olojo, R.; Olagunju, O.; Otoikhian, A.; Simoyi, R. Oxyhalogen-sulfur chemistry: Oxidation of N-acetylcysteine by chlorite and acidic bromate. *Journal of Physical Chemistry A* **2003**, *107* (46), 9834-9845.
99. Attia, S. M. Deleterious effects of reactive metabolites. *Oxidative Medicine and Cellular Longevity* **2010**, *3* (4), 238-253.
100. Simoyi, R. H.; Svarovsky, S. A.; Mundoma, C. M.; Makarov, S. V. Reactive oxygen species and sulfoxyl radicals in the aerobic decomposition of thioureas dioxides. *Abstracts of Papers of the American Chemical Society* **1999**, *218*, U375.
101. Hsu, D. Z.; Chu, P. Y.; Li, Y. H.; Chandrasekaran, V. R.; Liu, M. Y. Role of flavin-containing-monooxygenase-dependent neutrophil activation in thioacetamide-induced hepatic inflammation in rats. *Toxicology* **2012**, *298* (1-3), 52-58.
102. Tian, X.; Sun, X.; Su, J. Biochemical mechanisms for metaflumizone resistance in beet armyworm, *Spodoptera exigua*. *Pestic. Biochem. Physiol* **2014**, *113*, 8-14.
103. Hu, S. X.; Soll, R.; Yee, S.; Lohse, D. L.; Kousba, A.; Zeng, B.; Yu, X.; McPherson, A.; Renick, J.; Cao, J.; Tabak, A.; Hood, J.; Doukas, J.; Noronha, G.; Martin, M. Metabolism and pharmacokinetics of a novel Src kinase inhibitor TG100435 ([7-(2,6-dichloro-phenyl)-5-methylbenzo[1,2,4]triazin-3-yl]-[4-(2-pyrrolidin-1-yl-ethoxy)-phenyl]-amine) and its active N-oxide metabolite TG100855 ([7-(2,6-dichloro-phenyl)-5-methylbenzo[1,2,4]triazin-3-yl]-{4-[2-(1-oxy-pyrrolidin-1-yl)-ethoxy]-phenyl}-amine). *Drug Metab Dispos.* **2007**, *35* (6), 929-936.
104. Kousba, A.; Soll, R.; Yee, S.; Martin, M. Cyclic conversion of the novel Src kinase inhibitor [7-(2,6-dichloro-phenyl)-5-methyl-benzo[1,2,4]triazin-3-yl]-[4-(2-pyrrolidin-1-yl -ethoxy)-phenyl]-amine (TG100435) and Its N-oxide metabolite by flavin-containing monooxygenases and cytochrome P450 reductase. *Drug Metab Dispos.* **2007**, *35* (12), 2242-2251.

105. Schott, M. Hyperthyroidism. *Internist* **2013**, *54* (3), 315-326.
106. Korelitz, J. J.; McNally, D. L.; Masters, M. N.; Li, S. X.; Xu, Y. L.; Rivkees, S. A. Prevalence of Thyrotoxicosis, Antithyroid Medication Use, and Complications Among Pregnant Women in the United States. *Thyroid* **2013**, *23* (6), 758-765.
107. Kampmann, J. P.; Hansen, J. M. Clinical Pharmacokinetics of Antithyroid Drugs. *Clinical Pharmacokinetics* **1981**, *6* (6), 401-428.
108. Paterson, J. R.; Hood, H. T.; Skellern, G. G. The Role of Porcine Thyroid Peroxidase and Fad-Containing Monooxygenase in the Metabolism of 1-Methyl-2-Thioimidazole (Methimazole). *Biochemical and Biophysical Research Communications* **1983**, *116* (2), 449-455.
109. Podrez, E. A.; Abu-Soud, H. M.; Hazen, S. L. Myeloperoxidase-generated oxidants and atherosclerosis. *Free Radical Biology and Medicine* **2000**, *28* (12), 1717-1725.
110. Waldhauser, L.; Uetrecht, J. Oxidation of Propylthiouracil to Reactive Metabolites by Activated Neutrophils - Implications for Agranulocytosis. *Drug Metabolism and Disposition* **1991**, *19* (2), 354-359.
111. Marchant, B.; ALEXANDE.WD Thyroid Accumulation, Oxidation and Metabolic Fate of S-35-Methimazole in Rat. *Endocrinology* **1972**, *91* (3), 747-&.
112. Skellern, G. G.; Steer, S. T. The Metabolism of [Methimazole-2-C-14 in the Rat. *Xenobiotica* **1981**, *11* (9), 627-634.
113. Wang, Q.; Chen, K. F.; Li, J.; Xu, J.; Liu, S. S. Simultaneous Determination of Chlorine Dioxide and Hypochlorous Acid in Bleaching System. *Bioresources* **2011**, *6* (2), 1868-1879.
114. Peintler, G.; Nagypal, I.; Epstein, I. R. Systematic Design Chemical Oscillators - Kinetics and Mechanism of the Reaction Between Chlorite Ion and Hypochlorous Acid. *Journal of Physical Chemistry* **1990**, *94* (7), 2954-2958.
115. Jia, Z. J.; Margerum, D. W.; Francisco, J. S. General-acid-catalyzed reactions of hypochlorous acid and acetyl hypochlorite with chlorite ion. *Inorganic Chemistry* **2000**, *39* (12), 2614-2620.
116. Jones, J. B.; Chinake, C. R.; Simoyi, R. H. Oxyhalogen Sulfur Chemistry - Oligooscillations in the Formamidinesulfinic Acid Chlorite Reaction. *Journal of Physical Chemistry* **1995**, *99* (5), 1523-1529.

117. Nicoson, J. S.; Margerum, D. W. Kinetics and mechanisms of aqueous chlorine reactions with chlorite ion in the presence of chloride ion and acetic acid/acetate buffer. *Inorganic Chemistry* **2002**, *41* (2), 342-347.
118. Yin, G. H.; Ni, Y. H. Quantitative description of the chloride effect on chlorine dioxide generation from the ClO₂--HOCl reaction. *Canadian Journal of Chemical Engineering* **1998**, *76* (5), 921-926.
119. Olagunju, O.; Siegel, P. A.; Olojo, R.; Simoyi, R. H. Oxyhalogen-sulfur chemistry: Kinetics and mechanism of oxidation of N-acetylthiourea by chlorite and chlorine dioxide. *Journal of Physical Chemistry A* **2006**, *110* (7), 2396-2410.
120. Abraham, P.; Avenell, A.; Watson, W. A.; Park, C. M.; Bevan, J. S. Antithyroid drug regimen for treating Graves' hyperthyroidism. *Cochrane Database of Systematic Reviews* **2005**, (2).
121. Rostron, C. a. B. J. *Inorganic Chemistry in Pharmacy*. 1 ed.; 2013; p 237.
122. Russo, M. W.; Galanko, J. A.; Shrestha, R.; Fried, M. W.; Watkins, P. Liver transplantation for acute liver failure from drug induced liver injury in the United States. *Liver Transplantation* **2004**, *10* (8), 1018-1023.
123. Rivkees, S. A.; Mattison, D. R. Propylthiouracil (PTU) Hepatotoxicity in Children and Recommendations for Discontinuation of Use. *Int J Pediatr Endocrinol.* **2009**.
124. Rousu, T.; Pelkonen, O.; Tolonen, A. Rapid detection and characterization of reactive drug metabolites in vitro using several isotope-labeled trapping agents and ultra-performance liquid chromatography/time-of-flight mass spectrometry. *Rapid Communications in Mass Spectrometry* **2009**, *23* (6), 843-855.
125. Heidari, R.; Niknahad, H.; Jamshidzadeh, A.; Mohammad A, E.; Abdoli, N. An Overview on the Proposed Mechanisms of Antithyroid Drugs Induced Liver Injury. *Adv Pharm Bull*, **2014**, *74* (1), 1-8.
126. Sartori, E. R.; Trench, A. B.; Rocha, R. C.; Fatibello, O. Determination of Propylthiouracil in Pharmaceuticals by Differential Pulse Voltammetry Using a Cathodically Pretreated Boron-Doped Diamond Electrode. *Journal of the Brazilian Chemical Society* **2013**, *24* (9), 1504-1511.
127. Madej, E.; Wardman, P. The oxidizing power of the glutathione thiyl radical as measured by its electrode potential at physiological pH. *Archives of Biochemistry and Biophysics* **2007**, *462* (1), 94-102.

128. Poole, L. B.; Karplus, P. A.; Claiborne, A. Protein sulfenic acids in redox signaling. *Annual Review of Pharmacology and Toxicology* **2004**, *44*, 325-347.
129. Mansuy, D.; Dansette, P. M. Sulfenic acids as reactive intermediates in xenobiotic metabolism. *Archives of Biochemistry and Biophysics* **2011**, *507* (1), 174-185.
130. Turell, L.; Carballal, S.; Botti, H.; Radi, R.; Alvarez, B. Oxidation of the albumin thiol to sulfenic acid and its implications in the intravascular compartment. *Brazilian Journal of Medical and Biological Research* **2009**, *42* (4), 305-311.
131. Gupta, V.; Carroll, K. S. Sulfenic acid chemistry, detection and cellular lifetime. *Biochimica et Biophysica Acta-General Subjects* **2014**, *1840* (2), 847-875.
132. Sujit, R. A. a. S. K. B. S. Formation and Disproportionation of Arene Sulfenic Acids. *Journal of Applied Chemistry* **2013**, *3* (6), 40-45.
133. Zhang, X. Mass spectrometric and theoretical studies on dissociation of the C-S bond in the benzenesulfonic acid and benzenesulfinic acid anion series: Homolytic cleavage vs heterolytic cleavage. *Journal of Molecular Structure* **2012**, *1028*, 1-6.
134. Ranguelova, K.; Rice, A. B.; Lardinois, O. M.; Triquigneaux, M.; Steinckwich, N.; Deterding, L. J.; Garantziotis, S.; Mason, R. P. Sulfite-mediated oxidation of myeloperoxidase to a free radical: Immuno-spin trapping detection in human neutrophils. *Free Radical Biology and Medicine* **2013**, *60*, 98-106.
135. Nassar, A. F.; Holenberg, P. F.; Scantina, J. Drug Metabolism Handbook concepts and Applications. 39 ed.; 2009; pp 302-303.
136. Henderson, M. C.; Siddens, L. K.; Morre, J. T.; Krueger, S. K.; Williams, D. E. Metabolism of the anti-tuberculosis drug ethionamide by mouse and human FMO1, FMO2 and FMO3 and mouse and human lung microsomes. *Toxicology and Applied Pharmacology* **2008**, *233* (3), 420-427.
137. DeBarber, A. E.; Mdluli, K.; Bosman, M.; Bekker, L. G.; Barry, C. E. Ethionamide activation and sensitivity in multidrug-resistant *Mycobacterium tuberculosis*. *Proceedings of the National Academy of Sciences of the United States of America* **2000**, *97* (17), 9677-9682.
138. Henderson, M. C.; Krueger, S. K.; Stevens, J. F.; Williams, D. E. Human flavin-containing monooxygenase form 2 S-oxygenation: Sulfenic acid formation

from thioureas and oxidation of glutathione. *Chemical Research in Toxicology* **2004**, *17* (5), 633-640.

139. Krueger, S. K.; Williams, D. E. Mammalian flavin-containing monooxygenases: structure/function, genetic polymorphisms and role in drug metabolism. *Pharmacol. Ther.* **2005**, *106* (3), 357-387.
140. Eswaramoorthy, S.; Bonanno, J. B.; Burley, S. K.; Swaminathan, S. Mechanism of action of a flavin-containing monooxygenase. *Proc. Natl. Acad. Sci. U. S. A* **2006**, *103* (26), 9832-9837.
141. Cashman, J. R.; Zhang, J. Human flavin-containing monooxygenases. *Annu. Rev. Pharmacol. Toxicol.* **2006**, *46*, 65-100.
142. Koukouritaki, S. B.; Hines, R. N. Flavin-containing monooxygenase genetic polymorphism: impact on chemical metabolism and drug development. *Pharmacogenomics.* **2005**, *6* (8), 807-822.
143. Henderson, M. C.; Krueger, S. K.; Stevens, J. F.; Williams, D. E. Human flavin-containing monooxygenase form 2 S-oxygenation: Sulfenic acid formation from thioureas and oxidation of glutathione. *Chemical Research in Toxicology* **2004**, *17* (5), 633-640.
144. Genter, M. B.; Deamer, N. J.; Blake, B. L.; Wesley, D. S.; Levi, P. E. Olfactory Toxicity of Methimazole - Dose-Response and Structure-Activity Studies and Characterization of Flavin-Containing Monooxygenase Activity in the Long-Evans Rat Olfactory Mucosa. *Toxicologic Pathology* **1995**, *23* (4), 477-486.
145. Mizutani, T.; Yoshida, K.; Murakami, M.; Shirai, M.; Kawazoe, S. Evidence for the involvement of N-methylthiourea, a ring cleavage metabolite, in the hepatotoxicity of methimazole in glutathione-depleted mice: Structure-toxicity and metabolic studies. *Chemical Research in Toxicology* **2000**, *13* (3), 170-176.
146. Rankin, G.; Anestis, D.; Racine, C. Role of renal biotransformation in 3,4,5-trichloroaniline nephrotoxicity in vitro. *Faseb Journal* **2014**, *28* (1).